The Role of Alkali Metals in Biomass Thermochemical Conversion

by:

Abha Saddawi

Supervised by: Professors Jenny Jones and Alan Williams

Submitted in accordance with the requirements for the degree of
Doctor of Philosophy

The University of Leeds
Energy and Resources Research Institute
School of Process, Environmental and Materials Engineering

September, 2011

Acknowledgements

I would like to express my most heartfelt gratitude to my supervisors, Professor Jenny M. Jones, and Professor Alan Williams, who have been so generous with their time, support, and advice. I feel so incredibly lucky to have had the opportunity to study and work with both of you. Jenny, thank you for having been the best advisor anyone could ask for. Thank you also, Alan, your wisdom has been invaluable, and your encouragement during seemingly hopeless times is very much appreciated.

I would like to express my gratitude to the EPSRC for funding this work.

Many thanks to Mr. Simon Lloyd for all his help with my experiments, and for being such a great person to work with. My gratitude also extends to Dr. Adrian Cunliffe for always being helpful.

This thesis has benefitted from some laboratory work conducted by one visiting and two MSc students, and I would like to thank them for their efforts. Thank you Esther Fuentes, Martin Ross, and Camille Le Coeur.

Thank you also to my fantastic colleagues and friends: Kostas Anastasakis, Patrick Biller, Nikos Giannakeas, Guarav Nahar, Bijal Gudka, Xiaomian Baxter, Rob Johnson, thank you all for being there for me, and for making work such a happy place to be. Thank you Dr. Leilani Darvell and Dr. Andy Ross for all your help, excellent book recommendations, and coffee time chats. I would also like to thank our past group members who have helped me along the way: Toby Bridgeman, and Emma Fitzpatrick.

Finally, I would like to thank my wonderful family. Thank you to my husband Adel Jebar, for all his unconditional love, encouragement, and understanding. Thank you also to my parents; my mother Salma and my father Shafa Saddawi, who have been with me through every step of not only this degree, but all of life. Words cannot express all of my gratitude and love for you.

Dedicated to my parents,

Dr. Salma & Dr. Shafa Saddawi

Abstract

Environmental preservation concerns, coupled with those of energy supply security, are leading to a push for alternative fuels that are both green and sustainable. Therefore, biomass, which is a renewable low carbon energy source, is being increasingly utilized worldwide. The use of biomass in thermochemical conversion is not without problems, some of which are related to the inherent alkali metal content present in these types of fuels.

The work conducted for this thesis mainly deals with topics related to thermal degradation kinetics of biomass and the influence of alkali metals on these kinetics, as well as their effects on the thermal behaviour of the fuel. Torrefaction is also studied with respect to kinetics studies, and the effects of mineral content.

Thermal degradation was studied using thermogravimetric analysis (TGA) and kinetic models were evaluated to address two questions; first, what method of data analysis is appropriate for extracting reliable kinetic data from TGA experiments? Second, what kinetics are most suitable for high heating rate situations such as those present in pulverized fuel power stations? It was found that for low heating rate experiments (10 K/min), the global first-order reaction kinetic models that tend to yield low activation energies (E), such as the reaction rate constant method, work well. High E kinetics can also work well at low heating rate, but only if the reaction is assumed to be due to the sum of a number of individual steps. For example, those derived when assuming the biochemical components degrade independently, or using the functional group approach. For higher heating rates (>10^3 K/s) high E kinetics predict conversion well, and this can be rationalized since primary cracking reactions will dominate under these conditions. However, at heating rates of 10^5 K/s and temperatures of 1500 °C (i.e., flame conditions), a compensation on the rates is seen and the choice of rate parameters is less critical. Two sets of kinetic data, E = 178.7 kJ/mol, A = 2.2 × 10^{13} s^{-1} and E = 48.7 kJ/mol, A = 6.84 × 10^3 s^{-1}, both predict conversions in keeping with the available experimental data.

The effects of alkali metals (K, Na, Cs) on thermal degradation kinetics of SRC willow in pyrolysis, combustion were studied using TGA, and single particle burning in a methane-air flame. The results revealed that all three metals had a

strong and similar catalytic effect on pyrolysis and combustion. Combustion under flame conditions also showed a stark contrast between the strongly catalyzed degradation of samples in the presence of alkali metals, and the uncatalysed degradation of mineral-free samples. As with the low heating rate results, at flame conditions, the metal-impregnated samples behaved similarly to each other, implying that a similar thermal degradation mechanism is followed when woody biomass contains any of the alkali metals.

A mathematical expression directly linking the inherent potassium and sodium content of SRC willow to its thermal degradation kinetics was developed through modifying a Langmuir-Hinshelwood relation and applying it to pyrolysis data. This relation yields a maximum reaction rate and a metal saturation constant that can be used to predict a reaction rate of willow based on the pyrolysis temperature and the concentration of either of the metals in the biomass sample. I.e. the maximum reaction rate constant of 3.26×10^{-3} (s^{-1}) and the potassium saturation constant of 0.56 wt% can be used to derive the pyrolysis reaction rate of any willow sample with a known potassium concentration. Similarly, a maximum reaction rate of 3.27×10^{-3} (s^{-1}) and a sodium saturation constant of 0.36 wt% can be used to derive a reaction rate for any willow sample with a known sodium concentration. *Ab initio* (Density Functional Theory method) modelling was employed to explore the chemical mechanisms involved. Cellobiose was used as a model for cellulose. The cellobiose structure was first optimized at the HF level, and then at the B3LYP DFT level with a 6-31G(d) basis set and the structure frequency was checked to ensure the system was at ground state. The models showed that that both metal ions form multiple interactions with the hydroxyl and ether bonds in the cellulose structure. Structures with metal chelated at the C6 position in the ring have interactions with four oxygen atoms, while metals at the C2 position have interactions with only two oxygen atoms, although inter-molecular chelation between cellulose chains has not been considered. Structures are more stable when potassium or sodium can coordinate to more oxygen groups. Nevertheless, in all the structures investigated, chelation of potassium or sodium causes a change in the conformation of the rings (twisting) which may activate the structure towards cracking.

The final area of investigation in this thesis is in torrefaction, a mild pyrolysis process. Torrefied biomass has many advantages over untreated biomass, but its ash

characteristics remain similar to the parent biomass. In this thesis, inherent metals were removed prior to torrefaction. Impact on ash behaviour of this resultant fuel and the torrefaction process itself are reported. More specifically, the work examined the effects of altered mineral content (through a chemical fractionation procedure involving successive washings of the fuel in water, ammonium acetate, and hydrochloric acid), on the torrefaction of four biomass fuels (SRC willow, Miscanthus, eucalyptus, and wheat straw), as well as on the pyrolysis and the ash behaviour of the torrefied material. Washing prior to torrefaction significantly reduced the ash content of the fuels, and ameliorated the ash fusion temperatures. The pyrolysis reaction rates of the HCl treated and torrefied fuels were found to be the highest, presumably due to the changes in the biomass structure caused by the acid. The results suggest that water washing is the most useful pre-treatment for the preparation of torrefied fuels. Washing with ammonium acetate or HCl would not be feasible because of the small advantage gained, the high costs induced, and the environmental implications. The significance of the impact of these changes in composition and reaction rates depends on the end application, power station or domestic heating. In the case of power station applications, washing with water reduces the ash content, and improves the ash melting behaviour of the remaining ash, which may be advantageous particularly in the case of straw; the slight increase in N would not be significant because of the normal NOx reduction methods used in power stations. In domestic applications the reduction of ash is not so important but the increase in N may be a significant disadvantage.

Contents

Figures

Tables

Nomenclature and Abbreviations

Nomenclature		Units
A	Pre-exponential factor	s^{-1}
α	Reaction progress	
B	Heating rate	°C/min
[B]	Amount of biomass	
$[B_o]$	Total number of pyrolysis sites	
[BM]	Biomass-metal intermediate active species	
E	Activation energy	kJ/mol
k	Reaction rate	s^{-1}
k^o	Maximum reaction rate constant	s^{-1}
m	Mass of sample	mg
m_o	Initial mass of sample	mg
[M]	Amount of metal	
R	Gas constant	kJ/mol K
S_k	Metal saturation constant	wt%
T	temperature	K or °C
t	time	s

Abbreviations

CV	Calorific value
db	Dry basis
daf	Dry, ash free
DTG	Differential thermogravimetric analysis
DFT	Density functional theory
EPSRC	Engineering and Physical Sciences Research Council

EDX	Energy dispersive X-Ray
ERRI	Energy and Resources Research Institute
FC	Fixed carbon
FPS	Frames per second
HF	Hartree Fock
HHV	Higher heating value
ICP	Inductively coupled plasma
L-H	Langmuir Hinshelwood
LHS	Left hand side
Mtoe	Million tons of oil equivalent
NOx	Nitrogen oxides
RHS	Right hand side
SOx	Sulphur oxides
SPCE	Single particle combustion experiments
SRC	Short rotation coppice
TGA	Thermogravimetric analysis
VM	Volatile matter

Chapter 1
Introduction

1.1. Energy, Environment, and Renewable Fuels

1.1.1. Rising Energy Consumption

The 2011 Annual Energy Outlook, published by the independent U.S. Energy Information Administration, has predicted sharp increases in world energy consumption over the next twenty years. Energy demand, rising globally by nearly 50% by 2035 from 2009 values, is increasing more rapidly in non-OECD countries (countries with developing economies that do not belong to the Organization for Economic Cooperation and Development) [1]. Figure 1.1 illustrates past and predicted future energy consumption amounts by world region.

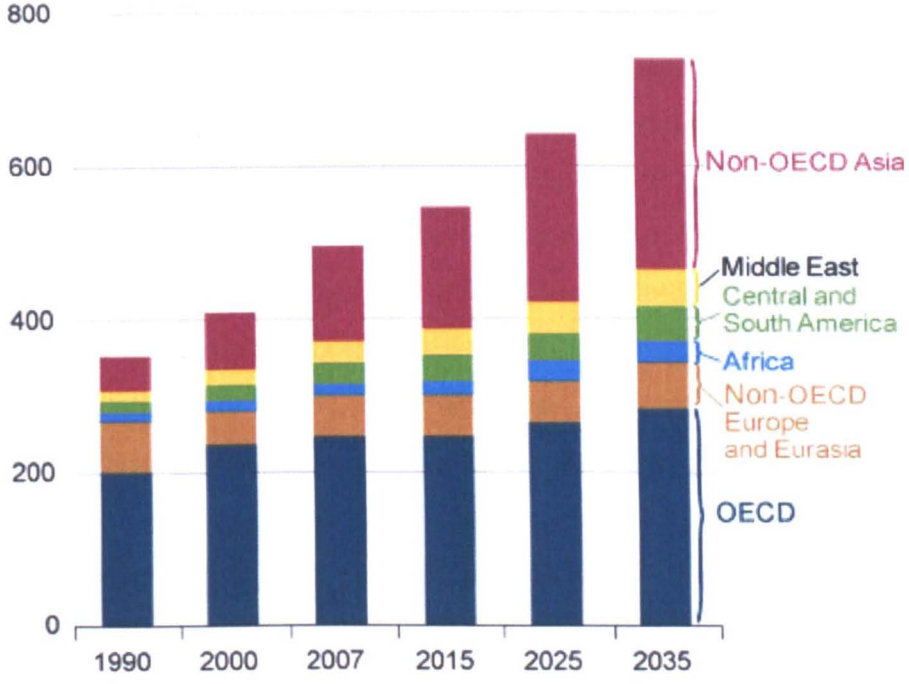

Figure 1.1 World energy consumption by region, 1990 – 2035 (quadrillion Btu (i.e. 10^{15})) [1], where 1 million barrels of oil equivalent = $5.8 * 10^{-3}$ quad.

Although there is a sharp predicted increase in energy consumption, British Petroleum's research claims that there are enough worldwide proven reserves of oil, natural gas and coal to meet energy needs for decades[2]. Ample supply of non-renewable fuel however, does not negate security of supply issues as most fuels in the UK are imported from politically unstable regions. The UK Energy White paper of 2003 states a need for investment in low carbon fuel infrastructure and also a need for managing the risks carried with a dependence on energy imports as the worldwide competition for energy supplies rises[3].

Supply concerns apart, it can be argued that with increased energy demand and production, the most pressing issue is environmental. This will especially be true if reliance upon fossil fuels does not rapidly diminish.

1.1.2 Environmental Concerns

It is well known that the combustion of fossil fuels for energy produces air pollutants including carbonaceous particles such as soot, together with sulphur dioxides, nitrogen oxides, and volatile organic compounds along with some heavy metals. Also of great importance is the release of large amounts of greenhouse gases, including carbon dioxide, nitrous oxide, and methane. These greenhouse gases have a long lifetime and gradually increase in concentration in the troposphere and trap an excessive amount of solar energy reflected from the earth. The trapped radiation then causes the ambient temperature of the earth to rise considerably. Approximately 30 years ago, the US. National Research Council concluded that if the concentration of carbon dioxide in the atmosphere were to double, a global surface warming of 2 to 3.5% could occur, and that temperatures could rise even further at higher latitudes [4]. Figure 1.2 shows that even over the relatively short period of time from 1990 to 2009, worldwide carbon dioxide emissions from the consumption of energy have greatly increased.

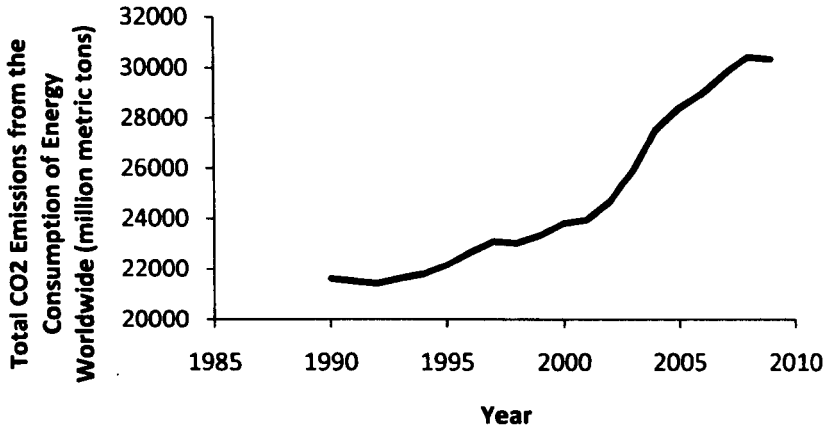

Figure 1.2 Total CO_2 Emissions from the Consumption of Energy Worldwide [5].

Most scientists now agree that continued release of green house gases at the current rates will significantly raise global temperatures which could have devastating effects such as rising sea levels, a shift in agricultural zones, and significant changes in the polar ice caps.

1.1.3 Growth in the Use of Renewables

Environmental preservation concerns, coupled with those of energy supply security, are leading to a push for alternative fuels that are both green and sustainable. The Renewable Energy Strategy aims to help mitigate the trend towards an increased dependence on imported fossil fuels. The report states that if 15% of the UK's energy is generated from renewables then a reduction in overall fossil fuel demand by around 10% and gas imports by between 20–30% can be achieved [6].

The UK aims to cut 18% of green house emissions measured in 2008 by the year 2020 and also plans to meet 40% of the country's energy demand with low carbon sources by then [3]. The UK Energy White Paper also states that by 2020, 15% of the country's energy for electricity, heating, and transport is to come from renewable sources such as wind, sunlight, tides, and biomass.

The Renewable Energy Policy Network for the 21st Century states, in its 2010 report, that there are worldwide increases in the use and production of renewable energy across all the different forms [7]. In 2008, renewable accounted for 19% of the global energy consumption.

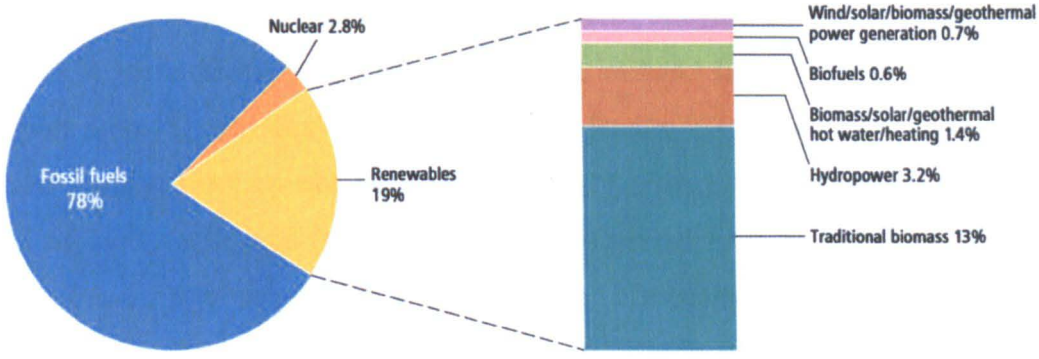

Figure 1.3 Renewable energy share of global final energy consumption, 2008 [7].

As figure 1.3 shows, globally, the largest share of the energy coming from renewables belongs to traditional biomass which in this case is defined as unprocessed biomass, including agricultural waste, forest products waste, collected fuel wood, and animal dung, that is burned in stoves or furnaces to provide heat energy for cooking, heating, and agricultural and industrial processing, typically in rural areas [7].

1.2 Biomass, Introduction and Advantages

Biomass is a renewable low carbon energy source that is being increasingly utilized worldwide. The term biomass refers to various forms of living matter, and there are many sources of biomass including forestry-derived material, agricultural by-products, biodegradable wastes, and purpose-grown energy crops [8, 9]. The main source used for energy is derived from vegetation and residuals from human and animal activity. This includes woody and non-woody biomass and also animal waste [10]. Biomass is seen as a renewable and low carbon energy source because the fuel can be re-grown or cultivated, and the carbon dioxide released in biomass to energy conversion, is used by other growing biomass crops as part of their

photosynthesis cycle, where the carbon dioxide is converted to organic compounds. It must be pointed out, however, that practices that reduce the size of the photosynthetic sink such as "slash-and-burn" agriculture [4], large scale wood burning, and rain-forest destruction can obviously reduce the amount of CO_2 captured by the natural photosynthetic process and must be avoided.

There are several advantages associated with biomass over other renewables. Biomass is versatile in its end uses and can be utilized for heating, electricity and transport fuels [8]. Perhaps the most attractive feature is that, unlike wind and solar derived energy, biomass can be stored to supply energy when needed. Various forms of solid, liquid and gaseous fuels can be derived from biomass and as stated earlier, these fuels can be used for heating, electricity, and transport. Most commonly in the UK, biomass is used for electricity, and heating through combustion. Another benefit of biomass conversion is that existing coal powered infrastructure can be easily adapted to for biomass usage. The UK government has introduced financial incentives for using biomass grown specifically for electricity production, therefore, energy crops such as Short Rotation Willow Coppice (SRC), and Miscanthus have received much attention [11].

1.3 Biomass Composition and Structure

Knowledge of the structure and composition of biomass is useful for the improvement of the various processes biomass undergoes in the production of energy and chemicals.

The dominant organic components in biomass are celluloses and hemicelluloses. Biomass, in general, is comprised of close to 50 wt % cellulose. Other components such as the hemicellulose, lignin, proteins, and triglycerides are present in smaller amounts. From a solid fuel and thermal conversion technology perspective, cellulose, hemicellulose, and lignin are the three most influential organic constituents as they play an important role in the decomposition reactions that occur during combustion and pyrolysis, and also influence the fuel's performance in physical conversion processes. The three components are often referred to collectively as lignocellulose.

1.3.1 Cellulose

The primary cell wall's tensile strength comes from cellulose. The cellulose molecule is made up of a linear chain that has more than 500 glucose residues that are covalently bonded to each other forming a structure that is stabilized by hydrogen bonds within the chain. Intermolecular hydrogen bonds between adjacent cellulose molecules cause them to stick to one another in "overlapping parallel arrays" forming cellulose microfibrils [12]. Figure 1.4 illustrates the chemical structure of cellulose.

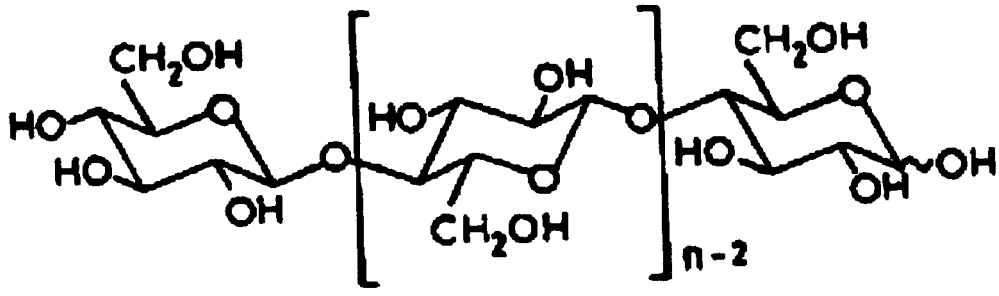

Figure 1.4 The Chemical Structure of Cellulose [13].

The average molecular weight of cellulose is between 300,000 to 500,000. Partial hydrolysis of cellulose yields cellobiose (glucose-β-glucoside), cellotriose, and cellotetrose. Wood cellulose always occurs in association with hemicellulose and lignin, unlike, for example, cotton which is made up of mostly α-cellulose [4].

1.3.2 Hemicellulose

Hemicelluloses make up a heterogeneous group of branched polysaccharides that are closely bound to the surface of each cellulose microfibril and also to each other. Through these bonds, hemicellulose helps to cross-link the microfibrils into a complex network. There are several different kinds of hemicellulose, but the variety all have in common a long and linear backbone composed of a sugar molecule. From these sugar units, short side chains of other sugars protrude. These sugars are hydrogen bonded with the cellulose microfibrils [12]. Hemicellulose molecules

usually consist of 50 to 200 monomeric units and some simple sugar residues. The most common hemicellulose is xylan which consists of D-xylose units linked in the 1- and 4- positions. Xylans exist in softwoods and hardwoods in amounts between 10 and 30 dry weight % (dw %) [4]. Figure 1.5 shows the chemical structure of xylan.

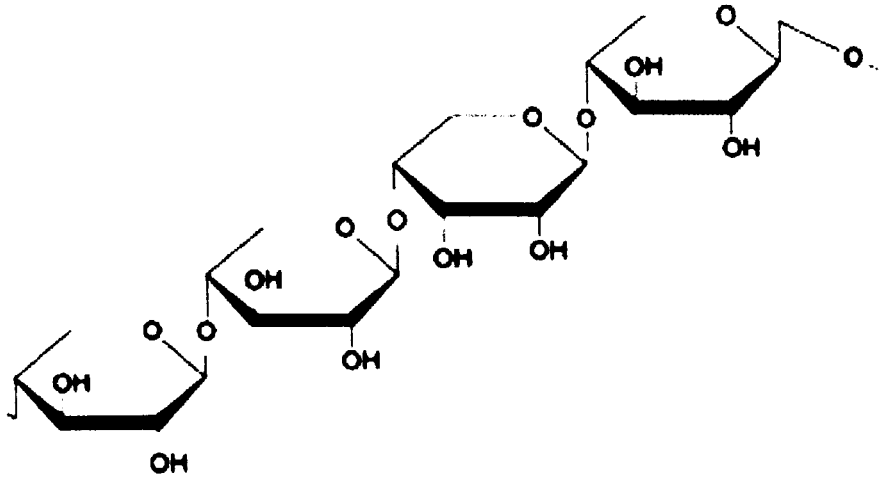

Figure 1.5 The Chemical Structure of xylan [14].

1.3.3 Lignin

Lignins are mostly found in the cell walls of woody biomass species. They are frequently bound to adjacent cellulose fibres. Lignins consist of highly branched, substituted, mononuclear aromatic polymers. They are often difficult to convert both through microbial and chemical means. The main monomeric units of the lignins are benzene rings, bearing methoxyl, hydroxyl, and propyl groups that can attach to other units. Figure 1.6 shows some of the structural units that lignins consist of.

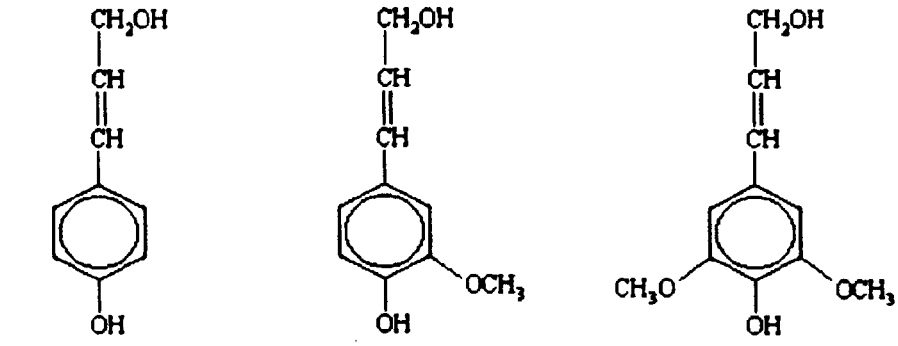

Figure 1.6 Some Structural Units of Lignin [15].

Lignins make up approximately 25 wt% of the parent hardwood or softwood biomass [4].

1.4 Biomass Fuel Properties

As with all fuels, the characterization of biomass is crucial for the design of conversion applications. Knowledge of the fuel characteristics such as the moisture, the amount of volatiles, the amount and quality of the ash, the energy content and so on, is necessary. There are several databases available such as the Phyllis data base (available at http://www.ecn.nl/phyllis/) and a similar US DOE database (available at http://www1.eere.energy.gov/biomass/feedstock_databases.html), that contain a plethora of biomass compositions.

1.4.1 Moisture, Volatiles, and Ash

In general, newly harvested biomass can contain between 40 to 60% moisture [4]. The amount of moisture present in the fuel will depend upon factors such as weather conditions, the type of biomass, time of harvesting. Primary drying (such as storing in a covered area) can reduce the moisture content significantly. Further drying at elevated temperatures is sometimes used (e.g. pellet production) to reduce moisture to less than 10 wt%. However, if stored for prolonged periods of time, the

hydrophilic nature of biomass will allow the fuel to re-absorb moisture, and this can lead to degradation of the biomass. The moisture content of the fuel is crucial in applications such as combustion, where valuable energy is lost if the fuel is wet and so must be dried prior to ignition [4].

The volatiles or volatile matter (VM) is considered to be the fraction of the biomass that is released upon decomposition (excluding moisture) when the fuel is heated at temperatures close to 400 °C in an inert gas. What remains of the biomass sample, excluding the ash (discussed below) is considered to be the fixed carbon content (FC), although this term is associated with coal analysis and is sometimes referred to as char fraction when dealing with biomass.

Ash is the inorganic or mineral content of the biomass that remains as a solid residue once the biomass sample has been further heated in an oxidative atmosphere. In biomass, ash is mainly comprised of elements such as potassium, sodium, calcium, phosphorus, magnesium, iron, aluminium, and silicon. The mineral content of the fuel has many ramifications on combustion systems such as lowering the combustion efficiency, and often high ash content results in undesirable fouling within the systems.

The moisture, VM, FC, and ash of a biomass sample can be ascertained by a standard fuel analysis method that is called a proximate analysis. The method can be found both in the British Standard Methods, as well as in the American Standard Methods.

1.4.2 Elemental Content

The elemental composition of a biomass sample can be determined by measurements of the five most common elements present in the fuel which are carbon, hydrogen, oxygen, nitrogen, and sulphur, where the oxygen content is often attained by difference. This measurement is referred to as the ultimate analysis, and is often used to determine the amount of air or oxygen necessary to cleanly combust a given fuel [16].

1.4.3 Energy Content

The energy content of a fuel can either be reported as the calorific value of that fuel (CV) or as the higher heating value (HHV) or lower heating value (LHV). As the carbon content increases, the heating value also increases [4]. The HHV is defined as the potential combustion energy when water vapour from combustion is condensed to recover the latent heat of vaporization. The LHV, on the other hand, is the potential combustion energy when water vapour from combustion is not condensed [17]. The difference between these two values shows the proportionality between the decrease of the heating value of the fuel, and the increase of its moisture content. Sometimes the energy content of a fuel is reported as energy density by volume. In such instances, densified fuels such as pellets will have higher reported energy by volume values than the parent biomass fuel. For example, the UK Biomass Energy Centre lists the energy density for wood chips as 3100 MJ/m^3 where as the energy density of wood pellets rises to 11000 MJ/m^3 [18].

1.5 Biomass Conversion Processes

1.5.1 Physical Conversion and Pre-Treatment

The physical conversion of biomass involves various processing and handling applications to achieve dewatering or drying, size reduction of the biomass fuel, densification and so on. These applications are often vital steps preceding further fuel conversion applications.

1.5.1.1 Dewatering and Drying

Dewatering and drying are rather similar processes that involve the removal of water or moisture from the fuel. Dewatering (for example pressure assisted mechanical dewatering) involves removal of moisture in liquid form, whereas drying, involves moisture removal in its vapour phase. It may be necessary, depending on the moisture content of the fuel and the intended processing application, to remove a certain amount of the moisture from the fuel to ensure that

less energy is consumed by the conversion process than will ultimately be produced. The most economical way of removing moisture from a biomass fuel is through open-air solar drying. Unfortunately, some fuels are not stable enough to withstand solar drying, and have to be dried more quickly with industrial dryers or ovens. Large scale drying applications often involve forced-air furnaces. Sometimes hot stack gases are used to dry moist fuels [4].

1.5.1.2 Size Reduction and Densification

It is often necessary to reduce the physical size of a biomass feedstock or fuel prior to direct fuel use, pellet production, or conversion [4]. Size reduction and densification improves handling and transportation. Size reduction also increases the exposed surface area of the fuel, thereby facilitating drying. End applications such as combustion, gasification, or biological processing, all have different operating parameters that dictate the necessary particle size distributions of the intended biomass fuel. There is a plethora of machinery and many techniques available for fuel size reduction purposes. There are grinders, shredders, impactors, choppers, chippers, crushers and so on [4]. Due to the fibrous nature of biomass, however, size reduction tends to be energy intensive and costly. Often, especially in the case of co-firing with coal, pre-existing machinery, originally designed for coal handling, cannot satisfactorily contend with a high biomass throughput.

1.5.1.3 Torrefaction

The term torrefaction comes from the Latin word torrere which means to roast or scorch. It is a term that was previously associated with coffee roasting. In the context of biomass pre-treatment, torrefaction refers to a mild pyrolysis (see section 1.5.2.2) process operated at a temperature between 200 and 300 °C. Industrial and academic interest in torrefaction has recently gathered much pace. It is seen as a way to improve solid fuel characteristics in terms of increased density, improved grindability, and gain of hydrophobic properties. Torrefied fuel has been shown to outperform wood in terms of higher energy density, improved physical properties, and reduced moisture content. A more detailed review of torrefaction studies is given in Chapters 2 and 6.

1.5.2 Thermochemical Conversion

Biomass can be thermally treated either to directly obtain energy or to make useful intermediate species used in further applications to make products such as biofuels. There are four processes that fall under the category of thermochemical conversion, namely: combustion, pyrolysis, liquefaction, and gasification.

1.5.2.1 Combustion

Combustion is the burning of a fuel that produces heat and light. Complete combustion of biomass involves a rapid chemical reaction between the fuel and oxygen which releases energy and the products carbon dioxide and water. A stoichiometric representation of the combustion of wood, represented by the formula for cellulose, is given in Equation 1.1 below.

$$(C_6H_{10}O_5)_n + 6nO_2 \rightarrow 6nCO_2 + 5nH_2O \quad \text{.....Eq. (1.1)}$$

The combustion process involves the evaporation of the high-energy volatiles that burn in the gas phase with flaming combustion [4]. The lignocellulosic components in the solid fuel then, under high temperatures, decompose and form pyrolysis products which also burn in the gas phase with flaming combustion. What is left is called char and that burns at a slower rate via surface oxidation or glowing combustion. The cellulose and hemicellulose are mostly converted to volatiles (both combustible and non-combustible) and the lignin forms significant amounts of char (around 40%). Combustion occurs in several steps, first the biomass dries when it is exposed to the heat, for example, in a furnace. Once all of the moisture has vaporized, thermal decomposition and devolatilisation begins on the fuel's surface and volatile organic compounds evolve and burn; the remaining carbonatious residue then combusts with the aid of oxygen diffusion to the fuel's solid surface.

The incomplete combustion of biomass can produce large amounts of particulate matter and toxic partially oxidized derivatives. Nitrogen and sulphur, naturally occurring in biomass are oxidized to nitrogen and sulphur oxides, and

various other pollutants (chlorine derivatives, unburned hydrocarbons, trace metal oxides etc) are also formed when incomplete combustion occurs. Therefore, combustion systems should be designed to run as close to complete combustion as possible. It is noteworthy that flyashes form regardless of whether combustion is complete or incomplete.

The combustion of solid fuels has been the centre of extensive research for many decades. A great wealth of information exists on combustion processes available for conversion of biomass to heat, steam, and electric power both for dedicated biomass combustors or for co-firing with fossil fuels such as coal [4]. Combustion remains the leading biomass conversion technology in current use.

1.5.2.2 Pyrolysis

Pyrolysis in biomass can be defined as the direct thermal degradation of the organic components in the absence of oxygen, and yields various useful gas, liquid, and char products. It is the first chemical step in both combustion and gasification [9, 19]. Advanced biomass pyrolysis processes have been developed based on detailed studies of the effects of parameters like biomass feedstock type, composition, residence time, reaction temperatures, the effects of catalysts on reaction rates, product selectivities, product yields, and so on.

The properties that a biomass exhibits during pyrolysis will depend upon the biomass' lignocellulosic components as well as upon extractives and the contained inorganic materials. Detailed discussions of the specific effects of inorganics upon the kinetics of pyrolysis will be discussed in subsequent chapters. A series of reactions, which occur both simultaneously and consecutively, proceed during pyrolysis and yield a large variety of products. Pyrolysis conducted at low temperatures (usually below 300 °C) results in a reduction in molecular weight, the evolution of water, carbon dioxide, carbon monoxide, and the formation of char; this process is known as torrefaction. At higher operating temperatures (300 to 500 °C), the fuel's molecules rapidly depolymerise and form anhydroglucoses that react further and form tars and cracked products. At temperatures above 500 °C, the anhydrosugars undergo significant cracking rearrangement reactions that produce low molecular weight gases and volatiles [20].

1.5.2.3 Gasification

Biomass gasification can be achieved in three ways; through pyrolysis, partial oxidation, or reforming. At sufficiently elevated temperatures, pyrolysis will achieve predominantly gaseous products. Partial oxidation, or starved-oxygen combustion, involves the combustion of biomass at less than stoichiometric concentrations of oxygen. Biomass reforming is gasification in the presence of another reactant. For example, steam reforming, involves the reactions of biomass and steam and of their secondary reaction products [4]. There has been considerable interest in gasification as the syngas produced can not only be used as a fuel itself, but can also undergo further synthesis through catalytic processes into valuable chemicals.

1.6 Concerns Associated with Biomass Studies and Utilization

1.6.1 The Need for Accurate Biomass Thermal Decomposition Kinetics

Several factors influence the performance of large scale industrial applications such as power stations when combusting biomass. These factors include decomposition kinetics, properties of the particles such as the metal contents, biomass particle size, and fuel moisture content. Often there is an economical and environmental play-off between these factors. There has been extensive effort expended on kinetics studies of the thermal decomposition of biomass as it is a major step in biomass combustion [21, 22]. Knowledge of the kinetics of this step is useful in modelling combustion processes and reactor kinetics. Flame ignition, stability, and temperature profiles in the radiant part of furnaces are influenced by the release of volatiles, their quantities and composition. This information is important in burner design in pulverized fuel power stations, where they influence NOx reduction mechanisms. Generally, thermal decomposition kinetics have been studied by slow pyrolysis and assumptions of first order reaction kinetics [23, 24]. A review of biomass decomposition kinetics is presented in Chapters 2 and 3. There

has been, however, little agreement in the literature regarding a systematic way of calculating these kinetics.

1.6.2 Effects of Alkali Metal Content

Plants require certain nutrients for their growth. The primary plant nutrients are nitrogen, phosphorous, and potassium. Other alkali metals, such as sodium, are also present in crops. The metal species in biomass play an important role in combustion applications as their presence could lead to fouling, slagging, and corrosion. As mentioned previously, they also form volatiles that are environmental pollutants. In addition to the release of adverse products, there have been many publications (discussed in Chapters 2, 4, and 5) stating that there is a catalytic effect that alkali metals have on thermochemical conversion processes. Further detailed studies of these catalytic mechanisms and studies on the influence of alkali metals on reaction kinetics would be useful.

1.7 Thesis Outline

This thesis is divided into seven chapters. **Chapter 1** briefly introduces the current situation of energy demand worldwide and touches on environmental issues that are driving political policy in a greener and more sustainable direction. Biomass is introduced as a fuel and described in terms of its main constituents. Conversion technologies are also noted leading into **Chapter 2**, which provides an overview of the research that has been conducted in this area. Chapter 2 terminates with the aims and objectives of the thesis, which arise naturally from the gaps and some of the unanswered topics that have been raised in the research overview.

The first of these topics deals with the kinetics of biomass thermal degradation. **Chapter 3** presents work conducted on the kinetics of the thermal degradation of Short Rotation Coppice (SRC) willow, and examines various well known mathematic methods for the extraction of kinetic parameters.

In **Chapter 4**, the effect of alkali metals (K, Na, Cs) on degradation kinetics is explored. The chapter also includes studies on combustion and single particles burning in a flame.

Chapter 5 utilizes the findings from Chapter 3 of the most appropriate and effective kinetic parameter extraction methods and examines the effects of potassium and sodium on degradation kinetics of slow pyrolysis. A method is developed to predict thermal degradation reaction rates based directly on the concentration of potassium or sodium in the parent biomass. Chemical models are also studied to explore the chemical mechanisms involved.

Chapter 6 is the ultimate experimental section and presents work conducted on the torrefaction of various biomass fuels. The effects of alkali metal removal through chemical fractionation pre-treatment are explored with the aim of ameliorating the ash behaviour of the fuels. The experimental chapters contain their own specific discussion and conclusions sections.

Chapter 7 serves as a concise summary of the findings of this thesis. It also contains some thoughts and recommendations for relevant future research.

Chapter 2
Project Overview

2.1 Overview of Thermal Degradation Kinetics

Combustion technology has been evolving over the last 10 years due to the new availability of foreign coal and also because green policy drivers have lead to the introduction and use of many kinds of biomass [23]. The characterization of alternative fuels has thus become very important. The development of accurate experimental methods to yield pyrolysis and char combustion rates has been the focus of much research. Various methods have been developed for solid fuel characterization which use different heating rates, top temperatures, and naturally yield differing data results. Some of the most common methods include using a drop tube reactor, thermal gravimetric analysis (TGA), differential thermal analysis (DTA), electrically heated wire mesh reactor, and methods involving a pyroprobe [23, 24].

The rate of pyrolysis and of char oxidation or combustion, are quantified by kinetic parameters such as the reaction order (n), the pre-exponential factor (A), sometimes reported as lnA and the apparent activation energy (E). In many instances, a reaction order of 1 is assumed, and only the E and A are calculated [23, 25]. Experimentally derived kinetic parameters also depend upon the particle size, the ambient gas environment, and the presence of mineral matter in the biomass fuel [26, 27].

If there is a range of the experimental data that has constant activation energy, it can be assumed that the reaction process progresses according to the Arrhenius equation. Variations in the activation energy usually involve catalytic effects, pore structure changes and so on. Accurate determination of the activation energy and the pre-exponential factor are vital for successful fuel characterization. For biomass pyrolysis, literature has reported a wide range of apparent activation energies anywhere from 30 to over 200 kJ/mol, calculated for an experimental temperature range from 100 to 1000 °C [23, 26, 28, 29]. A wide range of variation is also seen for the pre-exponential factor values reported in the literature.

2.1.1 Isothermal Versus Pre-Set Heating Rate Experiments

Experimental characterization of reaction rates can be conducted either isothermally, or with a pre-determined heating rate. For isothermal experiments, the fuel sample is kept at a constant temperature while its weight loss is determined as a function of time. This process is repeated over several temperatures in order to determine the activation energy. This applies mostly to TGA instruments. In drop tube reactors, wire mesh reactors, and pyroprobes, it is often assumed that the heating rate is high and that the fuel reaches isothermal temperature in the order of milliseconds or less. As one may expect, this isothermal approach for TGA experiments is time consuming, not only due to the necessity of repetition at various temperatures, but also because the sample must be kept at a certain temperature for prolonged periods of time to achieve a necessary degree of conversion. Furthermore, this method cannot be applied to the entirety of TGA data derived from pyrolysis. In this case, it is possible to heat a sample at a pre-set heating rate and simultaneously measure the mass loss as a function of both time and temperature. Such an approach has the added advantage of convenience and speed.

Once the mass loss with time/temperature data has been acquired, it is necessary to use mathematical procedures to extract the kinetic parameters. It is important to note, that often, these procedures are subjective, in terms of which data is included and what certain parameters (such as terminal mass) are taken to be, and there is no agreed standard procedure. It is possible to get variations in E's and A's even if the same experimental data is considered for a given fuel depending on which mathematical method is used to extract the kinetic parameters [24, 27], and in some cases, depending on the subjective choices made by the researcher. Some kinetic models developed describe biomass thermal degradation as a single step, while others consider the decomposition process as a system of parallel and consecutive reactions [19]. In woody biomass pyrolysis kinetics studies, for example, some authors have described the process as three independent parallel reactions resulting from the thermal decomposition of each of the main components of the parent biomass (cellulose, hemicellulose, and lignin) [19]. Examples and details of such methods are discussed further in Chapter 3.

2.2 Effects of Alkali Metals on Biomass Thermal Degradation

Inorganic species are present in biomass as they are necessary for plant growth. The presence of certain species greatly influences the thermal degradation of the biomass, thus affecting processes such as pyrolysis, combustion, and gasification. This section is meant to function as a brief introduction to this rich topic; Chapters 4 and 5 deal with alkali metals and their effects in more detail.

2.2.1 Catalyzing Thermal Degradation

Alkali metals, in particular, tend to act as catalysts during the thermal degradation reactions of biomass. Potassium can make up a few wt% of the dry fuel and a large fraction of this is retained in the biomass char, and catalyzes the combustion or gasification of the solid residue [30]. Potassium and sodium are two components of plants with a particularly strong influence on pyrolysis [30], as evidenced, for example, by the main peak degradation temperatures (measured with a TGA) being lowered by removing the minerals by either water or a stronger solvent [30-35], and also by lower activation energies [32, 33, 36]. Sometimes it is observed that the activation energies are not higher for samples that have been demineralized, but it is noted that in those cases, the pre-exponential factor is lower and therefore the result is a slower overall rate of reaction [10].

2.2.2 Influencing Product Composition

Published literature has focused on the effects of alkali metal content on char yield and of valuable chemicals from pyrolysis [31]. The inorganic content in a biomass fuel has been shown to cause a change in product distributions; that is the amount of voc (volatile organic compounds)/tar to gas, and char [30, 31]. Experimental work indicates that higher amounts of inorganics cause secondary reactions to occur more readily, breaking down larger molecules to smaller ones [30, 31, 34]. Researchers have discovered that the char yield increases with higher alkali metal concentrations in the fuel [35], while the amount of volatiles released decreases [32]. Also, it has been noted that with the presence of alkali metals, the yield of levoglucosan in pyrolysis products is significantly reduced [31, 34].

2.2.3 Problematic Ash

In combustion, potassium, sodium, and other inorganics such as sulphur and chlorine, influence ash chemistry and change the behaviour of the fuel in terms of its tendency to corrode equipment and cause slagging and fouling [10, 30]. The main causes of these undesirable effects are attributed to the reactions of alkali metals with silica to form alkali silicates which melt or soften at low temperatures (< 700 °C), and the reactions of alkali metals with sulphur which form alkali sulphates on heat transfer and combustor surfaces [10]. A fraction of the alkali metal content in the fuel also enters the vapour phase as chloride, or hydroxide, and these vapours cause fouling in the cooler region of the boiler. A slagging index, originally developed for coal fuels, is sometimes used to rate biomass according to its fouling tendency. The index corresponds to the mass of alkali metals as oxides per energy unit of the fuel [4]. Demineralization of the fuel, by water washing for example, is often a simple and effective method for removing a large fraction of the fuel's mineral content, thereby reducing the above mentioned ash problems [4, 33]. Demineralization and washing techniques and analyses will be discussed further in Chapters 4 and 6 (and briefly touched upon in Chapter 3).

2.3 Torrefaction

There are several drawbacks associated with the use of biomass as a fuel, especially when compared to coal and other fossil fuels. These shortcomings include low bulk densities, high moisture content, and low heating values.

Gaseous and liquid fuels can be easily transported, dispersed, mixed, and regulated. Solid fuels such as coal can be pulverized and aerated causing them to acquire flow properties similar to liquids; though handling fine solid fuels causes problems with erosion and also poses explosion hazards [37]. Unlike coal, biomass' fibrous nature makes size reduction rather difficult and very energy intensive. Approximately 10% of the energy expended on size reduction processes such as grinding or crushing or cutting is actually used to divide the material; the rest is lost as heat [37]. If the energy output, compared to that associated with fossil fuels, is to

remain the same, then the low bulk density and heating values of biomass necessitate larger boilers, and higher volumes of fuel delivery.

The process of torrefaction involves a mild pyrolysis of the fuel operated at a temperature between 200 and 300 °C. Approximately 30% of the biomass fuel's mass is lost upon torrefaction. This mass loss corresponds to only a 10% loss in the energy content of the fuel. There is therefore a net increase in the energy density of the biomass [38]. Torrefaction also removes the majority of the moisture content of the fuel which is valuable since some conversion processes require very low moistures and field drying alone, which leaves approximately 20% of the moisture, is not sufficient [37, 38]. The fuel is also rendered friable which makes it easier to pulverize or grind [38].

The literature on torrefaction agrees that the process occurs between 200 and at most 300 °C [39]. At temperatures higher than 300 °C, there is a risk of runaway exothermic reactions. Torrefaction involves the slow heating of biomass under an inert atmosphere for a given length of time, generally between 15 to 60 minutes. Researchers often report times that the biomass sample has spent at a desired temperature, however total residence time should be considered as the time that the fuel has spent at temperatures above 200 °C.

Below 160 °C, all that is lost from the biomass is its moisture [38]. At this stage, all of its other properties mostly remain unchanged. At temperatures above 180 °C, the biomass starts to appear brown in colour, and loses more moisture along with carbon dioxide, and significant amounts of acetic acid. Some phenols are also lost at this stage. Torrefied biomass loses its hygroscopic nature and also becomes more brittle, allowing for easier grinding compared to untreated biomass fuels [38]. Torrefaction is further discussed in Chapter 6.

2.4 Project Objectives

The work conducted for this thesis mainly deals with topics related to thermal degradation kinetics and the influence of alkali metals on these kinetics, as well as their effects on the applied behaviour of the fuel. Torrefaction is also studied and

linked to the other work not only through kinetics studies, but also in terms of the effects of mineral content.

The first experimental chapter (Chapter 3) aims to answer the following questions: Firstly, what method of data analysis is appropriate for extracting reliable kinetic data from TGA experiments? Secondly, what kinetics are most suitable for high heating rate situations such as present in pulverized fuel power stations?

The aim of the second experimental chapter (Chapter 4) is to investigate the effects of alkali metals (K, Na, Cs) on thermal degradation kinetics; more specifically, it deals with both pyrolysis and combustion, as well as single particle burning in a flame.

The objective of Chapter 5 is to develop a mathematical expression that directly links the inherent alkali metal content of a biomass fuel to its thermal degradation kinetics. This facilitates the prediction of fuel behaviour simply based on its metal content. *Ab initio* (DFT method) modelling is employed to explore the chemical mechanisms involved.

The final experimental chapter (Chapter 6) is concerned with torrefaction. Here, the goal is to study how effective pre-treatment can be in further improving torrefied fuel properties. The work examines the effects of minerals, reduced mineral content, or their absence, on torrefaction, as well as on the combustion and the ash behaviour of the torrefied material.

Chapter 3
Kinetics of the Thermal Degradation of Biomass

Biomass decomposition has been the focus of much academic and industrial attention because it is not only a major step in its combustion [21, 22] but also the key step during thermal processing methods, such as fast pyrolysis for the production of chemicals and bio-oils [40]. An understanding of the kinetics of this step is important in the modelling of both combustion processes and reaction kinetics. The rate of release, the quantity, and the composition of the volatiles influence flame ignition, stability, and the temperature profile in the radiant part of furnaces. These factors impact on NOx reduction mechanisms and are therefore important in pulverized fuel power stations and an understanding of these factors aids in the design of burners and so on. Similarly, in fast pyrolysis, the relative rates of thermal degradation, cracking, and repolymerisation/condensation reactions, influence not only the quantity and quality of the bio oil produced, but also the long-term stability of the oil.

The decomposition of biomass involves a number of simultaneous parallel reactions. The fact that the reactions involve a solid matrix means that heat and mass transfer processes may play an important role, often complicating the interpretation of kinetic analyses [4, 23, 26]. Most studies of thermal decomposition have been made using thermogravimetric analysis (TGA) at relatively slow heating rates, and temperatures up to 900 °C. Consequently, a criticism of TGA is whether the data are directly applicable to most industrial conditions where the heating rates are greater, and, in the case of combustion, the final temperatures can be much higher. Weber has pointed out the difficulty of using TGA derived kinetic data for high temperature situations [23].

A number of studies (using TGA) have examined the nature of the products and their rates of formation, and the rate of reaction of the parent biomass. Various authors have postulated the chemical steps that are involved in the decomposition of the constituents of biomass: cellulose, hemicellulose and lignin. Cellulose pyrolysis,

in particular, has attracted considerable attention, and the rate of reaction has been described as first order [41-45]. Biomass decomposition models have been suggested in which reactions for the three constituents occur simultaneously [46-48], but other evidence has been provided showing that under certain conditions there can be interaction between components [49]. However, in the case of TGA little interaction of components has been observed.

More recently a number of studies have been made at moderately high temperatures and with high heating rates to simulate the conditions pertaining to flash pyrolysis [50, 51]. Few kinetic studies have been made at high temperatures similar to flame conditions, but there are some examples [52, 53]. TGA is by far the most convenient technique for measuring reaction rates, but the issue arises whether it is possible to extrapolate the mechanisms and kinetic data derived at low heating rates and temperatures to high heating rate/temperature situations.

Reaction schemes consisting of multiple reactions are difficult to handle for moderately large organic molecules in the gas phase, and usually reaction scheme reduction systems are used to condense the large reaction mechanisms into more easily manageable systems. Alternatively, experimentally obtained data is used to generate empirical equations. In the case of biomass pyrolysis this latter approach is utilized with schemes that use one, two and up to six first order reactions. Other researchers have utilized the Distributed Activation Energy Model (DAEM) where the reactions are represented by a statistical method. For example, the functional group model, FG-Biomass, developed by Advanced Fuel Research Inc., uses multiple parallel, independent first-order reactions with a gaussian distribution of activation energies [54]. Simplifications of the DAEM have been used by various groups where multiple devolatilisation reactions have been lumped together [29, 48, 55, 56]. These lumped group kinetics give a more detailed insight into the devolatilisation process; however, they come at a greater computational cost [57]. Therefore, it is common for one first order reaction to be used for computational fluid dynamic (CFD) models [58, 59]. If the experimental data is from TGA, or similar studies, there appears to be no consensus or general agreement on which region of experimental data should be considered for kinetic calculations. Also, in the case of multiple first order reaction regions, the selection of the final mass (i.e. mass of reagent), utilized in some first order reaction kinetics calculation models,

can have a significant impact on the determined activation energy and pre-exponential factor values. Although non-linear calculations eliminate the need for final mass allocation, the question remains whether the kinetics should be determined on a global basis or divided into multiple regions. These are a few of the difficulties that have arisen in the way experimental data is interpreted. In addition, such data is frequently obtained using TGA experiments at 300 to 900 °C and then applied in high temperature combustion situations.

This chapter addresses two questions. Firstly, what method of data analysis is appropriate for extracting reliable kinetic data from TGA experiments? Secondly, what kinetics are most suitable for high heating rate situations such as those present in pulverized fuel power stations? It contains kinetic analysis of willow TGA data using a variety of approaches. A review of previously published work on biomass and its polymeric components helps ascertain the variation in kinetics, reasons for differences, and extrapolation to flame temperatures.

3.1 Isothermal Mathematical Kinetic Parameter Determination

Assuming that the fuel devolatilisation (or char combustion reactions) are first order, the rates can be expressed by the following equation:

$$\frac{d\alpha}{dt} = k(1-\alpha) \quad \text{.....Eq. (3.1)}$$

and

$$\alpha = 1 - \frac{m}{m_o} \quad \text{.....Eq. (3.2)}$$

where α represents the reaction progress, varying from 0 to 1, m is the current weight, and m_o is the original weight. k represents the reaction rate constant. As stated earlier, the reaction rate is assumed to follow the Arrhenius function:

$$k = A\exp\left(-\frac{E}{RT}\right) \quad \text{.....Eq. (3.3)}$$

where A and E are the pre-exponential factor and the activation energy, respectively. R is the gas constant and T stand for the temperature. Substituting equation 3.3 into equation 3.1 yields:

$$\frac{d\alpha}{dt} = A(1-\alpha)\exp\left(-\frac{E}{RT}\right) \quad \text{.....Eq. (3.4)}$$

Obtaining A and E is achieved by integrating equation 3.1 with respect to the initial conditions $\alpha = 0$ at $t = 0$ which yields equation 3.5.

$$-\ln(1-\alpha) = kt \quad \text{.....Eq. (3.5)}$$

Therefore, in isothermal experiments, plotting $-\ln(1-\alpha)$ versus t yields k as the slope and then the pre-exponential factor and activation energy can be easily determined from a plot of the following relation:

$$\ln k = \ln A - \frac{E}{R}\frac{1}{T} \quad \text{.....Eq. (3.6)}$$

where the slope is E/R and the pre-exponential factor is found from the intercept lnA.

The accuracy of the kinetic parameters found by this method depends upon the quality of the experimental data and on the value of the correlation coefficient of the plot of lnk versus 1/T from equation 3.6.

3.2 Non-Isothermal Mathematical Kinetic Parameter Determination

This section explains the mathematical kinetic parameter extraction methods that have been explored in this work. They range from simple methods that rely upon linear graphical means for the calculation of kinetic parameters, to more complex methods that employ non-linear regression to derive the desired parameters.

3.2.1 Reaction Rate Constant Method

The Reaction Rate Constant Method [58] is a simple and widely used mathematical method to derive the pre-exponential factor and activation energy based on TGA experiments. Although conducted under non-isothermal conditions, the method relies on the technique described in Section 3.1. If the weight loss with time curve is assumed to be the result of one or more first order reactions, then each reaction can be described by the following relation:

$$k_t = -\frac{1}{(m-m_\infty)}\frac{dm}{dt} \quad \text{.....Eq. (3.7)}$$

It is worth noting that the calculated values of k rely upon a chosen terminal mass, and can deviate greatly depending on what mass value is chosen as terminal (m_∞). Again, evaluation of A and E is straightforward using the relationship expressed in equation 3.6.

3.2.2 Integral methods

In experiments, the pre-determined heating rate (B) is expressed as B = dT/dt. The derivative of the devolatilisation (or char oxidation) rate is expressed as

$$\frac{d\alpha}{dt} = \frac{d\alpha}{dT}\frac{dT}{dt} = B\frac{d\alpha}{dT} \quad \text{.....Eq. (3.8)}$$

Therefore,

$$\frac{d\alpha}{dT} = \frac{A}{B}(1-\alpha)\exp\left(-\frac{E}{RT}\right) \quad \text{.....Eq. (3.9)}$$

If the initial conditions are take to be $\alpha = 0$ at $T=T_0$, then the lower integration limit T_0 of the integral of equation 3.8 can be taken to be zero under the assumption that the reaction does not progress, i.e. α remains zero, until the initial temperature is reached. By letting x = E/RT, the integration of equation 3.9 can be re-written as

$$\ln(1-\alpha) = \frac{AE}{BR}p(x) \quad \text{.....Eq. (3.10)}$$

Many methods have been developed to approximate the integral on the right hand side of equation 3.10, i.e. p(x). It is frequently referred to as either the temperature or the Arrhenius integral. [23]

3.2.2.1 Temperature Integral Approximation by Murray and White

The method of Murray and White, along with the two that follow in sections 3.2.2.2, and 3.2.2.3, provide different approximations to the temperature or Arrhenius integral.

The reactions are assumed to be 1st order. The Murray and White [60] approximation of the temperature integral yields the following relation:

$$\ln\left[\frac{-\ln(1-\alpha)}{T^2}\right] = \ln\left(\frac{AR}{EB}\right) - \frac{E}{RT} \quad \text{.....Eq. (3.11)}$$

where α = 1- m/m_o, m and m_o representing current and original sample weight, respectively, and B is a set heating rate. A plot of $\ln[-\ln(1-\alpha)/T^2]$ versus 1/T will yield the values of A and E from the intercept and the slope.

3.2.2.2 Temperature Integral Approximation by Doyle

Doyle [61] suggested a linear approximation to the temperature integral which yielded the following relation:

$$\ln[-\ln(1-\alpha)] = \ln\left(\frac{AE}{BR}\right) - 1.0518\frac{E}{RT} - 5.33 \quad \text{.....Eq. (3.12)}$$

Again, with a pre-determined heating rate B, A and E can easily be found from the intercept and slope of a plot of the left hand side of Equation 3.12 versus 1/T.

3.2.2.3 Temperature Integral Approximation by Senum and Yang

Senum and Yang approximated the temperature integral as a ratio of two polynomials [23, 62]. Once this ratio approximation is inserted in place of the temperature integral, a non-linear regression is employed to determine the pre-exponential factor and the activation energy. The temperature integral is as follows:

$$p(x) \cong \frac{\exp(-x)}{x^2} \frac{x^4 + 18x^3 + 86x^2 + 96x}{x^4 + 20x^3 + 120x^2 + 240x + 120} \quad \text{.....Eq. (3.13)}$$

where x = E/RT.

3.3 Materials and Sample Preparation

The biomass used for these experiments is Short Rotation Coppice (SRC) willow, obtained from Rural Generations Ltd. in Londonderry, Northern Ireland. The willow was ground and sieved. Only particles between 0.15-0.18 mm were used. Some samples were further demineralized.

3.3.1 SRC Willow Properties

Tables 3.1- 3.3 list the proximate, ultimate, and elemental content of the SRC willow samples studied in this chapter.

Table 3.1 Proximate analysis of (as received) willow [63].

	wt %
Volatile Matter	69.83
Fixed Carbon	17.53
Ash	5.2
Moisture	7.44

Table 3.2 Ultimate analysis of (as received) willow [64].

Carbon (wt %)	Hydrogen (wt %)	Nitrogen (wt %)	Sulphur (wt %)	Oxygen (wt %) (by difference)
51.65	5.84	0.51	<0.2	41.02

Table 3.3 Metal analyses for willow samples after drying at 333K [63].

willow treatment:	Moisture (wt %)	Al (mg/kg)	Ca (mg/kg)	Cd (mg/kg)	Co (mg/kg)	Cr (mg/kg)	Cu (mg/kg)	Fe (mg/kg)	K (mg/kg)	Mg (mg/kg)	Mn (mg/kg)
raw (untreated)	5.89	50	11020	6.35	<0.009	2.50	38.1	137	3770	1350	181
HCl treated	3.75	42	119	<0.005	<0.009	<0.007	<0.045	7.6	<107	5.3	<0.009
potassium impregnated (1 wt% K)	4.80	0.1	19	<0.005	<0.009	<0.007	0.9	6.8	17000	6.5	<0.009

3.3.2 Biomass Demineralization

The demineralisation process involves the use of hydrochloric acid. 10 g of sample was heated in 50 cm^3 of 2.0 M HCl for 6 hours at 333 K. The sample was then removed from the heat source and left for 48 hours. It was then heated again to 333 K for 6 hours. The biomass was then filtered and washed using de-ionized water until the filtrate runs Cl^- free, which was ascertained by the use of a 0.1 M silver nitrate solution.

3.4 Thermogravimetry

The pyrolysis of the SRC willow, both untreated and demineralized, was studied via thermogravimetric analysis (TGA). A Stanton Redcroft Analyzer STA-780 series was used. Samples in the range of 5 mg were heated in a purge of nitrogen at a rate of 25 °C/min to a final temperature of 550 °C. The results were interpreted in a number of ways, described earlier in section 3.2. A typical TGA pyrolysis profile for an untreated SRC willow sample is shown in Figure 3.1, where the mass loss and the first derivative of mass loss are plotted against temperature.

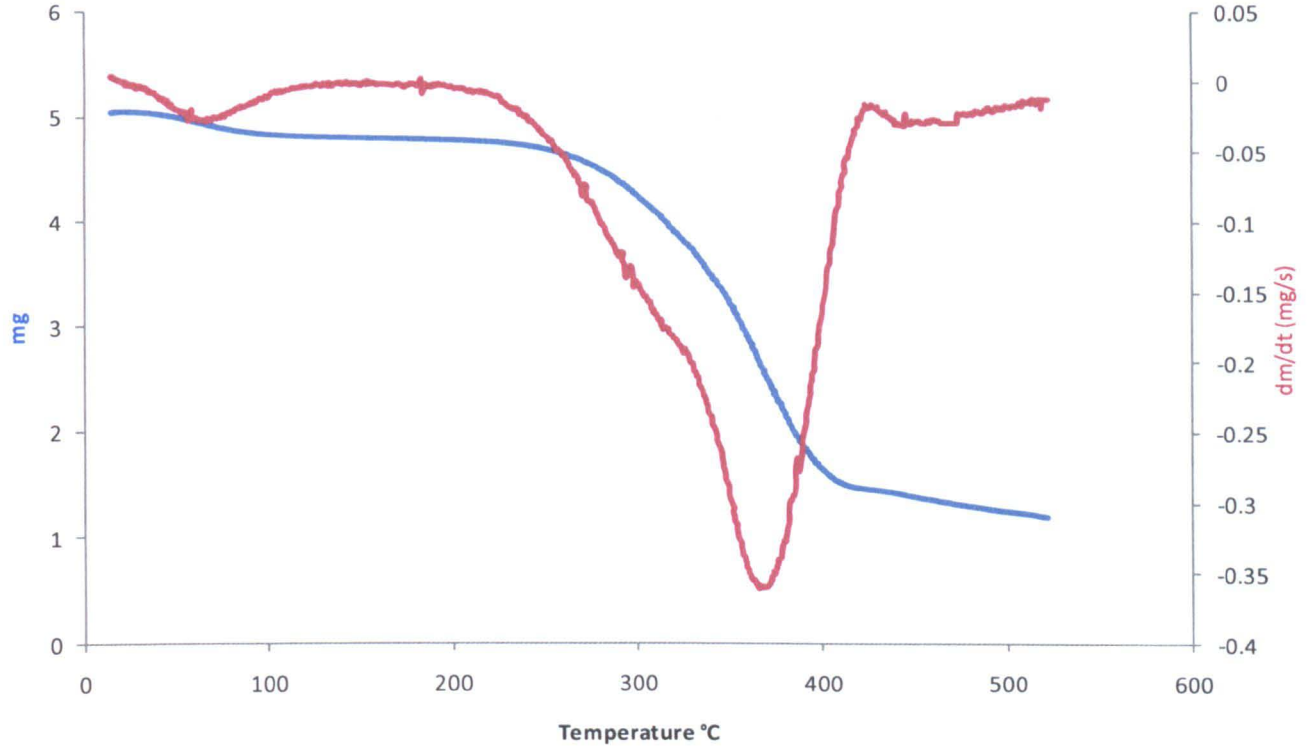

Figure 3.1 TGA pyrolysis profile for untreated SRC willow

The mass loss (TG) curve reveals three stages for this experiment. The first stage, corresponding to temperatures between 25 to 105 °C, is attributed to the loss of moisture from the sample. The next stage, perhaps more easily seen in the first derivative mass loss (DTG) curve in red, is due to the decomposition of hemicellulose and the initial stage of cellulose degradation, and can be seen between 250 to 320 °C in this case. The third stage is linked to the degradation of lignin and the final degradation of cellulose (giving a maximum rate of weight loss at 360 °C). In the case of TGA combustion experiments, the reaction profiles reveal an additional step after the main devolatilisation peak which is attributed to the burnout of char (discussed later in Chapter 4). The DTG profile also reveals useful information regarding the rates of pyrolysis. The positions of the peaks help to illustrate the ease or difficulty of removal of material (the lower the temperature associated with the peak the easier the removal of material). The height of the peaks shows the rates of devolatilisation. The area under the curve indicates the amount of volatiles released. The main peak temperature corresponds to the maximum rate of

volatile release, and is often used as a measure of a fuel's reactivity. It can therefore be utilized as a point of comparison between different fuels.

3.5 Data Interpretation of SRC Willow Pyrolysis

As this section will show, the method of analysis of weight loss data is vital for the extraction of kinetic parameters. Both high and low activation energies can be derived depending on the analytical method used and also on the range of the data selected.

3.5.1 Data Analysis Technique

Microsoft Excel was used for all of the computations involved in deriving kinetic parameters from the methods studied (Reaction Rate Constant, Senum and Yang, Murray and White, Doyle). Of these methods, the Senum and Yang approach is unique in that it requires the use of non-linear regression calculations to determine the activation energy and pre-exponential factor. To this end, the solver function in Excel was utilized. The left hand side (LHS) and right hand side (RHS) of equation 3.10 were defined where A (the pre-exponential factor) and M (M was substituted in place of E/RT) were named as unknowns. A column was created with subsequent values of difference between the LHS and the RHS (for every TGA data point). Then a goal cell was defined for the range of values in the LHS-RHS column and the solver was set to make the value of that goal cell as close to zero as possible by iterative guesses of the values of A and M. The solver ultimately converges on a solution where the values of A and M render the LHS and RHS of equation 3.10 equal.

3.5.2 Data Interpretation According to the Reaction Rate Constant Method

The apparent first-order reaction rate constant method is usually applied to the initial weight loss data generated by TGA pyrolysis or combustion, where the conversion is low and the approximation in equation 3.7 is valid. The conversion

value ranges from 0 to 1 and is defined as the fractional mass loss where at 0, no mass remains, and at 1, all mass remains.

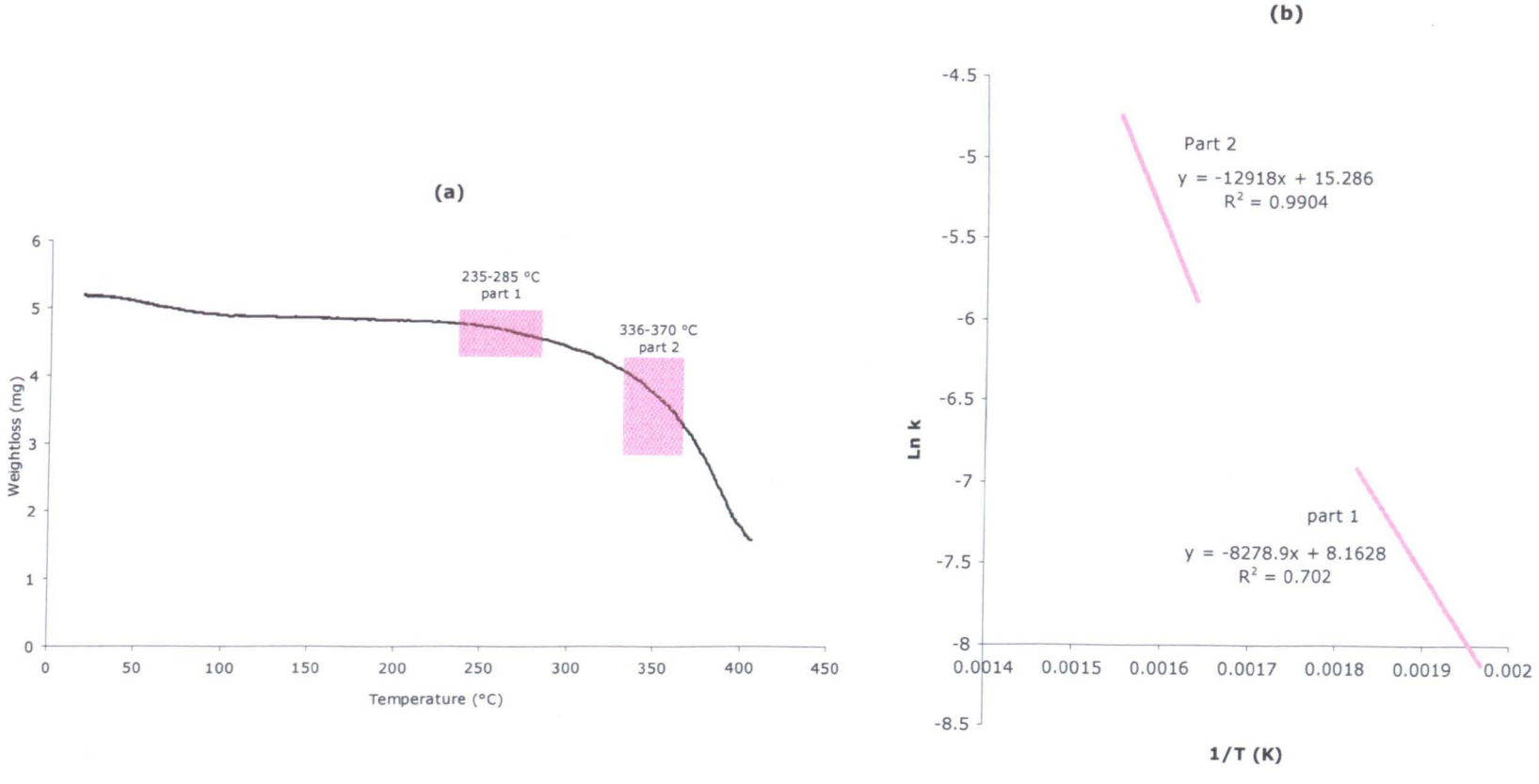

Figure 3.2 a) Pyrolysis weight loss curve for demineralized willow. Heating rate = 25 °C/min. (b) Linear regression curves according to the Reaction Rate Constant method (demineralized willow).

Two regions of the pyrolysis weight loss curve, highlighted in Figure 3.2a, were chosen to evaluate the initial kinetics and to compare the effect of deviation from this initial region on the values of the pre-exponential factor and the activation energy. The region labelled as "part 1" represents a data range corresponding to a 10% weight loss from 90 to 80% of the original mass and is mainly the degradation of hemicellulose. The second region, "part 2," represents a range of data slightly further along in the pyrolysis weight loss curve where 70 to 45% of the original mass remains. This second region was chosen as it includes data for the main decomposition peak. Kinetics were also evaluated on a more global basis encompassing data from both regions.

Linear regression plots, described in equation 3.6, were calculated and are shown in Figure 3.2b. Intuitively, the two regions yielded different pyrolysis kinetic parameter values. For the data range corresponding to part 1, the values for A and E were $3.51 \times 10^3 s^{-1}$ and 68.8 kJ/mol, respectively. For part 2, the pre-exponential factor was $4.35 \times 10^6 s^{-1}$, and the value of the activation energy rose to 107 kJ/mol.

In the more global region considered, the kinetic parameter values were in between those calculated for regions 1 and 3 (Table 3.4). In all cases, the final mass used in the analysis was that remaining at 550 °C, as this temperature is seen as the end of pyrolysis.

As noted above, this method is most valid when a small region of the weight loss curve data is examined. Since biomass is composed of three polymers which degrade over different temperature regions and the rate of mass loss does not remain linear (as can be seen in Figure 3.1), the kinetic parameters derived by this method are strongly dependent upon the weight-loss (α) regions selected.

3.5.3 Data Interpretation According to the Temperature Integral Approximations

The pre-exponential factors and the activation energies were calculated for various parts of the TGA curve with the three methods employing approximations of the temperature integral (Senum and Yang, Murray and White, Doyle), as well as

the reaction rate constant method. The results showed varying values for A and E in both the demineralized and raw willow samples. These results are detailed in Tables 3.4 and 3.5. It is clear that the models used to describe the demineralized sample kinetics can predict activation energies ranging from 44 kJ/mol (low) to over 107 kJ/mol (high), and from 58 kJ/mol (low) to 112 kJ/mol (high) for raw willow. Although there is variation in the kinetic parameters predicted by the different methods, there are similarities in the parameters each method predicts for the two different samples (demineralized and raw willow).

Table 3.4 Pre-exponential factor, activation energy, and variance values for various methods (demineralized willow).

	Senum & Yang	Murray & White	Doyle	Reaction Rate Constant
T range:	235-285 °C	235-285 °C	235-285 °C	235-285 °C
E (kJ/mol)	65	44.3	50.5	68.8
A (s^{-1})	1.28×10^{3}	7.49	9.97×10^{1}	3.51×10^{3}
Variance	1.92×10^{-5}	9.88×10^{-7}	7.98×10^{-3}	1.85×10^{-5}
T range:	336-370 °C	336-370 °C	336-370 °C	336-370 °C
E (kJ/mol)	67.1	63.8	70.5	107.4
A (s^{-1})	1.16×10^{3}	5.08×10^{2}	4.65×10^{3}	4.35×10^{6}
Variance	1.55×10^{-5}	7.63×10^{-6}	3.16×10^{-1}	6.92×10^{-4}
T range:	203-390 °C	203-390 °C	203-390 °C	203-390 °C
E (kJ/mol)	66.9	46.1	51.7	74.1
A (s^{-1})	1.18×10^{3}	1.25×10^{1}	1.70×10^{3}	9.24×10^{3}
Variance	2.38×10^{-4}	5.67×10^{-4}	2.00×10^{-1}	4.88×10^{-4}

Table 3.5 Pre-exponential factor, activation energy, and variance values for various methods (raw willow).

	Senum & Yang	Murray & White	Doyle	Reaction Rate Constant
T range:	235-285 °C	235-285 °C	235-285 °C	235-285 °C
E (kJ/mol)	64.6	61.7	67	74.6
A (s^{-1})	1.00×10^{3}	4.44×10^{2}	3.16×10^{3}	1.50×10^{4}
Variance	2.83×10^{-6}	2.93×10^{-6}	5.04×10^{-3}	5.44×10^{-5}
T range:	336-370 °C	336-370 °C	336-370 °C	336-370 °C
E (kJ/mol)	64.6	57.7	64.6	112
A (s^{-1})	1.00×10^{3}	2.04×10^{2}	2.21×10^{3}	1.61×10^{7}
Variance	4.46×10^{-5}	1.35×10^{-5}	4.59×10^{-1}	1.36×10^{-3}
T range:	203-390 °C	203-390 °C	203-390 °C	203-390 °C
E (kJ/mol)	64.5	60.7	65. 6	73.1
A (s^{-1})	1.01×10^{3}	3.83×10^{2}	2.61×10^{3}	1.03×10^{4}
Variance	3.36×10^{-5}	4.40×10^{-5}	3.43×10^{-1}	3.66×10^{-4}

The pre-exponential factors and activation energies obtained by each method are used in a back-calculation of the weight loss for the particular region considered, and this calculated weight loss is compared to the experimental data, to see how well the methods perform. The variance of each method from experimental values (for the three TGA weight loss regions examined) is listed in Tables 3.4 and 3.5 and is further illustrated in Figures 3.6 and 3.7. The reaction rate constant method, and the approximations by Murray and White and by Doyle, all rely on linear regression and are commonly employed for the derivation of kinetic parameters for smaller initial

ranges of weight loss data. Of these methods using linear regression, the reaction rate constant method is the only one requiring a selection of the appropriate terminal mass for its calculations. Although the two approximations eliminate the risk of error introduced by the potential erroneous selection of a terminal mass, the variance obtained by comparing the weight loss values derived from the predicted A and E values and the experimental weight loss data, listed in Tables 3.4 and 3.5, clearly shows that the reaction rate constant method is indeed reliable if care is taken in choosing the appropriate terminal mass for the weight loss region considered.

The Senum and Yang approximation is unique in that it employs non-linear regression and is thus generally much more accurate than the other methods considered in this work, and is also capable of application to wider ranges of the TGA data while maintaining this accuracy. The choice of weight loss region incorporated in the calculations, however, remains critical for meaningful kinetics, since TGA experiments can become mass transfer limited at high degrees of conversion.

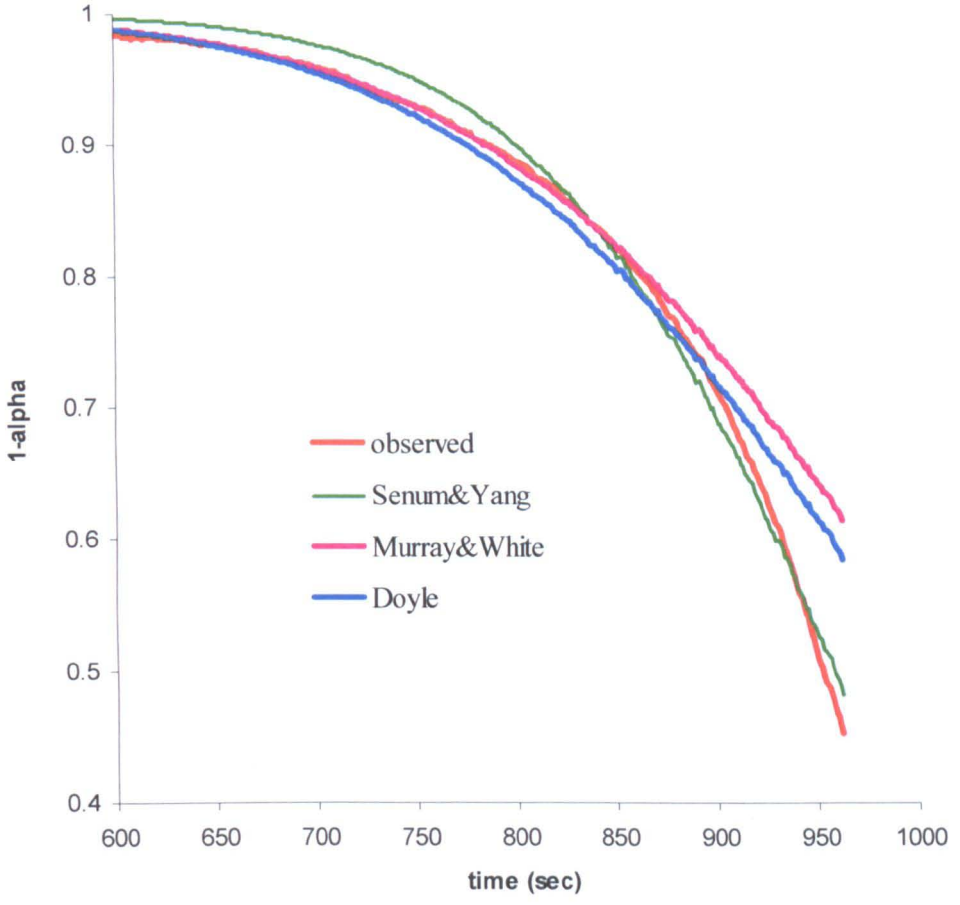

Figure 3.3 Weight loss data comparing various temperature integral approximation methods to experimental data for the 203-390 °C region (demineralized willow).

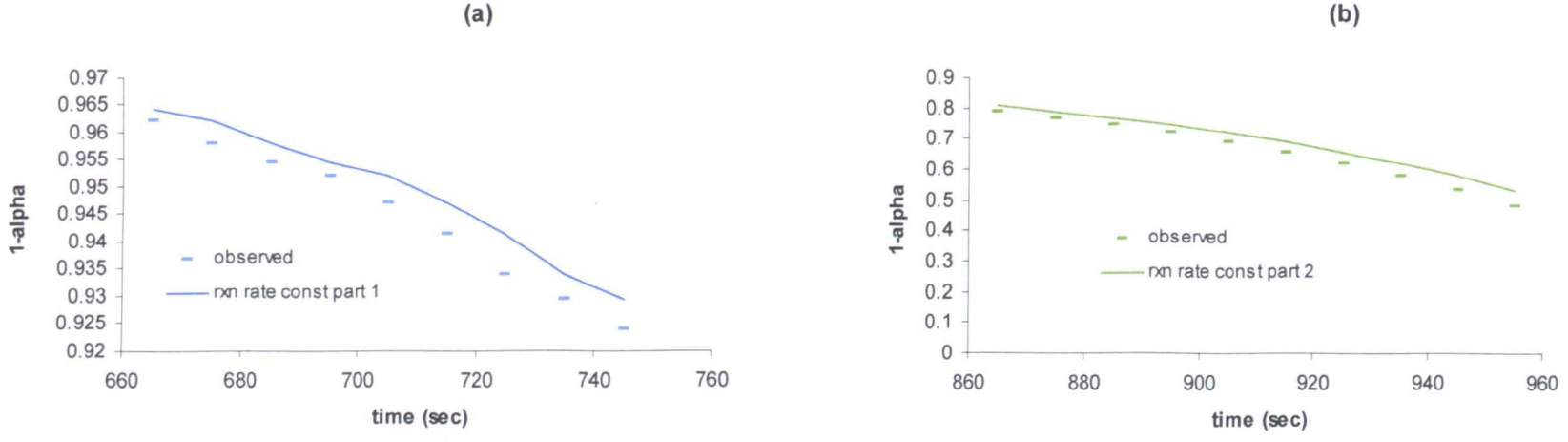

Figure 3.4 (a) Weight loss data comparing the Reaction Rate Constant method (part 1) to experimental data (demineralized willow). (b) Weight loss data comparing the Reaction Rate Constant method (part 2) to experimental data (demineralized willow).

Based on the fit of modelled versus actual weight loss, it is evident from Figure 3.3 that the Senum and Yang approximation is the most accurate of the considered methods on a global basis, predicting the activation energy to be in the region of 65 kJ/mol (low) with a pre-exponential factor on the order of 1 x 10^3 s^{-1} (raw willow). The Reaction Rate Constant method gives a respectable accuracy compared to the Senum and Yang approximation, predicting slightly higher activation energies of 75 kJ/mol (part 1), 112 kJ/mol (part 2) and 73 kJ/mol (global) and corresponding pre-exponential factors of 1.50 x 10^4, 1.61 x10^7 and 1.03x10^4 s^{-1}, respectively.

It is evident from these experiments and calculations, that of the methods studied, the Senum and Yang, Murray and White, and the Reaction Rate Constant Method are yielding kinetics which describe the initial pyrolysis of willow more accurately, but which suggest a low activation energy is appropriate (less than 80 kJ/mol in this case). The literature has reported both high and low activation energies for biomass and model compound pyrolysis. A review of these findings follows in section 3.6. It is intriguing that the same experimental data can yield different kinetic parameters depending upon the method used to extract them, and this may partly explain the wide variation of values reported in the literature. The kinetics most appropriate under flame conditions is of some interest to industrial design applications. A similar deliberation regarding coal pyrolysis kinetics occurred in the late 1900's and therefore similarities can be drawn, as discussed next.

3.6 Kinetics of Solid Fuels, Past Studies

Coal pyrolysis has been investigated at length and debated, particularly during the 30 years between 1970 – 2000. Since the 1990s, pyrolysis research has extended in earnest to biomass. Literature shows a wide scatter amongst the values derived for apparent first order kinetics, with similar fuels giving both high and low activation energies. The variation in coal pyrolysis rates was highlighted by

Solomon and Serio [65] and can be demonstrated on an Arrhenius plot in Figure 3.5, where the curve labels are in keeping with the publication by Solomon and Serio. Figure 3.6 gives a similar plot for apparent first order rates for pyrolysis of woody biomass, detailed in Table 3.3. Some of the curves in this figure were generated by TGA experiments while others have been generated by DFT, and various types of biomass are represented. The highlighted oval in Figure 3.6 shows the region of the curves generated by the present work on both demineralized and raw (or untreated) SRC willow.

These figures better portray what was stated earlier, that for both coal and biomass, "low" or "high" activation energies have been reported. If low activation energies are used in predictive modelling, then the decomposition rate becomes significant at lower temperatures compared to if a high activation energy is used.

In the past, the major application for these kinetics has been for modelling coal gasification at temperatures around 1000 °C and for coal combustion at higher temperatures where the coal particle devolatilises at temperatures of 500 to 1000 °C. A variety of kinetic parameter values have been used, and since the key temperature range is about 600-700 °C (for short residence times), the choice of these value has not been critical since most curves cross at about that temperature (see Figure 3.5).

Much effort has been expended on coal pyrolysis using TGA, wire mesh reactors, and drop tube furnaces, and it has been suggested that wide variations in the pyrolysis rates can arise due to the uncertainty in particle temperatures in the latter two cases . During coal pyrolysis, many simultaneous reactions occur which involve different kinetics. In addition to fragmentation and depolymerisation of the coal structure, char generation due to cross-linking also occurs. If fragmentation reactions are solely considered, then higher activation energies would be expected. However, if all these reactions are lumped together in an apparent first order reaction, lower activation energy ranges are derived. Also, if mass transport limitations are involved, then this would lower the apparent overall rate.

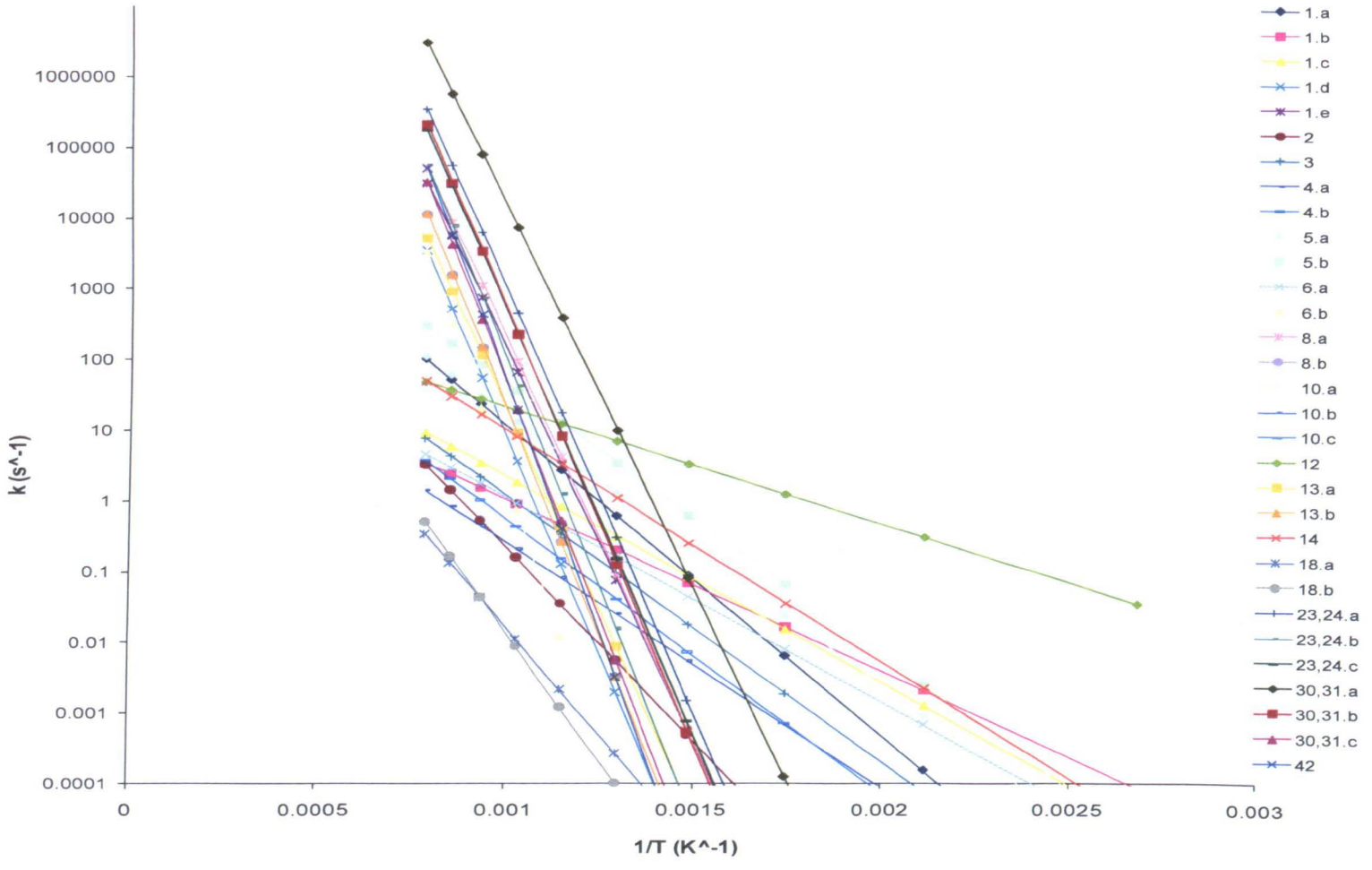

Figure 3.5 Comparison of apparent first order rate constants for coal pyrolysis (the numbers in the legend refer to references cited in Solomon and Serio [65].

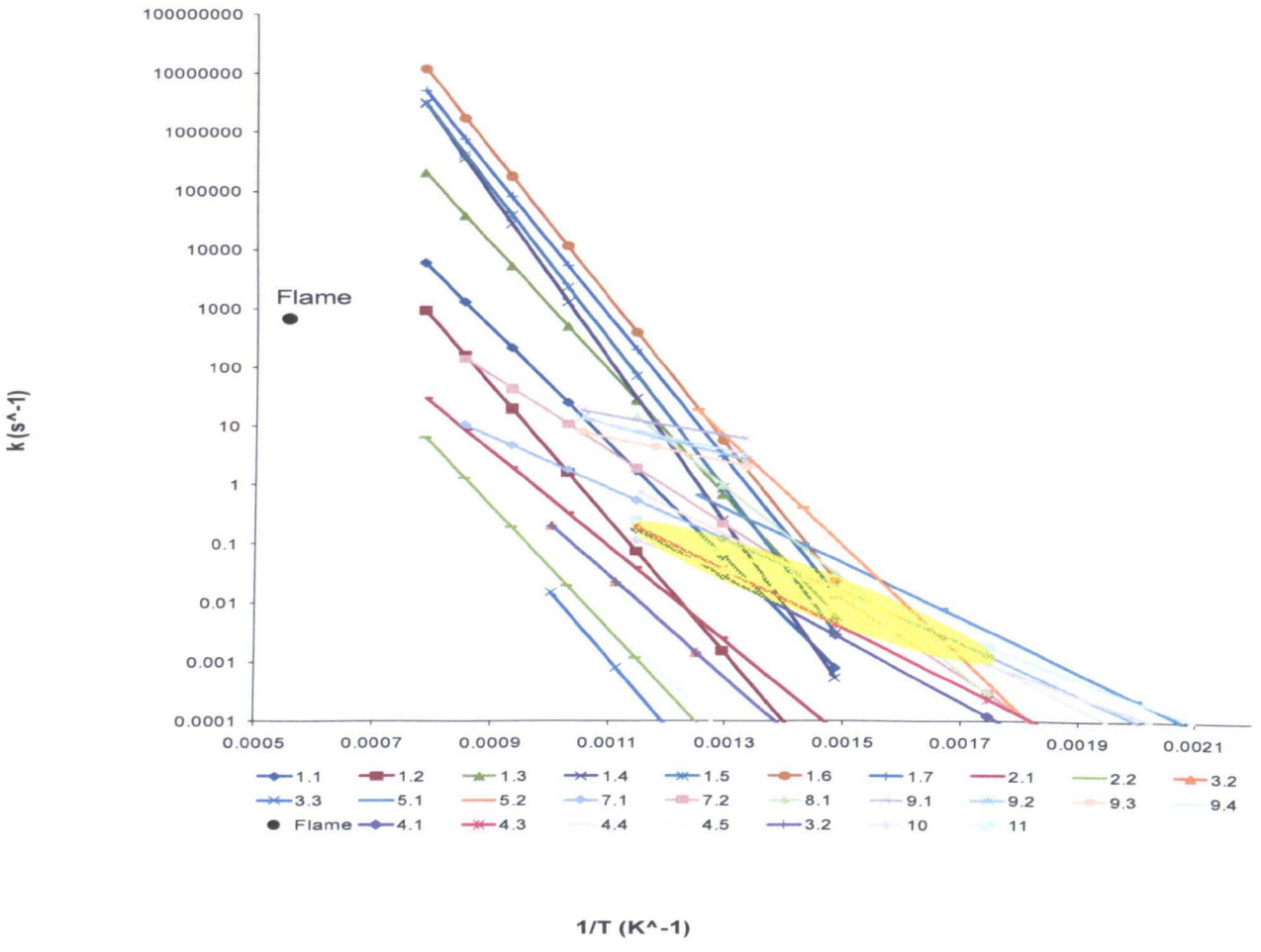

Figure 3.6 Comparison of apparent first order rate constants for biomass where solid lines represent pure species, and the oval highlights the curves (10, 11) generated by this present work (demineralized willow).

Table 3.6 Details accompanying curves in Figure 3.6 "comparison of kinetic rates for biomass".

Reference	Curve Number	Biomass	Particle Size	Heating Rate	Pre-exponential factor A (1/sec)	Activation Energy E (kJ/mol)
[25] (Table 3)	1.1	xylan	~40 μm	20 °C/min	3.18×10^{11}	188
[25](Table 3)	1.2	xylan	~40 μm	20 °C/min	8.38×10^{11}	218
[25](Table 3)	1.3	xylan	~40 μm	20 °C/min	5.95×10^{13}	206
[25](Table 3)	1.4	xylan	~40 μm	20 °C/min	2.93×10^{17}	267
[25](Table 3)	1.5	xylan	~40 μm	20 °C/min	3.95×10^{16}	246
[25](Table 3)	1.6	xylan	~40 μm	20 °C/min	7.16×10^{16}	238
[25](Table 3)	1.7	xylan	~40 μm	20 °C/min	2.09×10^{16}	234
[58](Table 4)	2.1	cellulose	N.A.	variable	6.53×10^{7}	154
[58](Table 4)	2.2	hemicellulose	N.A.	variable	9.71×10^{8}	199
[59](Table 4)	3.2	water washed rice hulls (2nd lump)	1-2 mg piece	3,10,30,60,100 K/min	8.81×10^{7}	165
[59](Table 4)	3.3	water washed rice hulls (3nd lump)	1-2 mg piece	3,10,30,60,100 K/min	2.92×10^{9}	216
[30](Table 5)	4.1	Scots pine (hemicelluloses 1)	<250 μm	10°C/min	1.98×10^{5}	101
[30](Table 5)	4.2	Scots pine (hemicelluloses 2)	<250 μm	10°C/min	7.16×10^{10}	262

[30](Table 5)	4.3	Scots pine (Lignin)	<250 μm	10°C/min	7.27×10^4	93
[30](Table 5)	4.4	Scots pine (cellulose 1)	<250 μm	10°C/min	2.95×10^5	93
[30](Table 5)	4.5	Scots pine (cellulose 2)	<250 μm	10°C/min	1.19×10^8	181
[60](Table 4)	5.1	raw willow	0.15-0.18 mm	25 K/min	4.56×10^5	89
[60](Table 4)	5.2	demineralized willow	0.15-0.18 mm	25 K/min	8.75×10^{12}	178.4
[52](Table 1)	7.1	raw willow	< 2.0 mm	25°C/min	5.99×10^4	84
[52](Table 1)	7.2	demineralized willow	< 2.0 mm	25°C/min	3.98×10^7	122
[61]	8.1	pine wood sawdust	100-212 μm	drop tube set at 380 °C	1.4×10^{10}	150
[49](Table 4)	9.1	wheat straw	50-70μm	104 K/s	1.05×10^3	31.7
[49](Table 4)	9.2	coconut shell	50-70μm	104 K/s	6.84×10^3	48.7
[49](Table 4)	9.3	rice husk	50-70μm	104 K/s	1.19×10^3	39.3
[49](Table 4)	9.4	cotton stalk	50-70μm	104 K/s	2.44×10^3	40.8

present work (Senum model)	10	Demineralized willow	0.15-0.18 mm	25°C/min	1.18×10^3	66.9
present work (rxn rate const model)	11	Demineralized willow	0.15-0.18 mm	25°C/min	3.51×10^3	68.8

A comparison of Figures 3.5 and 3.6, shows similarities in the variation of kinetics between coal and biomass. Closer inspection of Figure 3.6 and Table 3.3 reveals that very high activation energies are reported for the pure components, cellulose, and hemicellulose (or xylan). Lower values are reported for different biomass samples, again, due in part to the natural occurrence of metals such as potassium, which, as stated earlier, is a well known catalyst in thermal conversion.

When cellulose pyrolyses, a single dominant pathway is likely, and high activation energies have been measured for TGA experiments of this single pure compound. When biomass is considered on the whole, the three main polymers decompose in overlapping temperature regions, hemicellulose in the range of 423-623 K, cellulose in the range of 548-623 K, and lignin in the range of 523-773 K [63]. There are some contradictory studies as to whether these polymers can be considered to decompose independently, or whether there is some measurable interaction (synergy) between them. TGA experiments have generally suggested an additive behaviour when mixtures of the polymeric components in biomass have been studied [66]. Some authors have attempted to de-convolute the TGA weight loss curves to extract apparent first order kinetics for each of the individual lignocellulosic components [31, 67], and in these cases, high activation energies also dominate. Similarly, the functional group approach to biomass pyrolysis kinetics (the FG-BioMass model [54, 68, 69]) yields multiple simultaneous first order rates for various products. In this case, the pre-exponential factor constant is fixed at a suitable value and the activation energy extracted. The choice of high pre-exponential factor will be discussed later.

3.7 Discussion

Figure 3.6 presents a compilation of the available kinetic data for the pyrolysis of biomass, mainly wood or related materials, and the lignocellulosic model compounds. There is a wide range of the kinetic constants reported, and a similar variation is observed for coal. As coal has been studied for many more years, there exists already extensive discussion regarding this matter. Much of the variation observed for coal was attributed to different techniques, heating rates, and transport

limitations, rather than specifically assigned to different coal types. It is therefore natural to wonder whether there are differences in kinetics for different classes of biomass components, as has been suggested by various researchers.

Both Figure 3.6, and Table 3.3 show that pure compounds have high activation energies. During the decomposition of biomass, the fundamental reactions involve the decomposition of the biopolymers. For the case of cellulose, this is well-studied and the reaction involves an initial decrease in the degree of polymerization followed by hydrolysis reactions. Further decomposition cracks open monomer units to form gases and vapours. Decomposition of oxygenated heterocycles has been studied in a high temperature shock tube [70] and first order rate constants yield activation energies in the range 200-430 kJ/mol depending upon the reaction products, with corresponding pre-exponential factor values ranging from 10^{12}-10^{20} s^{-1}. Thus, for the model compound studies conducted in a TGA it is reasonable to expect a dominant reaction pathway with a high associated E and a high A for the first order kinetics. Similarly, in the functional group approach, or when TGA data is interpreted as the sum of its individual components i.e. cellulose, hemicellulose and lignin decomposing independently, high activation energies may be extracted.

A second question arising regarding biomass is whether different chemistry is applicable to the different reaction conditions or applications. The applications relate to slow pyrolysis (TGA), flash pyrolysis, and to flame studies; the rate constants deduced from these observations, detailed in Table 3.3 along with the heating rates and final temperatures that were involved in the measurements, are included in Figure 3.6. Figure 3.7 compares the predicted conversions with temperature for a heating rate of 25 K/min (i.e. typical TGA conditions) for the raw, or untreated willow fuel used in this thesis. The first order reaction kinetic parameters that were used to calculate these conversions were discussed earlier in Section 3.5 and are listed in Table 3.2. Here, conversion is defined as fractional volatile loss where 1 is no volatiles released and 0 is release of all volatiles. As discussed earlier, first order kinetics derived via the Senum and Yang, Murray and White, or the Reaction Rate Constant approach (global) give the best prediction of the slow pyrolysis reaction. These approaches have yielded low activation energies for willow pyrolysis (60.7-73.1 kJ/mol). It is probable that when biomass is studied under TGA conditions of

low temperature and heating rate, a large number of secondary reactions of cracking and cross-linking proceed, and the result is low E and A values for the apparent first order rate. The Reaction rate constant approach applied to "part 2" (E = 112 kJ/mol) also fits well over the whole data range, but "part 1" kinetics are too slow when extrapolated over the whole curve. FG-BioMass, which is validated via TGA experiments using multiple first order steps gives an excellent fit to the experimental data. The very low E kinetic data (9.2) is too fast at low temperature/heating rate to predict the decomposition well.

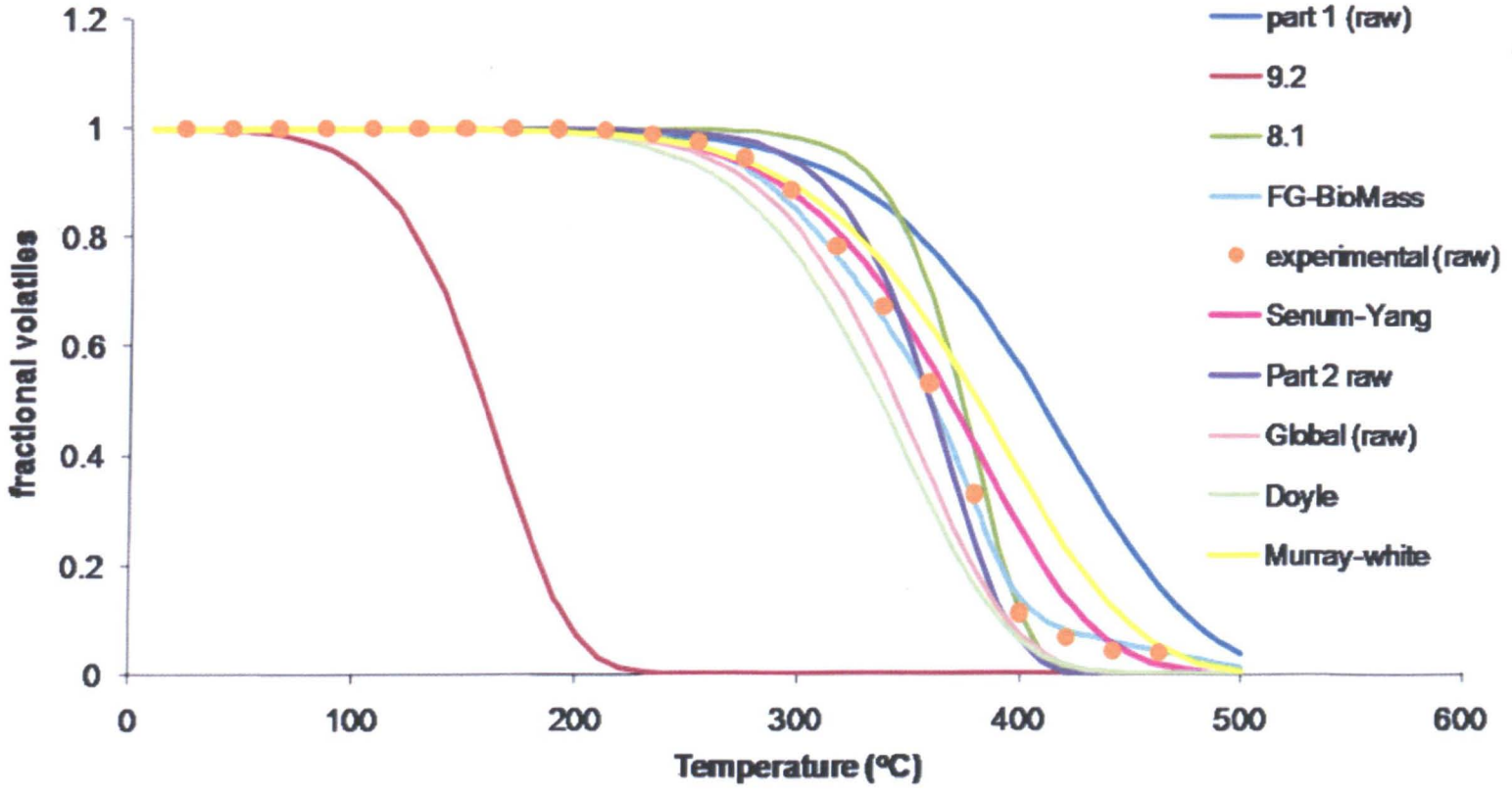

Figure 3.7 Predicted conversion with temperature (at a low heating rate) for raw willow using different apparent first order kinetics, as listed in Tables 3.4-3.6.

In flash pyrolysis, the typical temperature is 500 °C, and particles heat rapidly so that residence times are approximately 1 second. Under these conditions, secondary cracking reactions are minimized. Figure 3.8 shows the calculated conversions assuming no mass transfer limitations, using the kinetics reported here and by other workers, and assuming a heating rate of 10^3 K/s. Under these conditions it is expected that the reactions occurring will be simpler, and primary cracking pathways will be dominant, thus high values of E and A would be expected to predict the conversions well. From Figure 3.8 it is seen that high values of E and A (FG-BioMass) predict significant conversions under fast pyrolysis conditions (71% conversion). The DTR (Drop Tube Reactor) rates reported by Wagenaar (8.1, high E and high A) also predict reasonable conversions (42% conversion), but most of the apparent first order global TGA rates (low E) are too slow to predict conversion well (as are the low E, low A, DTR rates (not shown)). Curve 9.2, however, which was generated from kinetics measured during fast pyrolysis experiments of coconut shell, also gives good predictions of conversion. This can be explained by examination of Figure 3.6. The data for curves 9.1 - 9.4 predict reaction rate constants equivalent to those predicted for high E curves (1.3 - 1.7) due to the compensation effect. That is to say, this data will work well in the range of temperature under which it was derived experimentally.

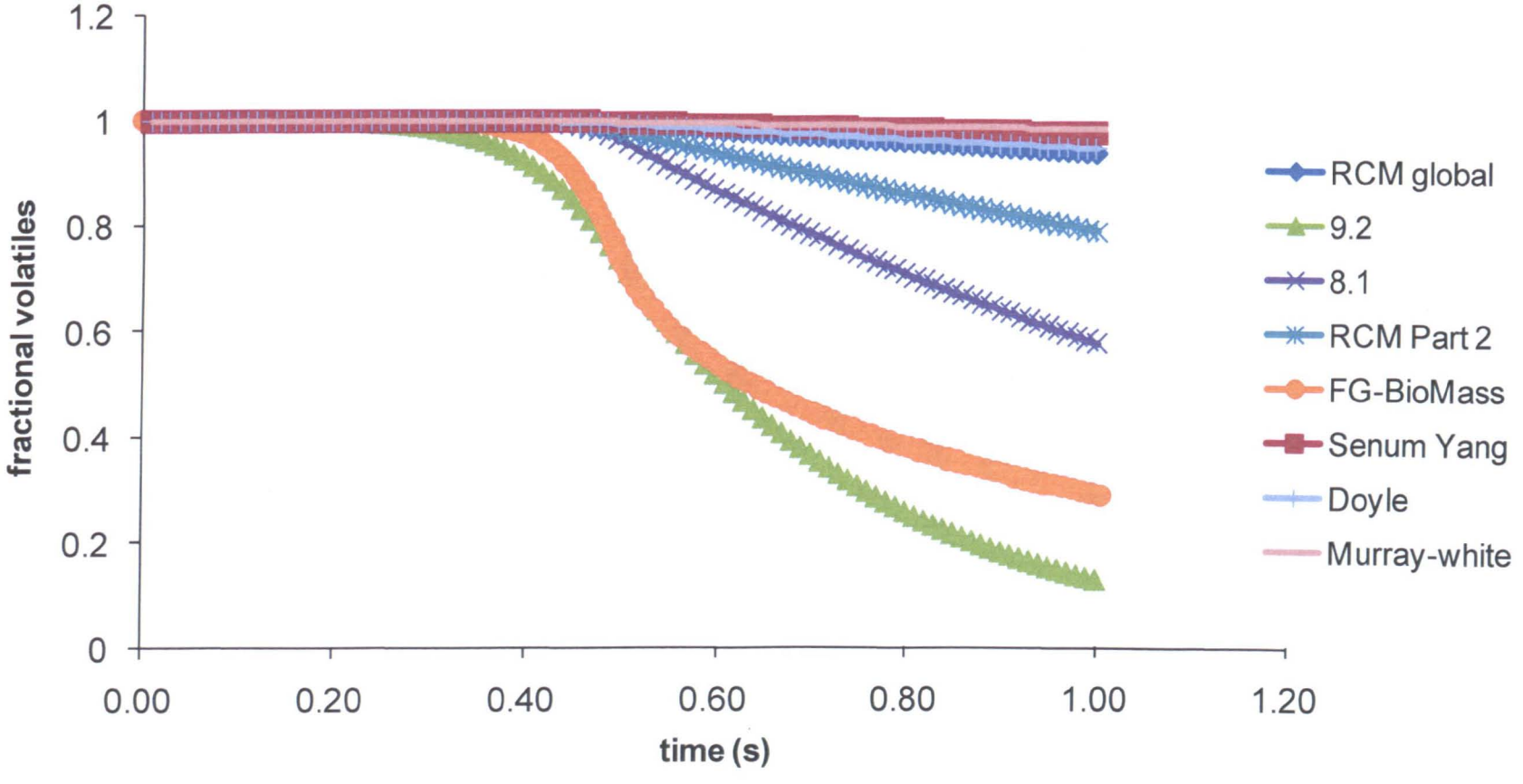

Figure 3.8 Predicted conversion for 10^3 K/s to 500 °C, 1 s residence time.

Figures 3.9 and 3.10 give similar results for conversion with residence time in a typical flame of temperature 1500 °C. Since residence time is short and heating rate is rapid (10^4 -10^5 K/s), it is expected here (as for the fast pyrolysis case) that primary cracking pathways will be dominant, and thus high values of E and A would be expected to predict conversions well. There have been very few studies of devolatilisation rates of biomass in flame conditions [71, 72], but for willow typical durations of devolatilisation are 10-40 ms for 2-4 mm particles entrained into a flat-flame methane-air burner. Figure 3.9 shows that if the heating rate is 10^4 K/s to 1500 °C, then all the rates are too slow (where particle devolatilisation is taking >80 ms) to predict accurate conversion (although FG-Biomass and 8.1 are the closest). If the heating rate is 10^5 K/s to 1500 °C, as in Figure 3.10, then there is a compensation effect and many rate parameters predict conversions within experimental error. The high E (8.1) or multiple reactions approach (FG-BioMass), each are predicting conversion in less than 10-15 ms. Since some compensation effect is seen, lower E kinetics (such as Rate Constant Method (RCM) global (E = 74.6 kJ/mol) and even curve 9.2 (E = 48.7 kJ/mol, but derived from 10^4 K/s heating rate experiments) are predicting conversions in timescales comparable to that seen experimentally (i.e. between 10-40 ms). The Senum-Yang rate and the Doyle rate, with low E and low A values are too slow at these heating rates to predict conversion correctly.

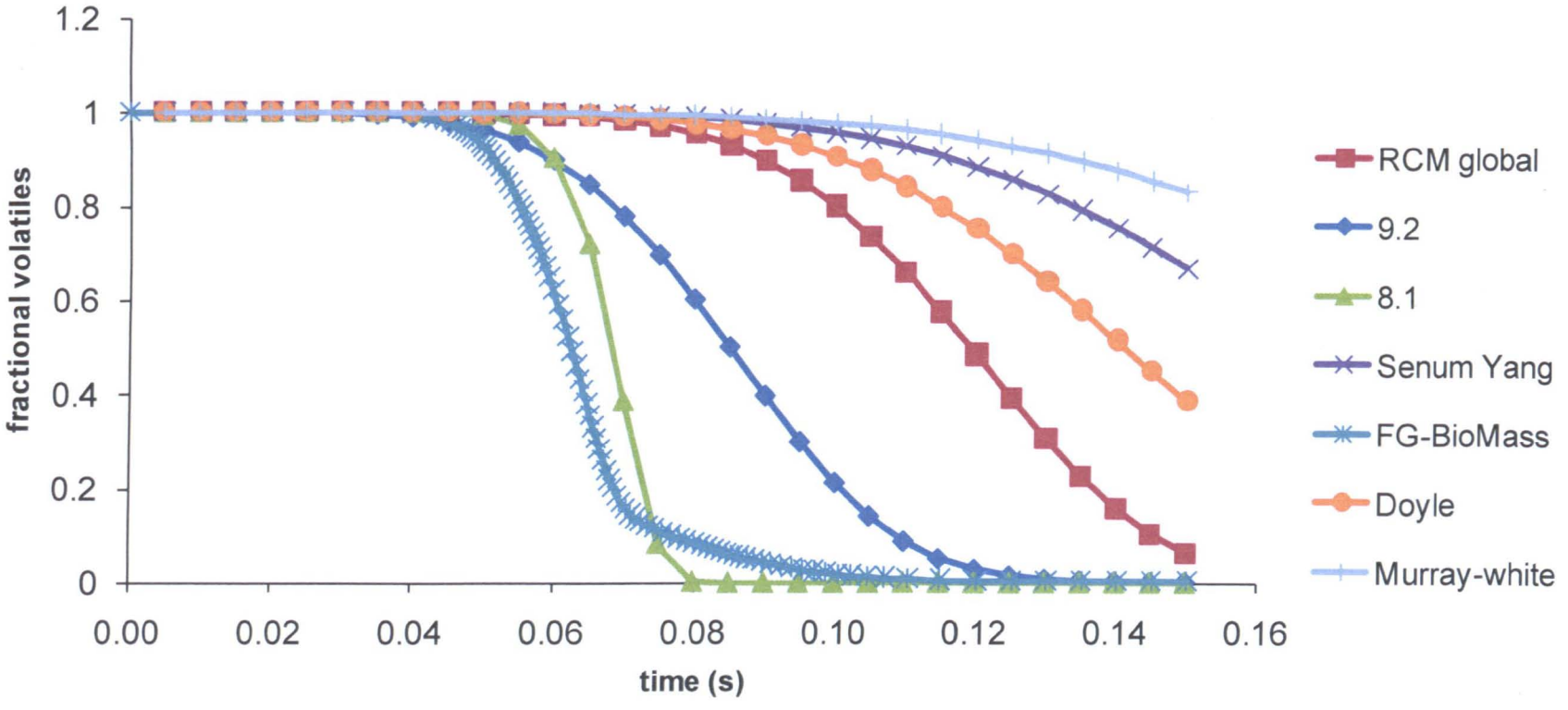

Figure 3. 9 Predicted conversion for 10^4 K/s to 1500 °C.

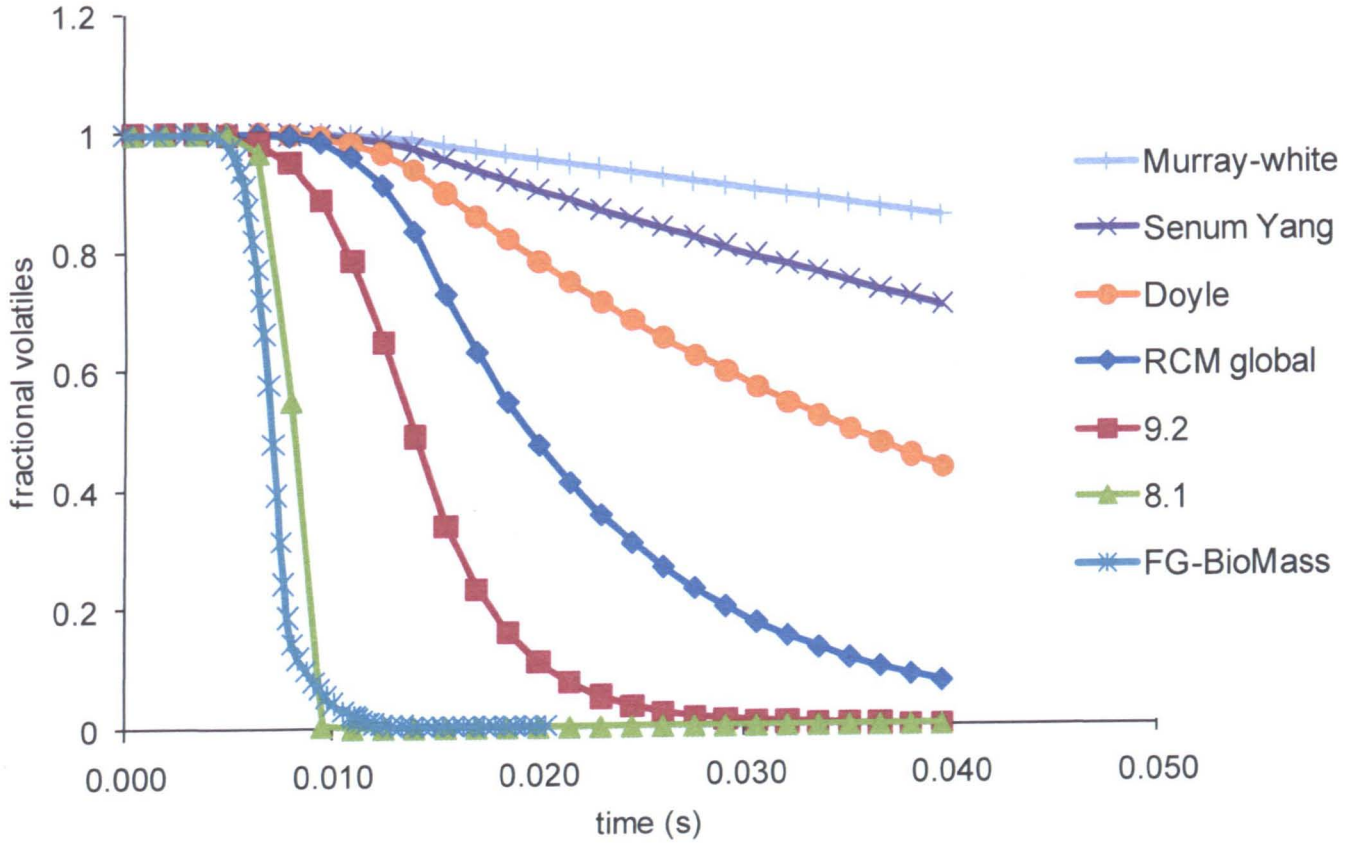

Figure 3.10 Predicted conversion for 10^5 K/s to 1500 °C.

3.8 Conclusions

In this work, different approaches have been analyzed for deriving apparent first order kinetics from TGA data of biomass pyrolysis. In addition, kinetic data from the literature has been compiled and compared. The data falls into two main categories: (1) Very high E and A values (> 100 and up to 270 kJ/mol, and up to 10^{17} s^{-1}) derived when model biomass components are studied, e.g. cellulose; or the data is interpreted as the sum of a number individual first order reactions, e.g. FG-BioMass; (2) Intermediate and Low E and A values (50-100 kJ/mol and <~ 10^5 s^{-1}) derived using a number of global approaches.

Of the global methods tested the "Senum-Yang" approach, the "Murray and White", and also the Reaction Rate Constant Method give apparent first order kinetics which give excellent predictions of pyrolysis under conditions of low heating rate. As might be expected, FG-BioMass also gives excellent predictions. For higher heating rates, such as those encountered in fast pyrolysis, those kinetics expressions with high E and A values typically give reasonable predictions of conversion. It is thought that under these conditions, the residence time is too short for secondary reactions and hence the kinetics are best described by the high E's and A's of primary cracking reactions.

The same is true under flame conditions of even higher theoretical heating rates (10^4 – 10^5 K/s); kinetics described by high E's and A's (typically E = 178.75 kJ/mol, A = 2.2 x 10^{13} s^{-1}) give rapid conversion of the correct magnitude to those seen experimentally. At very high heating rates (10^5 K/s) some compensation on the rates is observed, so that there is a greater range of kinetic parameters which give reasonable conversion rates. FG-BioMass and high E rates predict conversion in the order of 10 ms, while the Reaction Rate Constant method (global) predicts conversion in the order of 40 ms; both are within the range observed experimentally (10-40 ms for volatile combustion). Some kinetic approaches (e.g. Senum-Yang) still yield parameters which under predict the conversion at these heating rates.

In summary, "lumped" or detailed kinetics such as FG-Biomass (typically E = 178.75 kJ/mol, A = 2.2 x 10^{13} s^{-1}) give good predictions of conversions over a wide range of heating rates and temperatures (10 K/min – 10^5 K/s and 327 - 1500 °C). Rate parameters with low E values but measured under high heating rate conditions e.g. 10^3 or 10^4 K/s drop tube studies at 500 °C (typically E = 48.7 kJ/mol, A = 6.84 x 10^3 s^{-1}) give good predictions for modelling over the validated range and some extrapolation to higher temperature is possible because there is a compensation effect. High temperature, high heating rate modelling (10^5 K/s, 1500 °C, 1bar) is more forgiving of the rates used, than is low temperature (500 °C) high heating rate modelling. For 10^5 K/s, 1500 °C, 1bar, E = 178.75 kJ/mol, A = 2.2 x 10^{13} s^{-1} (FG-Biomass) or E = 73.1 kJ/mol, A = 1.03 x 10^4 s^{-1} (RCM global) will both predict conversions within experimental timescales. Whilst these results have discussed kinetics of one particular biomass, willow, the conclusions are equally applicable to similar woody biomass.

Chapter 4
Role of Alkali Metals in Biomass Pyrolysis and Combustion

4.1 Introduction

Alkali metals have a profound impact on the thermal reactions of biomass [73]. Some inherent alkali metals in biomass have been investigated in some detail, particularly for their effect on pyrolysis of lignocellulose biopolymers, and in carbon gasification reactions. A catalytic effect is evidenced by increased char formation, and gas/light volatiles being favoured over tar. The mechanism proposed for the catalyzed decomposition of cellulose involves heterolytic ring opening, rearrangement and cracking reactions [74]. This mechanism is usually written as a base-catalyzed process; therefore the exceptional impact of the alkali metals is still intriguing. The influence is further complicated by the fact that these metals are volatile under combustion conditions and hence concentrations in the fuel are in flux [72].

Previous research has shown that alkali metals present in biomass influence the rates of release and yields of various species during thermochemical conversion [72]. The effect of potassium in biomass thermochemical conversion has specifically been investigated. During pyrolysis, the presence of potassium increases the rate of decomposition, the gas and char yields, and decreases the tar products. Similarly, during combustion, the presence of potassium leads to higher conversion efficiencies. Potassium also changes product distributions which is indicative of a change in the reaction mechanism [35, 72, 73, 75]. This chapter details preliminary fundamental work on alkali metals (sodium, potassium, and cesium) to determine if group chemistry has an effect upon the catalytic process observed in SRC Willow thermal degradation. The same ratio of moles of metal to grams of biomass was used. The work deals with both pyrolysis and combustion, conducted under low heating rates with the use of thermogravimetric studies, and also investigates group effects under flame conditions with single particle combustion studies in a methane

air flame. The experimental work conducted in this chapter was conducted in part by Ms Esther Fuentes, and by Mr. Martin Ross.

4.2 Materials and Sample Preparation

The biomass used for the work in this chapter is the same SRC willow described in Chapter 3. The willow was ground and sieved and a size fraction between 0.15 and 0.18 mm was used in the TGA studies. Larger particles of 1 to 3 mm were kept for the single particle combustion experiments.

4.2.1 Demineralization and Impregnation

The ground sample and some larger particles were demineralized and impregnated with various amounts of potassium, sodium, and cesium. The demineralization was achieved with the use of hydrochloric acid. 10 g of the sample was heated in 50 cm^3 of 2.0 M HCl for 6 hours at 333 K. After 48 h the sample, left in the HCl solution, was re-heated at 333 K for another 6 hour period. The sample was then filtered, and washed using de-ionized water until the filtrate was Cl^- free (checked by a 0.1 M silver nitrate solution). The sample was then oven dried at 333 K until constant weight is achieved.

To impregnate the willow with the alkali metals, the biomass sample was mixed with the appropriate metal acetate (to achieve a 1 wt% potassium concentration, or equivalent molar concentrations of the other metals), then moistened by 5 cm^3 of de-ionized water, mixed and then oven dried at 333 K to constant weight. The molar concentration was 2.56×10^{-2} mol/100 g of willow and the weight percentages were 0.6, 1, 1.4 for Na, K, and Cs respectively.

4.3 Thermogravimetric Analysis

Pyrolysis tests were performed using a Station Redcroft Simultaneous Analyser STA-780 Series. A typical sample mass of 16 mg is heated at 10 °C /min in a purge of nitrogen with a final temperature of 110 °C. The sample is held at 110

°C for 5 min, is then heated at 25 °C /min to a final temperature of 900 °C, where it is held for an additional 15 min.

Combustion tests were performed with the same equipment. A typical sample mass of 4-5 mg was heated at a rate of 25 °C/min in a purge of air to a final temperature of 900 °C, and was held at this temperature for 15 min.

4.4 Single Particle Combustion

The single particle combustion experiments were conducted by piercing the particle (particle size ca. 2 mm) to suspend it, with a stainless steel needle which is then inserted into a holder; this allows the particle to be supported over a Meker burner. The needle and particle were both covered by a protective water-cooled sheath that was held in place until the digital video recording equipment was ready. The protective sheath was then retracted and the particle was directly exposed to a methane-air flame (air (kg)/methane(kg) ~ 10.5) at 1227 °C. Combustion was monitored and recorded with a Photo-Sonics Phantom V7 high-speed video system with a frame rate of 1000 frames per second (fps) [64]. Figure 4.1 shows the single particle combustion experimental set-up. Interrogation of the captured footage enables identification of several key stages in the process such as the time that the particle is first exposed to the flame, ignition and onset of volatile combustion (characterized by a volatile flame), the end of volatile combustion (characterized by the disappearance of the volatile flame), char combustion, and ash melting.

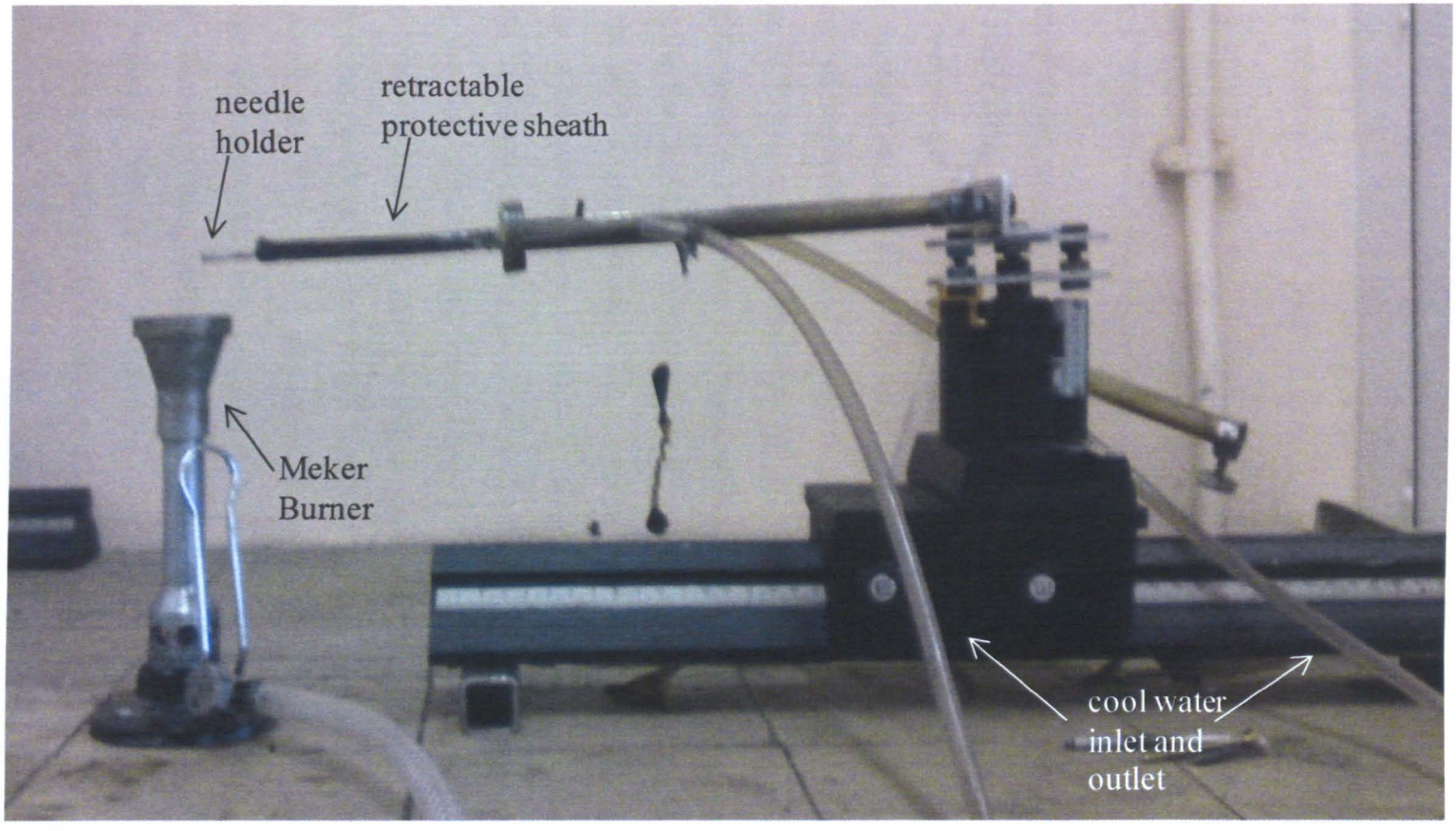

Figure 4.1 Single Particle Combustion Experimental Set-up.

4.5 Fuel Properties

The proximate, ultimate, and metal analyses of the SRC willow studied in this chapter were presented earlier in Tables 3.1-3.3.

4.6 Willow Pyrolysis and Combustion

Derivative thermogravimetric analysis (DTG) results comparing the pyrolysis of the three alkali metal-impregnated samples along with a demineralized and a raw or untreated sample are shown in Figure 4.2. The raw willow profile reveals that the thermal degradation occurs in two stages. The first stage is attributed to the decomposition of hemicellulose and the initial stage of cellulose degradation. The second stage is linked to the degradation of lignin and the final degradation of cellulose. If the profiles of the raw and the demineralized samples are compared, it is noted that the first peak, indicating the decomposition of hemicellulose, is much smaller in the acid treated sample. This implies that acid treatment not only removes most of the minerals from the willow sample, but also digests some of the hemicellulose in the process. Figure 4.2 shows a shift in peak temperatures from higher, with the demineralized and raw samples, to lower, with the alkali metal-impregnated samples, indicating that the alkali metals are catalyzing the pyrolysis reaction. It is also evident that the DTG curve of the raw, or untreated, willow sample has two peaks (270-350 °C, and 350-410 °C), whereas the curve belonging to the HCl treated sample only has one (350-410 °C). It is know that the biomass components, hemicellulose, cellulose, and lignin, decompose over varying temperature regions: 150-350 °C, 275-350 °C, and 250-500 °C, respectively [63]. Thus, for the untreated willow DTG curve in Figure 4.2, the first peak is attributed to the decomposition of hemicellulose together with the beginning of the decomposition of cellulose, and the second peak is linked to the degradation of lignin and with the final degradation of cellulose. The lack of this first peak in the curve of the HCl treated sample suggests changes in the hemicellulose content [63].

There is also a slight shift to a higher main peak temperature from the untreated to the HCl treated sample, indicative of a reduced catalytic activity in the acid treated willow. Figure 4.2 also shows the DTG curves of the metal-impregnated samples, and it is clear that all three metals have a strong catalytic influence on the degradation of the willow, with two clear peaks occurring at 220-280 °C, and 300-390 °C. The first main peak is attributed to the decomposition of cellulose since the hemicellulose content of these samples has decreased due to the acid treatment they have undergone prior to metal impregnation. The second main peak is also likely due to be mostly caused by cellulose degradation.

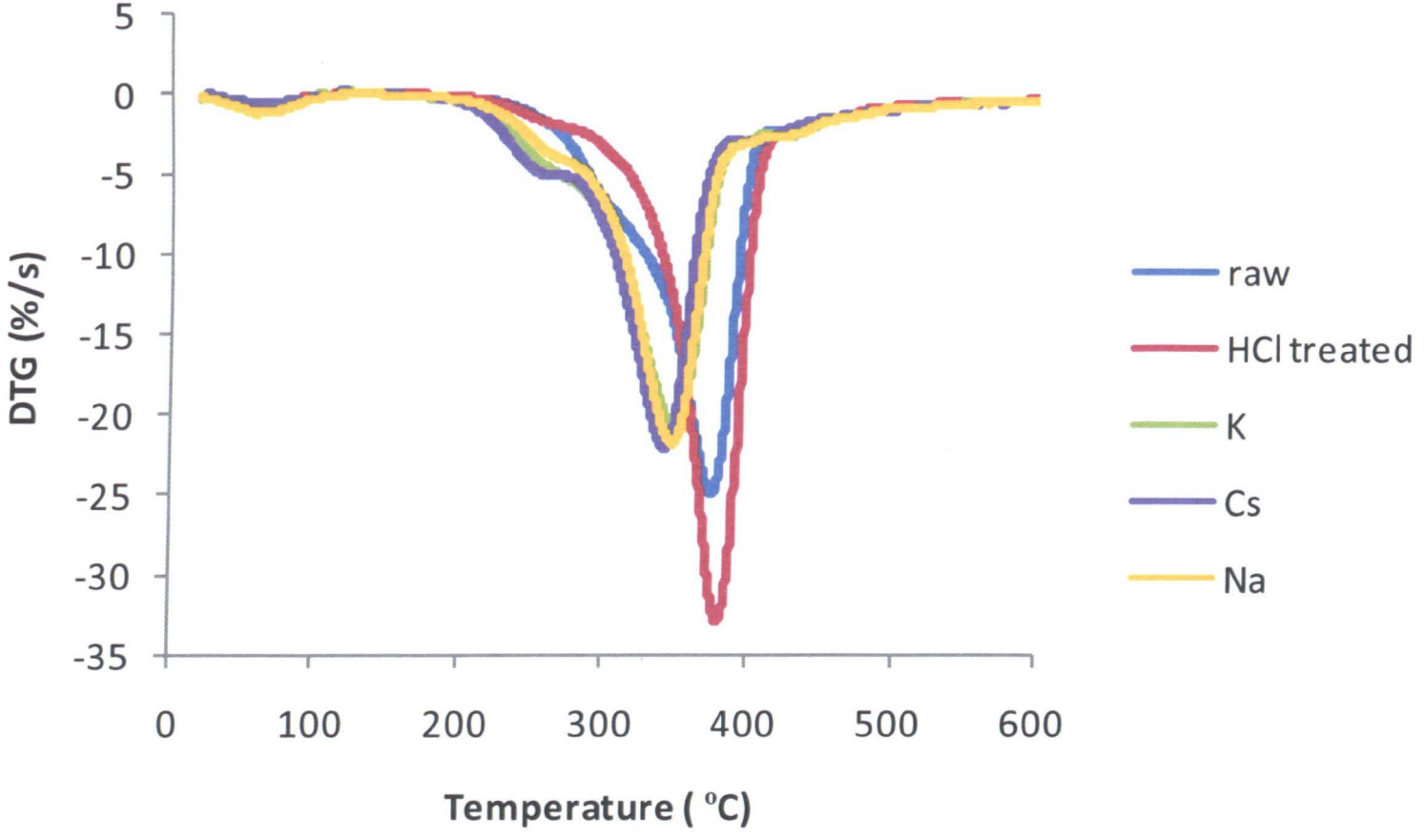

Figure 4.2 DTG pyrolysis profiles for raw, demineralized and metal-impregnated willow samples.

DTG results of the combustion of similar samples are shown in Figure 4.3. The first and main peak in the DTG combustion profiles represents the release of volatiles, ignition, and combustion. The smaller second peak is attributed to char combustion and in the case of the HCl treated sample is broader because char combustion is a much slower process in this case. As with pyrolysis, it is clear that sodium, potassium, and cesium all strongly catalyze devolatilisation as well as char combustion, as is evidenced by a shift of both main DTG peaks to lower temperatures when compared with the demineralized (HCl treated) sample. As one would expect, the raw, or untreated, sample with a 0.4 wt% concentration of potassium [63], exhibits devolatilisation and char combustion characteristics in-between those of the metal-impregnated and demineralized samples.

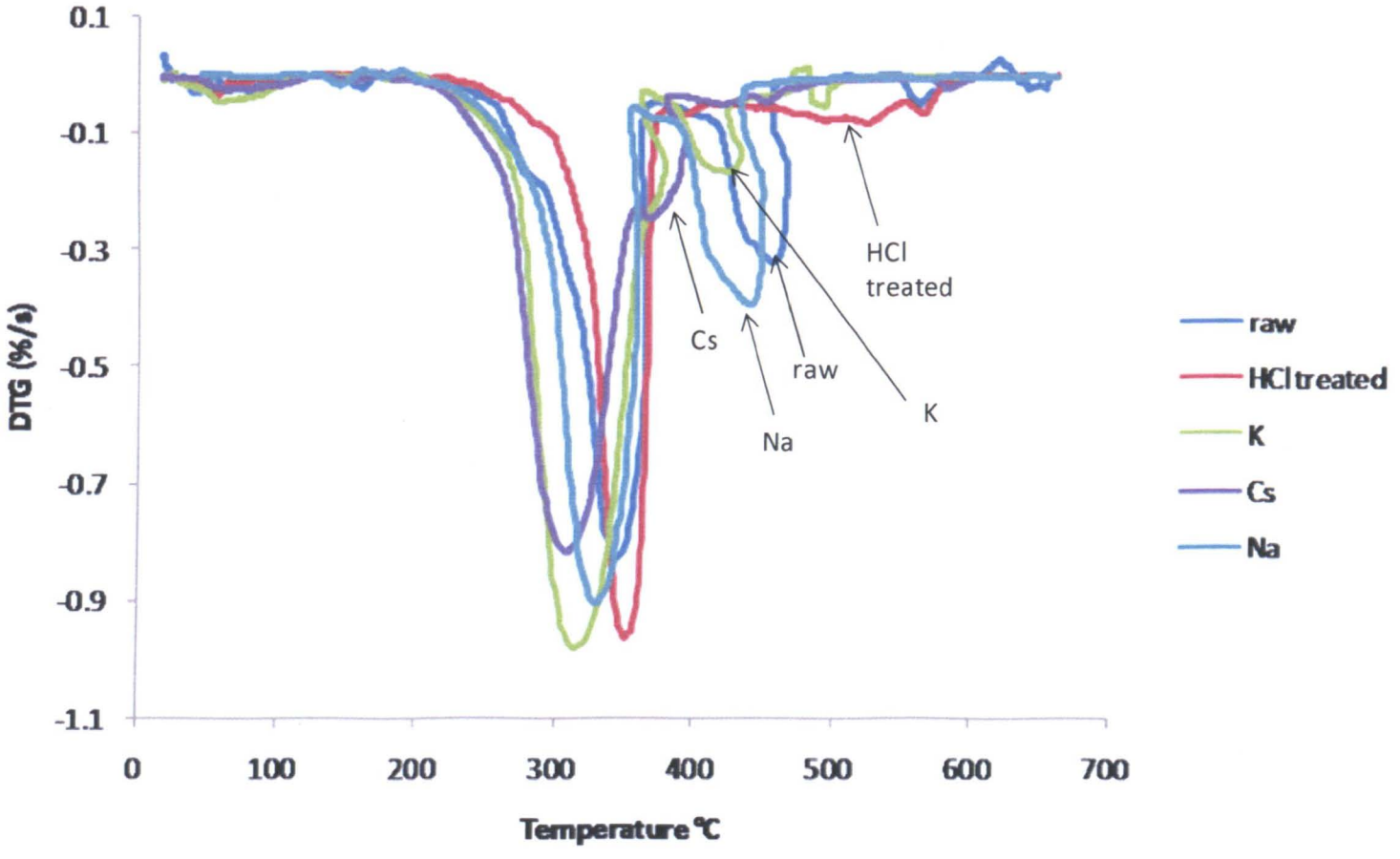

Figure 4.3 DTG combustion profiles for raw, demineralized and metal-impregnated willow samples.

Although the catalytic effect of the metals on pyrolysis and combustion is clear, in pyrolysis the three metal-impregnated samples all produce similar consequences. Table 4.3 lists the first order reaction kinetics of the various samples for the pyrolysis and combustion TGA runs. The activation energies and the pre-exponential factors were calculated according to the Senum and Yang approximation of the Arrhenius temperature integral as described in Chapter 3. The reaction rates are calculated at 300 °C according to equation 3.3.

Table 4.1 First order reaction kinetics of TGA runs (pyrolysis and combustion).

Pyrolysis Sample:	E (kJ/mol)	ln A (s^{-1})	$k_{300\,°C}$ (s^{-1})
HCl treated	119.8	17.5	4.6×10^{-4}
Raw	81.9	10.3	9.8×10^{-4}
Na	79.4	10.2	1.6×10^{-3}
K	80.5	10.3	1.4×10^{-3}
Cs	75.5	9.6	2.0×10^{-3}
Devolatilisation	E (kJ/mol)	ln A (s^{-1})	$k_{300\,°C}$ (s^{-1})
HCl treated	117.5	17.9	1.2×10^{-3}
Raw	80.4	10.8	2.2×10^{-3}
Na	79.0	10.6	2.4×10^{-3}
K	76.3	10.3	3.2×10^{-3}
Cs	57.1	6.2	3.0×10^{-3}

The activation energies for the demineralized samples, in both pyrolysis and combustion, are higher than those observed for the raw samples, which are in turn higher than those of the metal-impregnated ones. As is expected, the reaction rates for the demineralized samples are slower than those of the metal-impregnated samples. In pyrolysis the alkali metals all appear to catalyze pyrolysis to a similar extent. It is interesting that, in pyrolysis, all the alkali metals give similar peak positions in the DTG profiles (Figure 4.2), but this is not the case in the combustion tests (Figure 4.3). In Figure 4.3, the main peak temperatures follow the order Cs<K<Na<HCl for char combustion, although in the latter case this may not be accurate because of the strong exotherm in char combustion which gives uncertainties in peak temperatures. As seen in Table 4.3, a group effect is observed on the devolatilisation kinetics (E decreasing down the group). The mechanism of oxidative pyrolysis is even more complex than pyrolysis, but if metal-oxygen bonds are involved, then these bond strengths become influential in the reaction rates. Alkali metal-oxygen bond strengths follow the order Cs-O > K-O > Na-O [76]. Oxygen interaction with metals is also influential in char oxidation reactions. Unfortunately, kinetics could not be derived from the data in Figure 4.3 because of

the large exotherms observed in the catalyzed reactions. At the temperatures of char combustion, melting temperatures of metal salts may also become a factor. These would influence not only the concentration of catalytic sites on the char (through evaporation), but also the mobility of salts on the surface and their migration to active sites on the char where catalysis may occur at the salt/carbon interface.

4.7 Single Particle Combustion Results

Figures 4.4 and 4.5 depict a series of images captured during the single particle combustion experiments (SPCE). Analysis of a series of SPCE images for any given particle shows the onset of the various stages of combustion (such as ignition, devolatilisation, char combustion, and ash melting), and also allows the calculation of their duration. In these experiments, ignition occurs soon after the particle has been exposed to the flame, and is characterized by the beginning of a glow at the bottom of the particle. The onset of devolatilisation is detected when a luminous flame appears above the particle. Upon the extinguishment of this flame, all that is seen is the glow of the particle, and it is evident that the fuel is undergoing char combustion. For practical reasons, this point can be taken as the onset of char combustion, although the particles in these experiments often exhibit the "char combustion" glow at the bottom (part of particle closest to the flame) prior to the termination of the volatile flame. The particle retains its shape during the majority of the char combustion stage, and at the end, shrinks rapidly. When this shrinkage ceases, only ash remains. Eventually this ash becomes fluid, and this point is considered as ash melting.

Previous research on the single particle combustion of SRC willow has been carried out [72], where the willow samples were demineralized and some were also impregnated with potassium. Figure 4.4 shows SPCE images for two willow particles from this study. The top images in Figure 4.4 depict a K impregnated particle, and the images on the bottom show a demineralized particle.

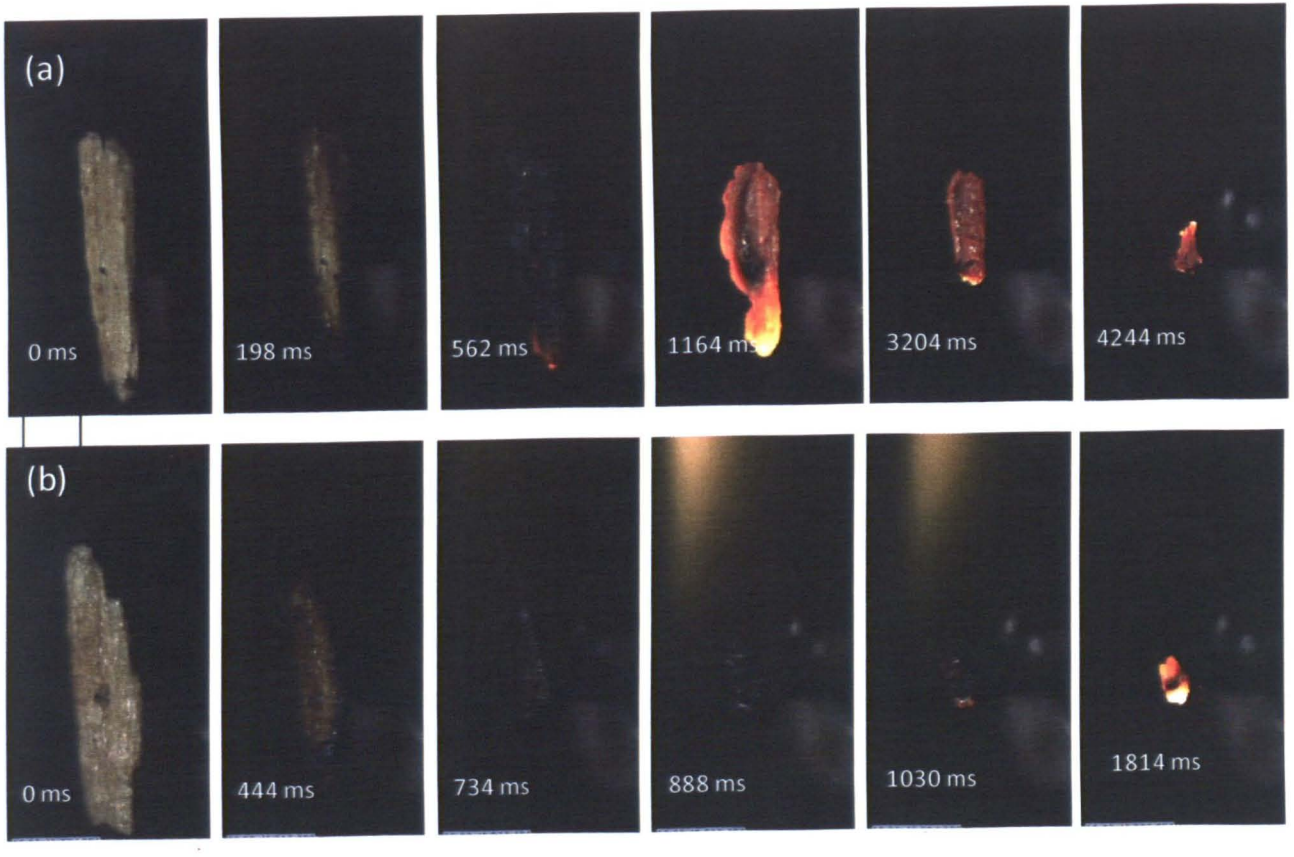

Figure 4.4 Close up view of combustion in the Meker burner of a (top) K-impregnated and (bottom) demineralised willow particle [72] (image reproduced with permission from the author).

In the case of the K impregnated particle (top of Figure 4.4), volatile combustion can be detected through the characteristic volatile flame above the particle (although this is not clearly visible in Figure 4.4). Upon the disappearance of the volatile flame, uniform char combustion began, and the particle integrity was retained while the particle slowly shrank. Toward the end of char combustion, the particle shrank more rapidly and left some ash at the end of the support needle. This ash was observed to have a glassy appearance [72].

In the case of the demineralized particle (bottom of Figure 4.4), the devolatilisation stage was characterized by the appearance of a black tar that boiled from the particle and rapidly coated its entire surface. At the same time, an increase in the brightness and luminosity of the flame above the particle was observed. The authors attributed this to the decomposition and evaporation of the formed tar. The demineralized particle was also seen to melt and shrink rapidly during this stage. Upon the disappearance of the tar and the luminous flame, the particle began to glow and it continued to shrink but more slowly than previously. The char combustion stage was reported to last for up to 20 seconds.

Figure 4.5 shows SPCE images for another demineralized SRC willow sample (top) and a sodium impregnated sample (bottom). In this case, the luminous volatile flame above the demineralized sample (attributed to the decomposition of the tar) can be more clearly seen. Similarly to the findings in [72], it was observed that the devolatilisation stage was short in comparison to the metal doped samples, and that the particle decreased in size rapidly. A comparison between the Na impregnated and the demineralized particles at 1 second (Figure 4.5) shows the contrast in particle size retention following devolatilisation where the demineralized sample has shrunk considerably. The char combustion stage for the demineralized sample continued well beyond the 3 seconds shown in Figure 4.5 (unlike the Na impregnated particle where char combustion has terminated at 3 seconds).

As with the potassium impregnated particle, examination of the SPCE images of the sodium impregnated particle reveal a greater char yield than that observed with the demineralized sample. Unlike the potassium impregnated sample studied in

[72], the sodium impregnated sample studied here exhibits a visible glow that continues throughout most of the SPCE, and is given off by the devolatilisation of sodium.

The SPCE demonstrate that both alkali metals have a catalytic effect on the thermal degradation of willow at flame conditions. This is apparent by the higher char yield, and shorter char burn-out times as compared with demineralized samples.

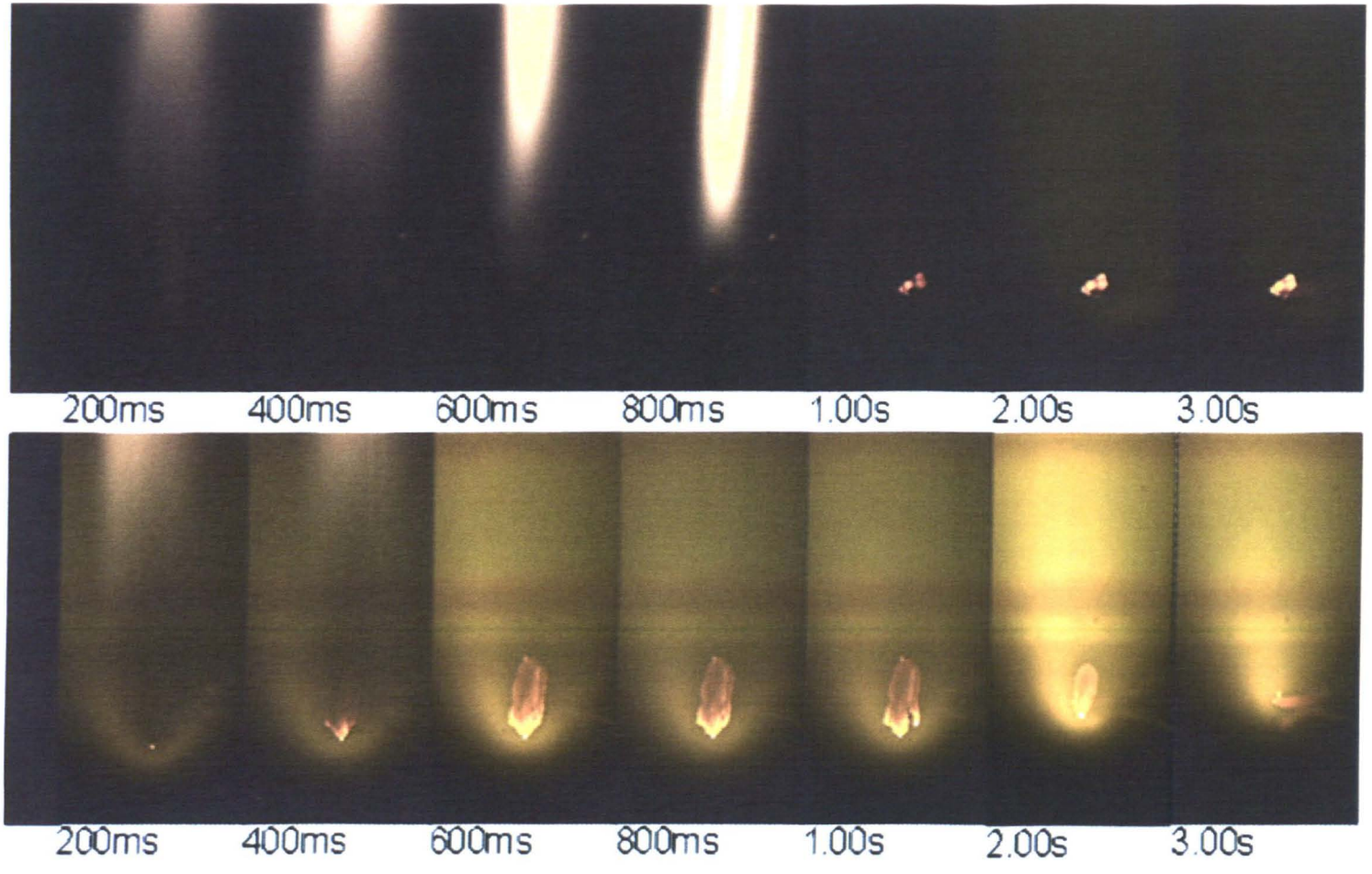

Figure 4.5 Single particle combustion of demineralized (top), and sodium impregnated (bottom) willow samples.

4.8 Conclusions

Pyrolysis and combustion studies under slow heating rate conditions, conducted with TGA, have revealed that sodium, potassium, and cesium presence in the SRC willow strongly catalyzes these reactions. This is evident not only from the shift of main DTG peak temperatures from higher to lower values in the impregnated samples, but also from first-order reaction kinetics which reveal faster reaction rates for these samples. No particular trend in pyrolysis reactivity is observed within the group 1 metals. Willow samples impregnated with the same molar concentration of the three alkali metals all behave in a similar fashion during pyrolysis. In oxidative pyrolysis, a group effect is observed on the devolatilisation kinetics with the activation energies decreasing down the group (Na>K>Cs).

Single particle combustion experiments comparing raw, demineralized and sodium impregnated samples again revealed a stark contrast between the degradation of samples with and without alkali metals. As with the low heating rate results, at flame conditions, samples impregnated with various group 1 metals behave in a similar fashion. Video interrogation shows faster reactions, lower tar yields and higher char yields compared to demineralized samples. These findings imply that a similar thermal degradation mechanism is followed when this woody biomass contains any of the alkali metals. These mechanisms will be considered more closely in Chapter 5.

Chapter 5

Influence of Potassium and Sodium on the Kinetics of SRC Willow Pyrolysis – Model Predicting Reaction Rates

5.1 Introduction

In Chapter 4, it was established that the alkali metals have similar catalytic influence in pyrolysis when present in the same molar concentrations in SRC willow. In the present chapter, the variation of pyrolysis kinetics with metal concentration is investigated.

In Chapter 3, various data analysis methods were studied to ascertain which kinetic extraction method is best suited for reliable kinetic parameter evaluation (based on thermogravimetric analysis (TGA) derived data). Kinetic ranges most applicable to industrial biomass processes were also explored. In many instances, single-step, apparent first order kinetics were seen to give satisfactory predictions of conversions for the time-temperature profile under study. The Senum-Yang approach to deriving first order kinetics from the TGA data was found to be an objective method, and a good approximation when applied to low heating rate data; this approach is therefore applied in the kinetic analysis of the current chapter.

Inherent alkali metal content in biomass has an influence on thermal decomposition [30, 77-79]. Potassium has specifically been discovered to act as a catalyst during pyrolysis reactions [11, 53, 63, 72, 73]. During pyrolysis, the presence of potassium increases the rate of decomposition, increases gas and char yields, and decreases the tar products. Similarly, during combustion, the presence of potassium leads to higher conversion efficiencies. Potassium also changes product distributions [11, 35, 72, 80] as was seen from the single particle combustion experiments in Chapter 4. In the case of sodium, pyrolysis studies have shown that the presence of this metal also lowers the activation energies of the fuels [81] (as seen previously in Chapter 4), and that biomass species with high ash content tend to

have high concentrations of sodium [82]. In general, the concentration of potassium in biomass is much higher than that of sodium. This is reflected in the literature as studies of the influence of potassium are more common than those of sodium. However, the direct influence of alkali metal content on biomass decomposition kinetics expressions has not been thoroughly investigated for any metal. This influence is made more complex by the fact that a portion of the metals is evolved during volatile release and thus the concentrations of metals are not static throughout decomposition. This chapter extends the previous work on short rotation coppice (SRC) willow decomposition to develop a preliminary expression that directly links the biomass degradation kinetics to the inherent alkali metal content. This is achieved with TGA studies on SRC willow samples that have been impregnated with gradually increasing amounts of potassium and others with a range of sodium. The impregnations and TGA experiments were conducted by Ms. Esther Fuentes. The implications on the chemical mechanisms of the observed catalytic activity of these metals on biomass thermal degradation are explored through *Ab initio* modelling.

5.2 Materials, Sample Preparation, and Methods

As with the samples described in Chapter 3, SRC willow was used. The willow was obtained from Rural Generation Ltd. (Londonderry, Northern Ireland). The sample is ground and sieved, and 0.15-0.18 mm particles are used in the TGA studies. The raw willow analyses are given in Tables 3.1-3.3.

5.2.1 Demineralization and Impregnation

Some of the ground sample is further demineralized and impregnated with various amounts of potassium. The demineralization is achieved with the use of hydrochloric acid. 10 g of the sample is heated in 50 cm^3 of 2.0 M HCl for 6 hours at 333 K. After 48 h the sample, left in the HCl solution, is re-heated at 333 K for another 6 hour period. The sample is then filtered, and washed using de-ionized water until the filtrate is Cl^- free (checked by a 0.1 M silver nitrate solution). The

sample is then oven dried at 333 K until constant weight is achieved. Energy dispersive X-ray (EDX) analysis was conducted on the demineralized samples to ascertain that the HCl treatment was effective, and the results showed the complete removal of minerals [63, 83].

To impregnate the willow with either potassium or sodium, 3 g of sample were mixed with potassium acetate, and sodium acetate, respectively, and then moistened by 5 cm^3 of de-ionized water, mixed and then oven dried at 333 K to constant weight. Willow samples with nominal potassium weight percentages of 0, 0.05, 0.1, 0.25, 0.3 0.5, 0.75, 1.0, 1.5, 2 wt% have been studied, along with samples with nominal sodium weight percentages of 0, 0.1, 0.25, 0.5, 1, 2 wt%. The 0.3 wt% K sample is the raw (starting) SRC willow material, as is the 0.1 wt% Na sample. These raw or untreated samples, of course, also contain other metals and an ash analysis revealed the following concentration of oxides: 36.7% CaO, 5.24% MgO, 0.29% Fe_2O_3, 17.1% K_2O, and 19.9% P_2O_5 [11].

5.2.2 Thermogravimetry

Pyrolysis tests were performed using a Station Redcroft Simultaneous Analyser STA-780 Series. A typical sample mass of 10 mg is heated at 10 °C /min in a purge of nitrogen with a final temperature of 110 °C. The sample is held at 110 °C for 5 min, is then heated at 25 °C /min to a final temperature of 900 °C, where it is held for an additional 15 min.

5.2.3 *Ab initio* Modeling

Gaussian 03W software [84] was used for the modelling study. Structures of interest were first geometry-optimized at the HF level and then at the B3LYP DFT level (6-31G(d) basis set). Ground state structures were confirmed from the absence of imaginary frequencies in a subsequent frequency calculation. There is a general agreement in the literature that the structures studied in this chapter (described in Section 5.6.2) can be modelled well at the density functional theory level with the B3LYP method and the 6-31G(d) basis set [85-87].

5.3 Willow Pyrolysis

Figures 5.1 and 5.2 show the TGA weight-loss profiles of the samples studied. It is evident that a general catalytic trend exists, with the samples containing more potassium and sodium being more reactive. The main peak temperatures of the differential thermogravimetric analyses profiles of the same samples portray this trend more clearly, and are plotted in Figures 5.3 and 5.4 as a function of potassium and sodium contents of the samples. There is a decrease in the temperature associated with the main peak of nearly 60 °C for the 2 wt% K-willow compared with demineralized (0% K) willow. Similarly for sodium, there is a decrease of 50 °C for the 2% Na sample as compared to the demineralized (0% Na) one. Tables 5.1 and 5.2 contain a cross reference of the main peak temperatures with the weight percent of each metal as well as the moles. On a molar basis, potassium and sodium have similar influences on the main peak temperature, although sodium appears to be slightly more active, as evidenced by the lower peak temperatures of the sodium doped samples versus those of equivalent moles of potassium shown in Figure 5.5. It is noteworthy that previous reproducibility work indicated that for these experiments the accuracy of the volatile peak was within 3 °C.

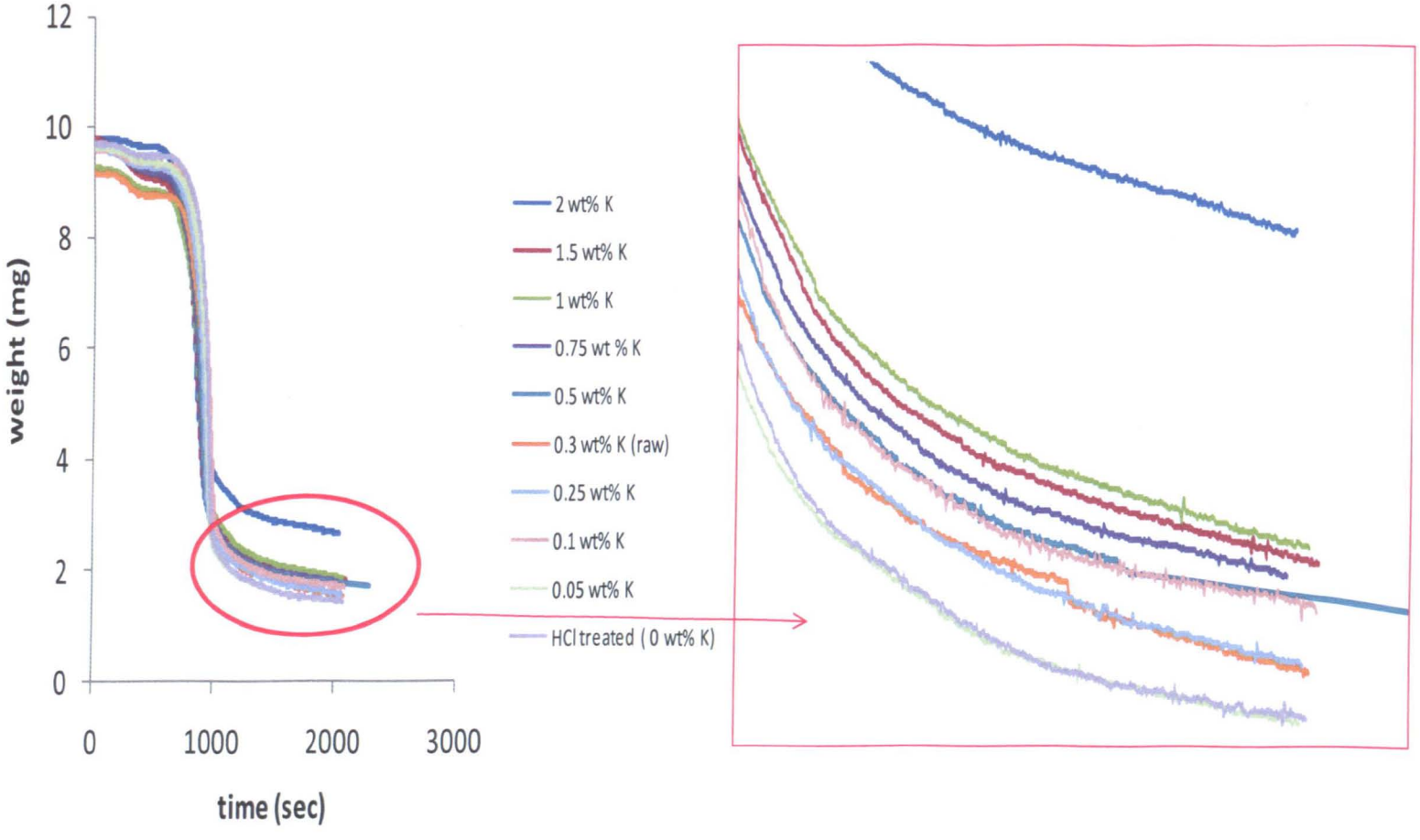

Figure 5.1 TGA weight loss profiles during pyrolysis, at a heating rate of 25 °C/min, of willow samples impregnated with various amounts of potassium.

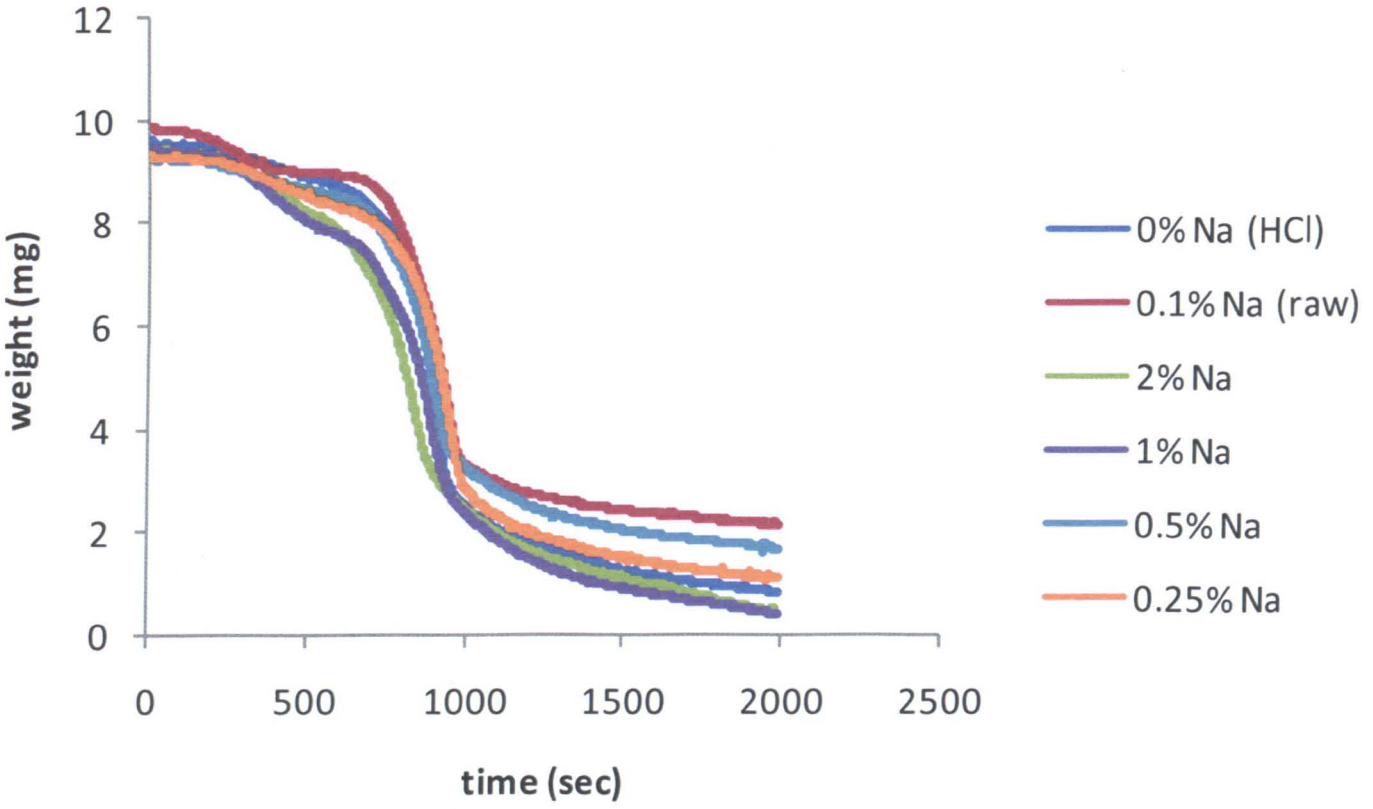

Figure 5.2 TGA weight loss profiles during pyrolysis, at a heating rate of 25 °C/min, of willow samples impregnated with various amounts of sodium.

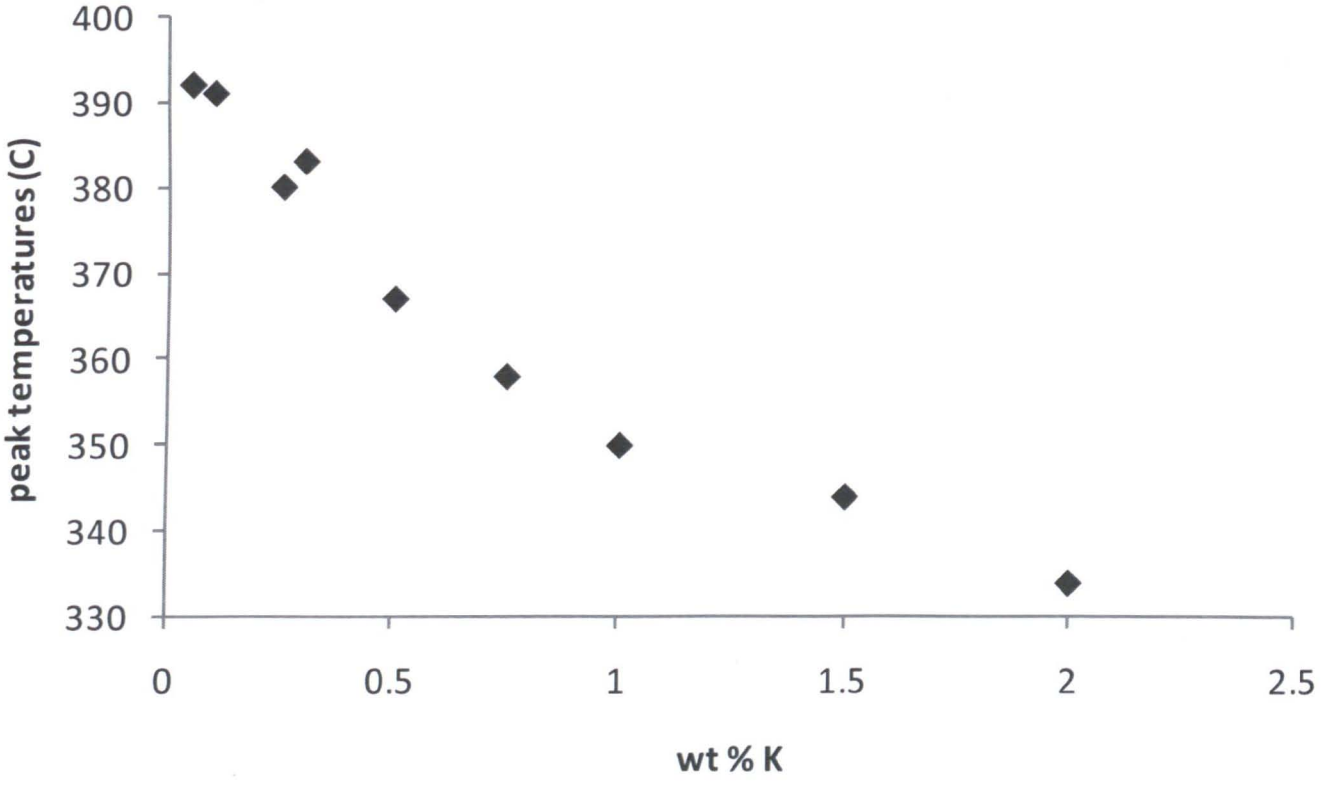

Figure 5.3 Main peak temperatures of the differential thermogravimetric analyses profiles of willow samples impregnated with a ranging amount of potassium.

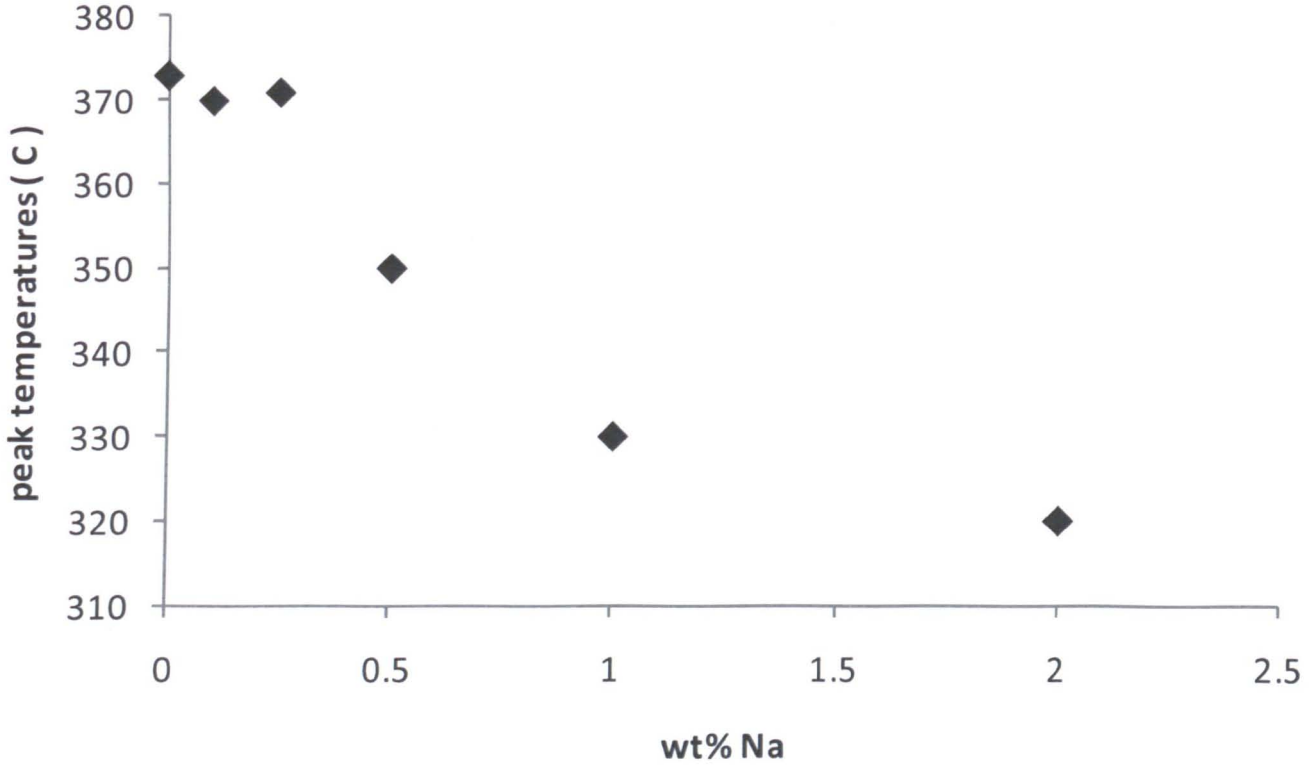

Figure 5.4 Main peak temperatures of the differential thermogravimetric analyses profiles of willow samples impregnated with a ranging amount of sodium.

Table 5.1 Main Peak Temperatures, wt %, and moles of Potassium.

wt % K	moles ($\times 10^2$) K per 100 g	main peak temperature (°C)
0 (HCl treated)	0	383
0.05	0.13	392
0.1	0.26	391
0.25	0.64	380
0.3 (raw)	0.90	383
0.5	1.28	367
0.75	1.92	358
1	2.56	350
1.5	3.84	344
2	5.12	334

Table 5.2 Main Peak Temperatures, wt %, and moles of Sodium.

wt% Na	moles ($\times 10^2$) Na per 100 g	main peak temperature (°C)
0 (HCl treated)	0	383
0.1	0.43	370
0.25	1.09	371
0.5	2.17	350
1	4.35	330
2	8.70	320

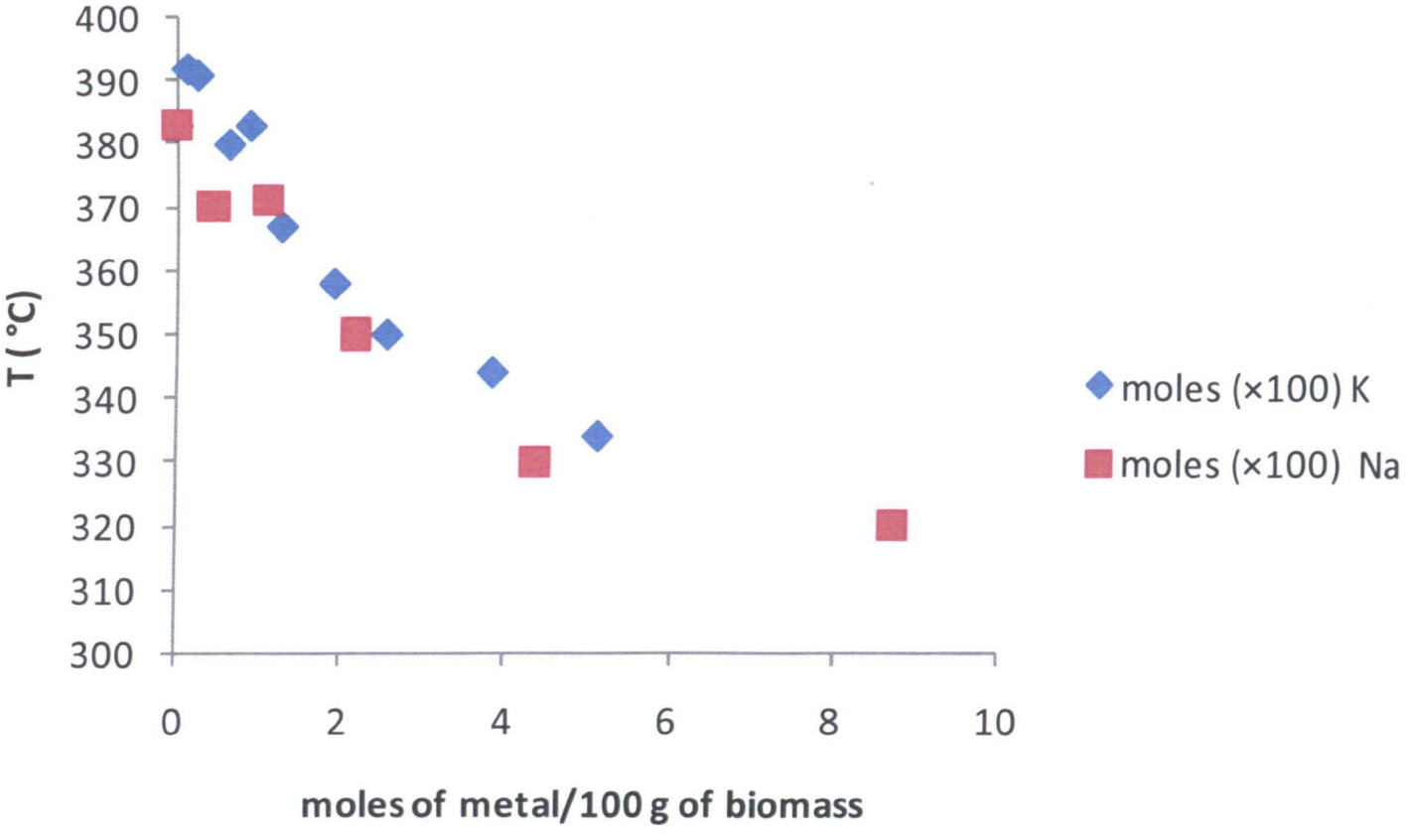

Figure 5. 5 Main peak temperatures and moles of metal

Figure 5.1 also shows that an increased amount of potassium relates to an increased char yield. Conversely, Figure 5.2 shows no particular trend, although samples with the highest sodium concentration have the lowest char yield. The case of sodium however is potentially misleading as the TGA measurements were taken to a higher temperature, perhaps causing more of the sodium to evaporate. For the case of potassium, this trend is more easily seen in Figure 5.6, where char yield has been plotted with respect to metal content. To verify that the trend in increased char yield with increasing potassium content is not simply due to an increase in ash content, char yield on a theoretical ash-free basis was calculated and is also plotted in Figure 5.6. It was assumed that the ash consists of K_2O as no other minerals are present in these samples (except in the case of the raw willow). For the data range studied, a linear fit can be applied to describe char yield, for both dry and dry ash free, with wt % K content although the regression coefficient is 0.55.

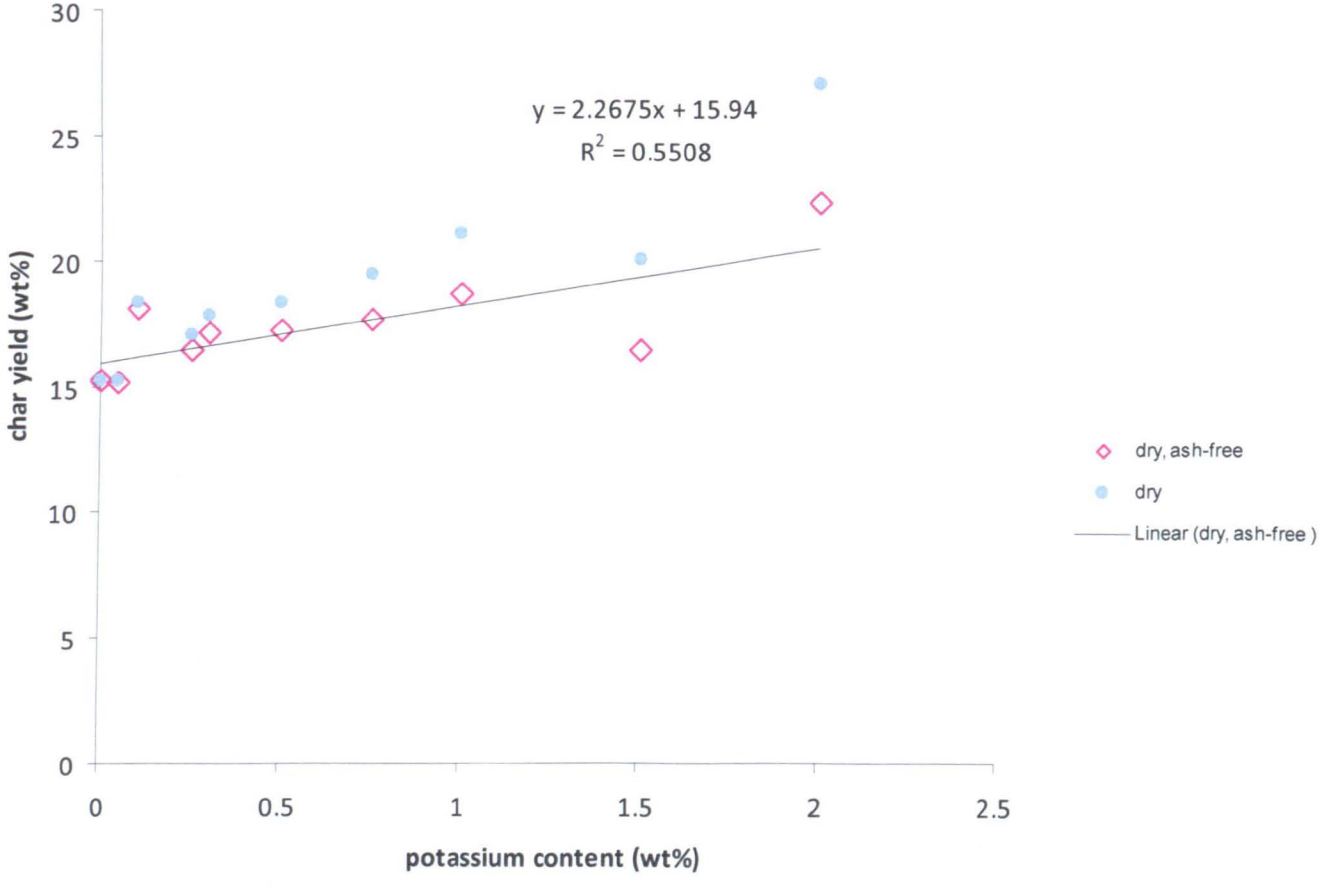

Figure 5.6 Char yield versus potassium content of samples.

Other authors have reported similar trends in char yields for washed (low metal) and unwashed (higher metal) samples of other types of pyrolysed biomass such as poplar [34] and Lolium and Festucia grasses [30]. Pyrolysed switchgrass, untreated and having a potassium content of 0.85 wt%, gave char yield values of ca. 19% [88].

5.4 Kinetic Analysis

The TGA-derived data was analyzed for apparent first-order pyrolysis kinetics and the pre-exponential factor and activation energies were derived for each sample, again, according to the Senum and Yang approximation [7] of the Arrhenius integral. The apparent-first order kinetics are valid over the experimental temperature range, and are given in Tables A.1 and A.2 in the Appendix.

5.4.1 Influence of Potassium on Reaction Kinetics

The influence of potassium on the initial pyrolysis of willow was studied examining the samples with a range of potassium concentrations; from 0 wt% potassium, achieved by acid-washing the willow, to 2 wt% K. The apparent first order pre-exponential factors and activation energies were calculated over a conversion range from approximately 10 to 50%. It is important to note that the proposed model, discussed in the following section, is based on assumptions that are valid during the early stages of pyrolysis. Therefore, earlier and smaller initial conversion ranges were tested (such, as 10 to 15% and 10 to 20% conversion), and minimal differences were observed in the resulting kinetic parameters (standard deviation of activation energy values were generally less than 0.2 and for lnA, less than 0.1) as compared to the more global conversion range of 10 to 50%. Thus, this larger conversion range was chosen as it covers conversions relating to the main pyrolysis decomposition peak. From these kinetics studies, it is evident that an

increase in the potassium concentration clearly causes a decrease in both the activation energies and the pre-exponential factors of the samples.

For illustration of the influence of K on reaction rate, the A's and E's reported in Figure 5.7 were used to calculate the corresponding reaction rate constant at 300 °C. A plot of the reaction rate and the potassium concentrations is shown in Figure 5.8. It is noticeable that the relationship deviates from linearity at the higher concentrations under study. Also, the efficacy of potassium as a catalyst appears to reach a limiting value and this is discussed further in Section 5.5.

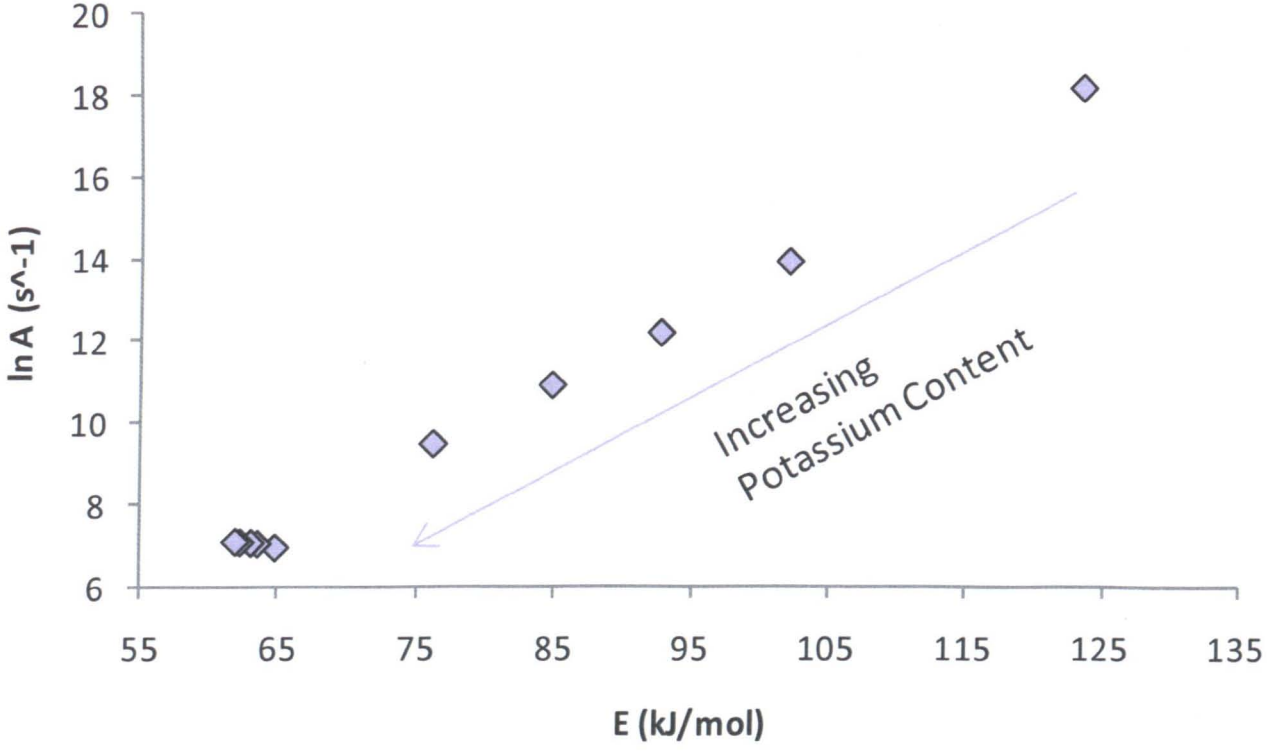

Figure 5.7 Kinetic parameters of particles with a range of potassium concentrations.

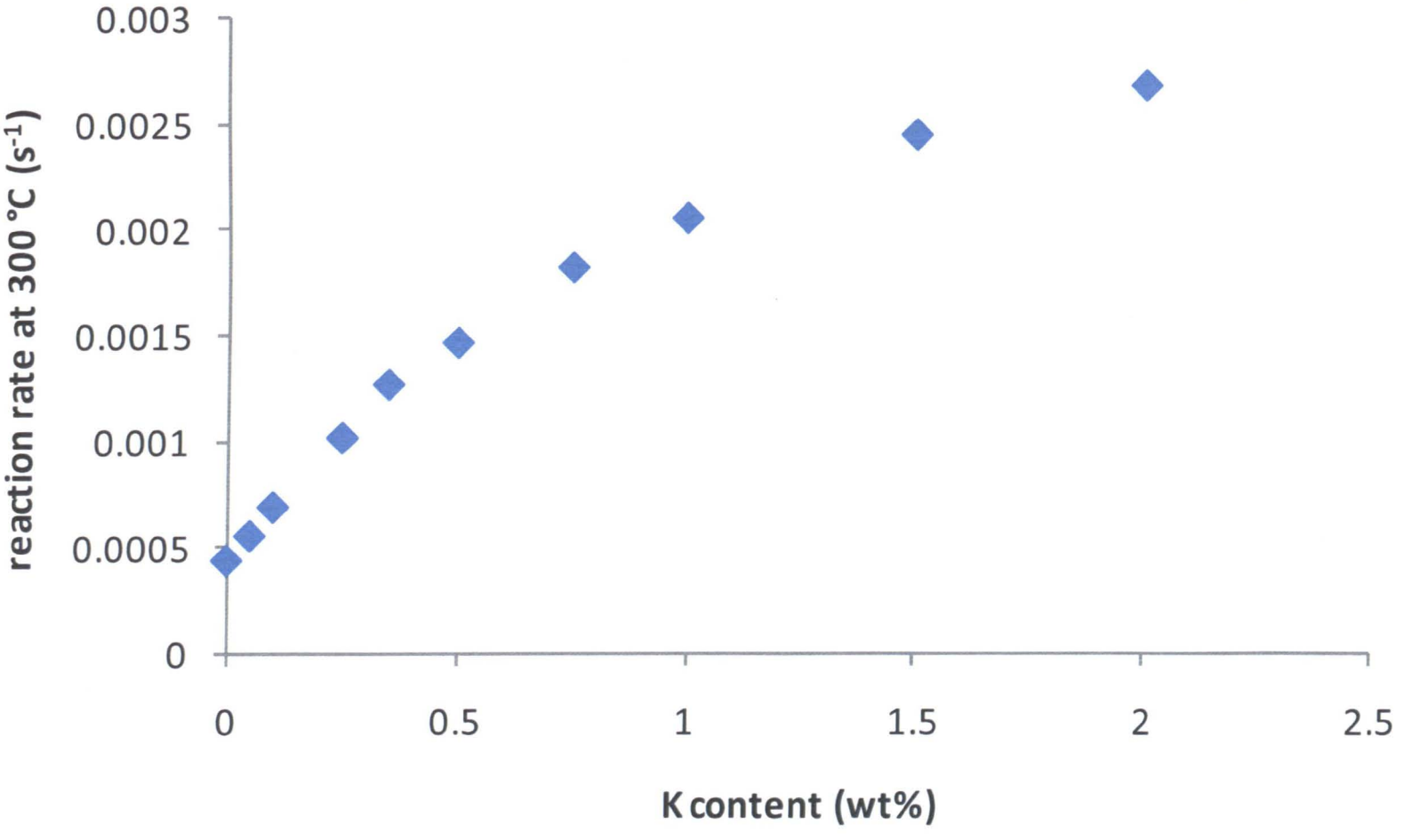

Figure 5.8 Dependence of reaction rate on potassium concentration.

5.4.2 Influence of Sodium on Reaction Kinetics

As with the case of potassium impregnated samples, the influence of sodium on the initial pyrolysis of willow was studied. Again, samples with a range of metal concentrations; from 0 wt% sodium, achieved by acid-washing the willow, to 2 wt% Na were examined. The apparent first order pre-exponential factors and activation energies were also calculated over a conversion range from approximately 10 to 50%, and are shown in Figure 5.9. An increase in the sodium concentration also causes a decrease in both the activation energies and the pre-exponential factors of the samples.

Figure 5.10 illustrates the influence of Na on the reaction rate. Again, the rate constant was calculated at 300 °C. There seems to be a similar limiting value (similar to the potassium case) of the catalytic activity of sodium as the concentration in the sample increases.

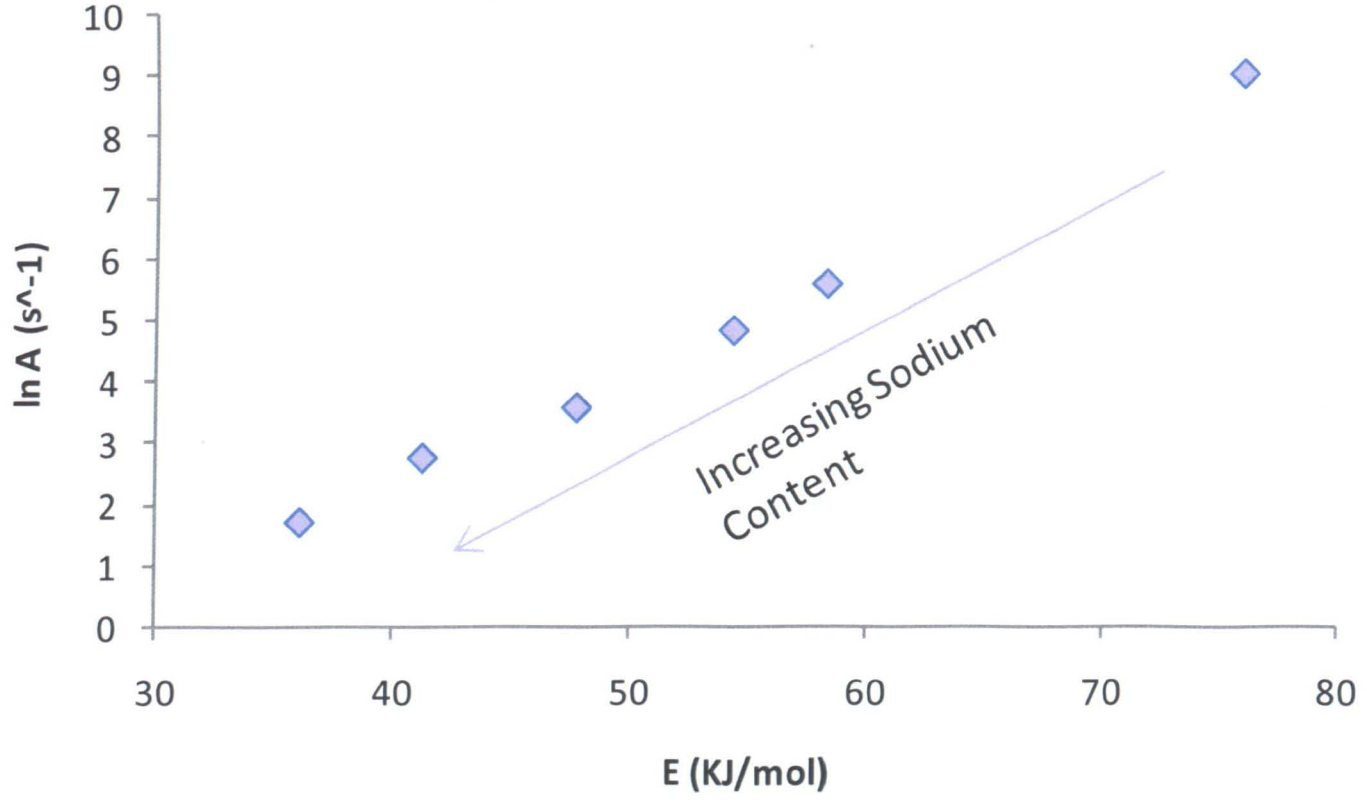

Figure 5.9 Kinetic parameters of particles with a range of sodium concentrations.

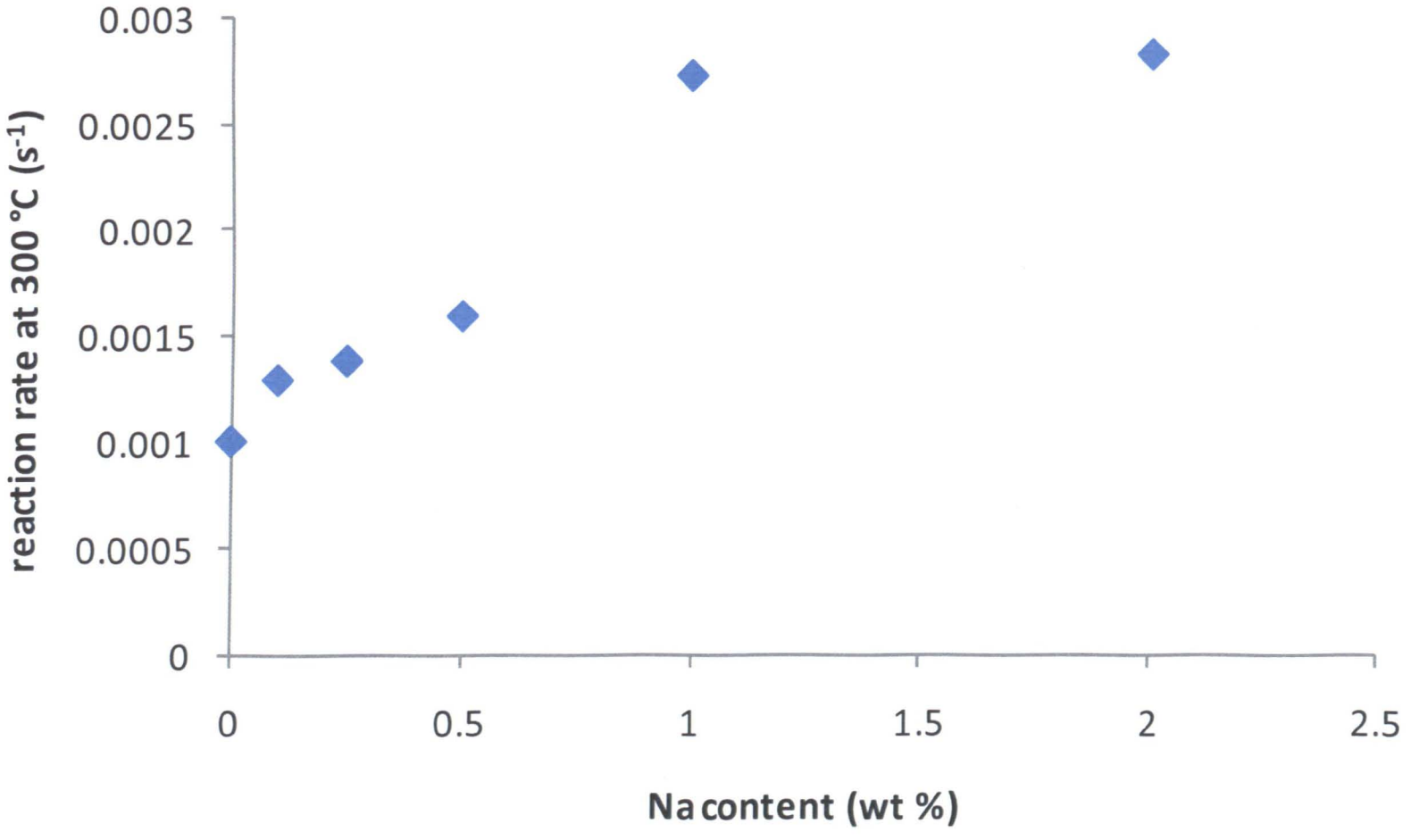

Figure 5.10 Dependence of reaction rate on sodium concentration.

5.5 Linking Metal Content to Rates of Pyrolysis

The possibility of linking early pyrolysis to metal content by modelling according to a Langmuir-Hinshelwood relation has been explored. Generally, the Langmuir-Hinshelwood relation refers to a surface coverage of active sites, but it has also been modified to describe the rate of biological growth on a substrate, as the substrate concentration changes [89]. In the present work, rate of reaction rather than growth, and potassium or sodium concentration is considered. The reaction proceeds as follows:

$$[B]+[M]\underset{k_{-1}}{\overset{k_1}{\rightleftharpoons}}[BM]\xrightarrow{k_2}[B]+[P] \quad \text{.....Eq. (5.1)}$$

where B stands for biomass, M for metal (in this case potassium or sodium), and P for products.

It is assumed that the intermediate active species [BM] is at steady state since as metal evolves, the amount or concentration of biomass also decreases i.e:

$$\frac{d[BM]}{dt}=0 \quad \text{.....Eq. (5.2)}$$

$$[B_o]=[B]+[BM]=\text{constant} \quad \text{.....Eq. (5.3)}$$

where $[B_o]$ = total number of biomass pyrolysis sites.

During early stages of pyrolysis these assumptions are reasonable. The rate of evolution of products, P, is given by:

$$\frac{d[P]}{dt}=k_2[BM] \quad \text{.....Eq. (5.4)}$$

Letting $S_k=\frac{k_{-1}+k_2}{k_1}$, then the following can be derived:

$$[BM] = \frac{[M][B_o]}{S_k + [M]} \quad \text{.....Eq. (5.5)}$$

Therefore,

$$\frac{d[P]}{dt} = k = k_2[BM] = k_2[B_o]\left(\frac{[M]}{S_k + [M]}\right) \quad \text{.....Eq. (5.6)}$$

Substituting k^o for $k_2[B_o]$, the modified Langmuir-Hinshelwood expression is:

$$k = \frac{dP}{dt} = k^o\left(\frac{[M]}{S_K + [M]}\right) \quad \text{.....Eq. (5.7)}$$

where k° is the maximum reaction rate constant, [M] is the potassium or sodium concentration and S_K is the potassium or sodium saturation constant, which, numerically, is the metal concentration where the reaction rate is half of its maximum. Simple re-arrangement of equation 5.7 yields the following relation:

$$\frac{1}{k} = \frac{S_K}{k^o} \times \frac{1}{[M]} + \frac{1}{k^o} \quad \text{.....Eq. (5.8)}$$

A plot of $1/k$ vs. 1/[M] reveals the maximum reaction rate constant and the potassium saturation constant to be 3.26 x 10^{-3} s^{-1}, 0.56 wt%, respectively. In the case of sodium, the maximum reaction rate constant and the sodium saturation constant are 3.27 x 10^{-3} s^{-1}, 0.37 wt%, respectively. These values can then be utilized to calculate an actual reaction rate constant for any concentration of potassium or sodium.

The $1/k$ vs. 1/[M] plots for the K and Na impregnated samples are shown in Figures A.1 and A.2 in the Appendix. Figures 5.11 and 5.12 show the predicted reaction rate constants at 300 °C calculated according to this model, compared with the measured values (obtained using the Senum-Yang approximation) for the potassium and sodium impregnated samples. For the model, the potassium concentrations were extrapolated to 7 wt%. It is clear from Figure 5.11 that the reaction rates obtained from equation 5.1 follow very closely to those predicted via the use of the Senum and Yang approximation. Similarly, from Figure 5.12, it is clear that the model works well for sodium. The data was again extrapolated to 7 wt%.

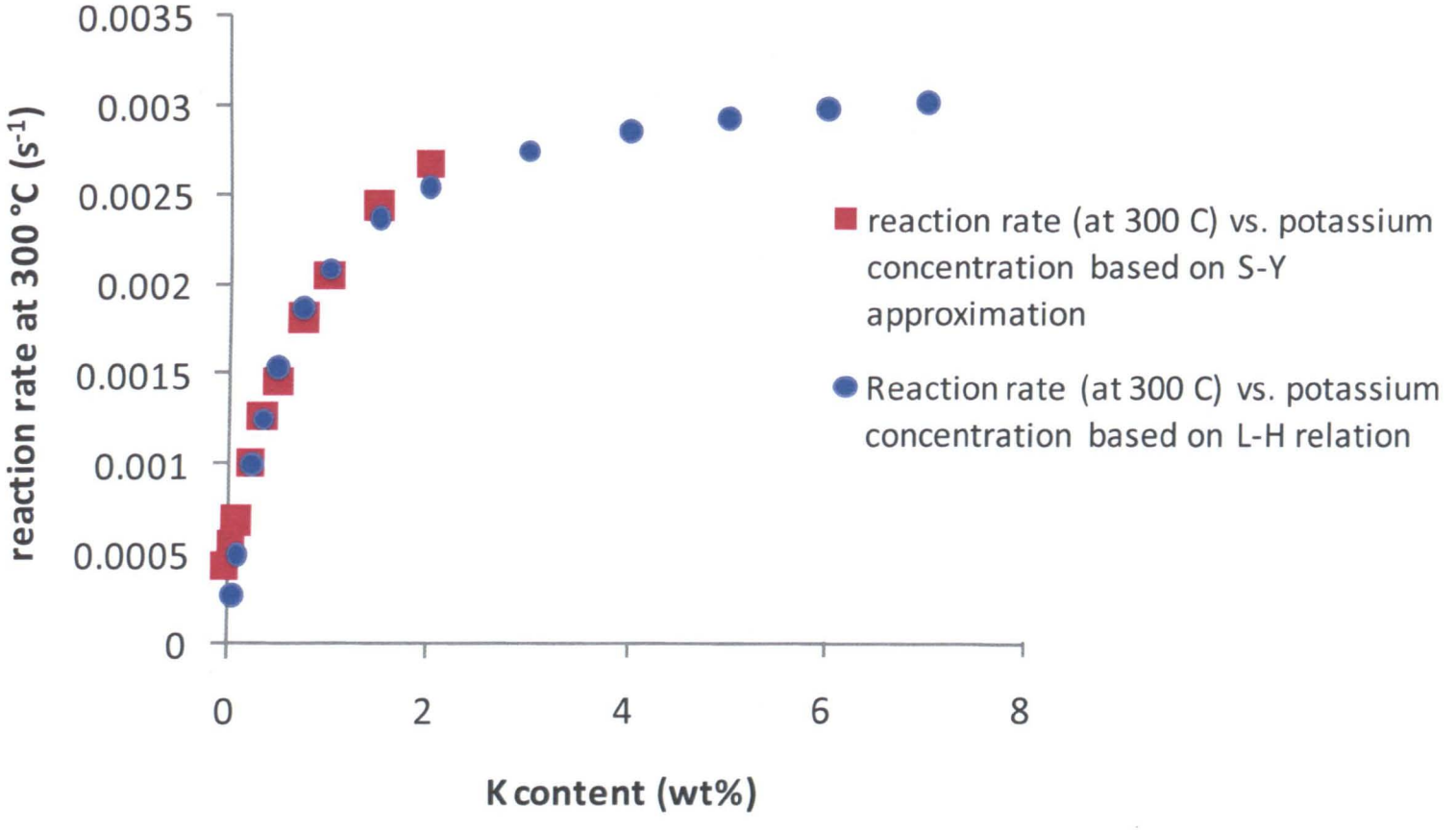

Figure 5.11 Potassium content vs. reaction rate constants calculated at 300 °C with both the Senum and Yang approximation and the Langmuir-Hinshelwood relation.

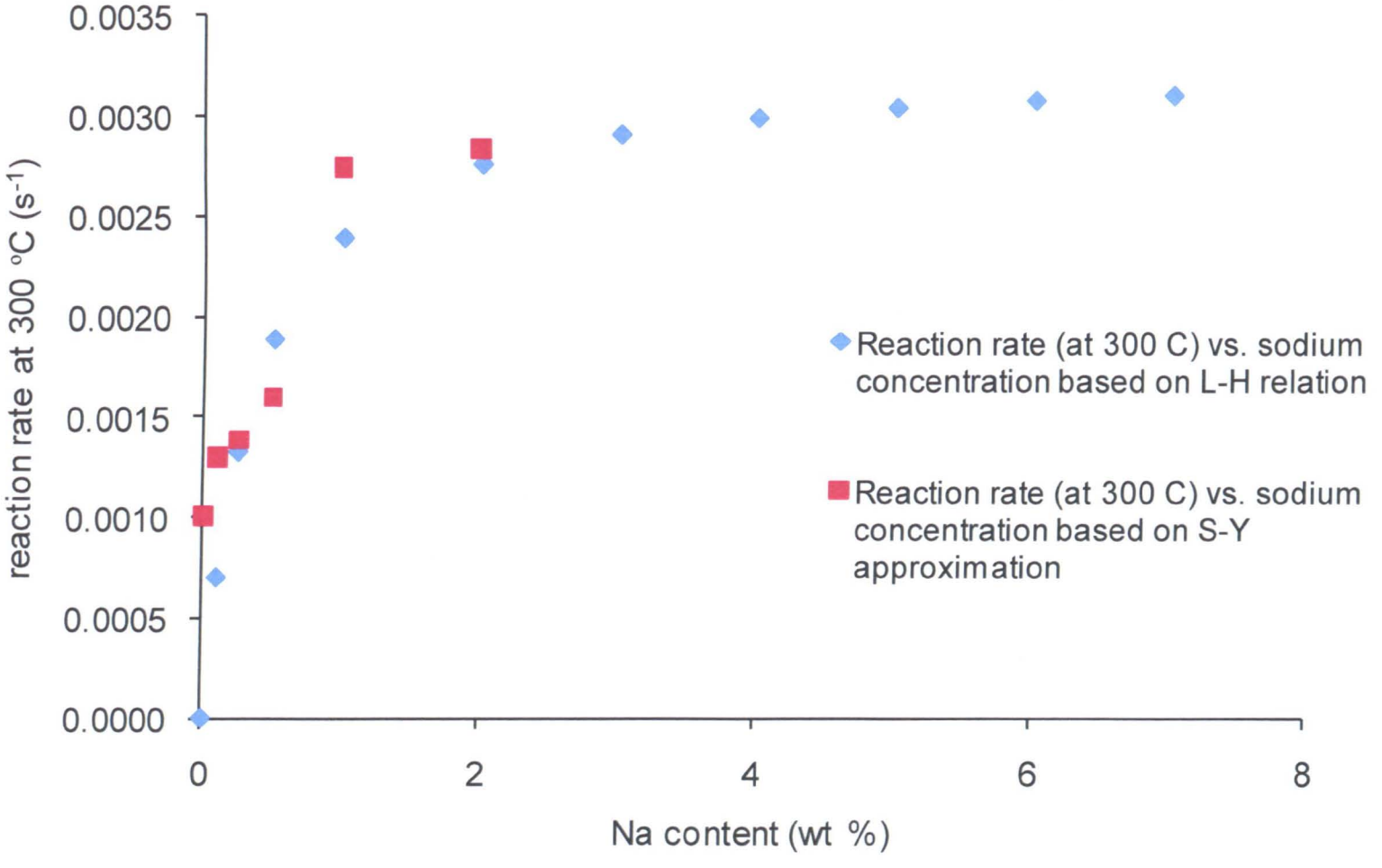

Figure 5.12 Sodium content vs. reaction rate constants calculated at 300 °C with both the Senum and Yang approximation and the Langmuir-Hinshelwood relation.

It is also noted that after a certain concentration (ca. 4 wt% for K and 3.5% for Na) an increased value of potassium or sodium concentration has little effect on the reaction rate. Tables 5.3 and 5.4 contain lists of maximum reaction rate constants and metal saturation constants for a range of temperatures.

Table 5.3 Predicted maximum reaction rate constants and potassium saturation constants for various temperatures according to the Langmuir-Hinshelwood relation.

temperature (°C)	maximum reaction rate constant (k°) (s^{-1})	potassium saturation constant (S_K) (wt%)
300	3.26×10^{-3}	0.56
310	4.15×10^{-3}	0.57
320	5.10×10^{-3}	0.54
330	6.23×10^{-3}	0.51
340	7.56×10^{-3}	0.49
350	9.12×10^{-3}	0.47

Table 5.4 Predicted maximum reaction rate constants and sodium saturation constants for various temperatures according to the Langmuir-Hinshelwood relation.

temperature (°C)	maximum reaction rate constant ($k°$) (s^{-1})	sodium saturation constant (S_{Na}) (wt%)
300	3.27×10^{-3}	0.36
310	3.66×10^{-3}	0.32
320	4.09×10^{-3}	0.27
330	4.56×10^{-3}	0.24
340	5.08×10^{-3}	0.20
350	5.64×10^{-3}	0.18

The Langmuir-Hinshelwood relation in this case describes a mechanism where the attachment of the potassium or sodium atoms to the biomass catalyzes a pyrolysis step. It is important to note that the metal not only catalyzes the pyrolysis reaction, but is also partially entrained in the volatiles. Consequently, the concentration of the potassium and the sodium is not static during devolatilisation. It is proposed that as the metals evolve during pyrolysis, new active sites are generated by the diffusion of metal ions from salt particles to chelation complexes. The assumptions in the model presented (Equations 5.2 and 5.3) hold in the early stages of pyrolysis when the biomass concentration (and metal concentrations) are assumed to be constant.

5.6 Mechanistic Implications

5.6.1 Introduction

The inherent mineral content of biomass exists in various forms, such as: salts, which are left within the cells during moisture evaporation; metal ions sometimes ion-exchanged within the biochemical polymers; and metal centres existing as organometallic compounds such as chlorophyll. In the case of potassium and sodium (potassium being naturally more abundant) this is mainly in the form of salts (chlorides, acetates, sulphates etc.), with a certain percentage associated with the organic fraction in the ion exchanged form. For potassium, as an example, Yu and Zhang [67] report this latter form to be 13% in the case of wheat straw. Various researchers have studied the evolution of alkali metals during thermal decomposition, and this work [67, 72, 90-93] suggests that the alkali metals are lost in two main stages. In the first stage (200-500 °C) there is loss of the metal associated with the organic phase during devolatilisation, while in the second stage (above 500 °C) there is evaporation of the inorganic metal, which is dependent upon the chlorine content of the biomass. The second stage has been modelled by evaporation of potassium salts based on their vapour pressure with temperature [67, 72]. The first stage has been modelled as release of K at the same rate as pyrolysis [67, 72] and is of relevance to the work presented here. The evaporation model, which was first developed by Yu and Zhang [67], was later modified by Jones et al. [72] so that as the particle is heated, its diameter is linked to, and changes with both temperature and time, and potassium is released. The authors [72] assume that most of the chlorine content of the fuel is released during the devolatilisation stage based on experimental work produced by Jensen et al. [94] concerning the release of potassium and chlorine to the gas phase during biomass pyrolysis. Therefore, for low Cl biomass, such as SRC willow, hydroxide is the main potassium salt that has a low enough vapour pressure to evaporate. The authors also assume that some of the inorganically bound potassium is fixed in the ash as sulphates and silicates. In the model, the particle temperature is raised with time up to a maximum, and it is assumed that the vaporisation occurs under a stagnant environment on a resistance-

free surface of a spherical particle. The partial pressure of the potassium hydroxide is considered to be zero far from the particle. Factors such as the possible erosion of the ash, the decomposition of potassium silicates or sulphates in the particle, are neglected.

Alkali and alkaline earth - carbohydrate complexes have been studied in solution in some detail, and the work was last reviewed some time ago [95]. Metal complexes with sugars have assisted separation in chromatography [96], and alkali metals are also known to enhance ionization of carbohydrates in mass spectrometric analysis [97]. All the alkali metals can complex to the hydroxyl groups of the carbohydrates, forming bonds to multiple OH groups, and with simple sugars, some of these complexes have been isolated and crystal structures established by X-ray crystallography [95]. For strong bases (e.g. KOH) it is suggested that there is removal of a proton by the anion to form an alcoholate; such a complex would be stabilized by chelation of the metal ion with neighbouring OH groups on the carbohydrate. Early studies have investigated the pH dependence of formation of these complexes (or adducts) and for higher concentrations of hydroxide, cellobiose can accommodate at least two KOH molecules [98]. The interaction between K^+ and carbohydrates has also been studied theoretically at different levels of theory with approaches involving *ab initio* modelling, as well as low level theory models like molecular mechanics, and dynamics, and semi-empirical molecular orbital calculations, though these later methods tend to be less accurate [99-102]. Many of these computations have been aimed at understanding the enhanced ionization of carbohydrates by alkali metals in mass spectrometric analysis [101, 103].

5.6.2 *Ab Initio* Modelling

Possible complexes in the solid state are investigated in the present work to assist in interpreting the mechanism of catalyzed pyrolysis of biomass. Two scenarios are considered: (1) A complex between a strong base (e.g. MOH), where the anion extracts a proton from the carbohydrate OH group. Here, the different possible alcoholates are evaluated for relative stability. (2) A complex between a very weak base (e.g. MCl), where the anion does not extract a proton from an OH

group. In the latter case, the complex under investigation carries a +1 charge, while the complex in the first case is neutral. Results of key bond lengths and bond/torsion angles are compared against the analogous free cellobiose moieties. These two cases are considered for potassium and sodium. Cesium complexes could not be studied under the same conditions as potassium and sodium because cesium has a sufficiently large atomic number to be out of the range for the 6-311 G basis set. Literature suggests that for elements past the third row of the periodic table, a basis set of LANL2DZ ought to be used [104]. Unfortunately as HF level computations with the LANL2DZ basis were being carried out, the program was adding a large number of connections to the Cs atom and due to limited available computational power, the computations always ended abnormally (or "crashed" due to errors in the internal coordinate system).

Many authors have reported that even small quantities of alkali metals change the product distribution favouring furfural and its derivatives, carbonyl compounds and increased char yield [74, 105]. Potassium is proposed to produce a rapid ionic reaction whereby ring opening of cellulose is favoured over the non-catalyzed mechanism involving glycosidic bond scission to form levoglucosan as a major product. The first step is thought to be activation via a change in ring configuration. The increased char is proposed to arise from polymerization reactions involving alkene intermediates, via the ionic mechanistic route [74]. The mechanisms proposed by Evans and Milne [74] for non-catalyzed and the alkali metal catalyzed pathways are shown in Figure 5.13 top and bottom, respectively.

(a)

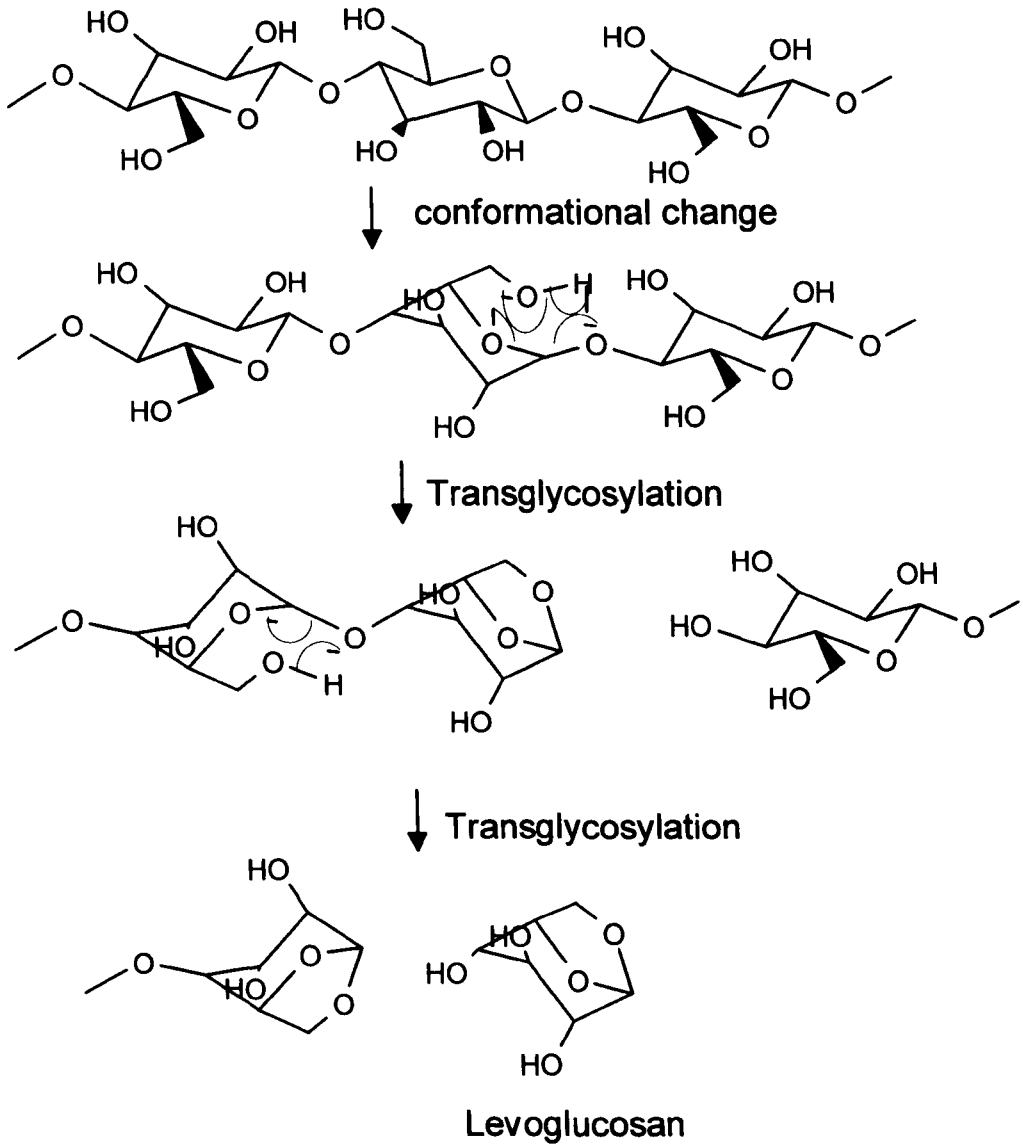
conformational change
Transglycosylation
Transglycosylation
Levoglucosan

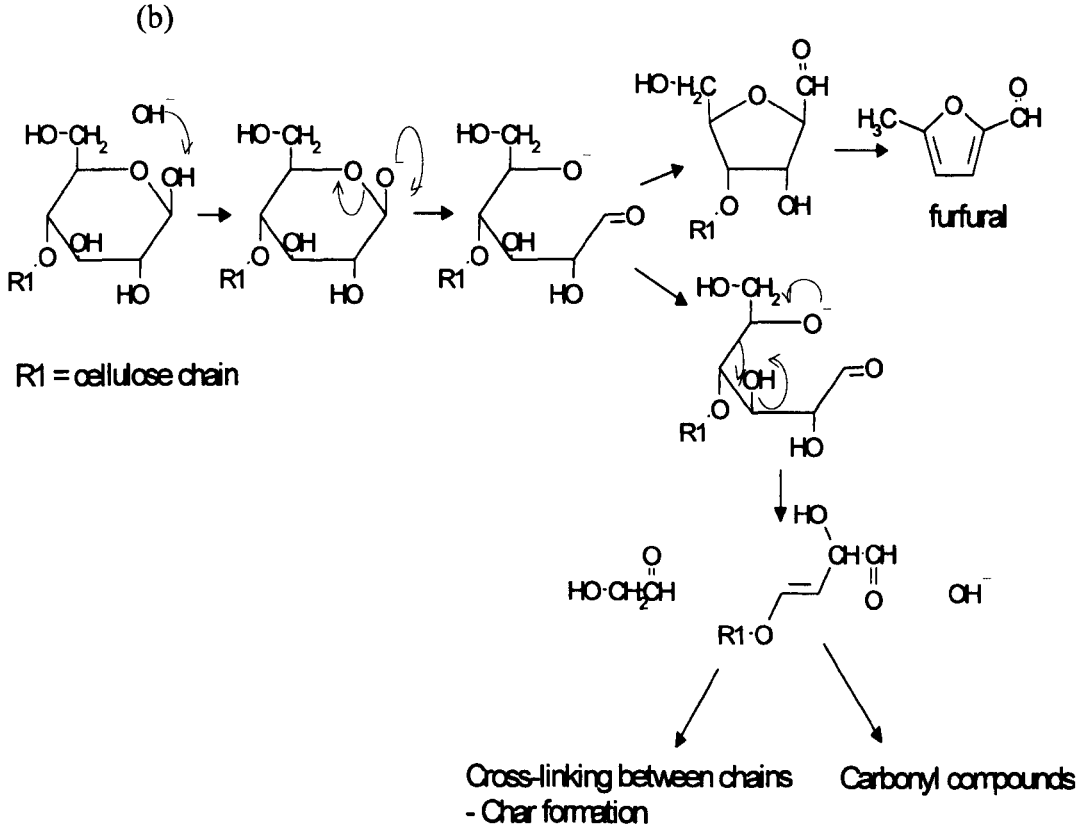

Figure 5.13 Non-catalyzed (a) and the alkali metal catalyzed (b) biomass pyrolysis pathways suggested by Evans and Milne [74].

A fraction of potassium is known to be evolved during pyrolysis/devolatilisation [72, 91, 93, 106, 107] but it is still to be established whether this is potassium which is complexed to the evolving organic species, or whether this is potassium salts entrained in the rapidly evolving vapours and gases. The current chapter will suggest that the interaction of metals in the carbohydrate structure, such as shown in Figures 5.14, 5.15, is critical to the catalytic action of these metals. This idea was suggested earlier this chapter, in the evaluation of the kinetics using a Langmuir-Hinshelwood type approach.

After pyrolysis/devolatilisation, a large fraction of the alkali metals remains in the biomass char. Potassium is also renowned for its catalytic activity in char oxidation/gasification reactions. The other alkali metals have also been shown to be catalytically active (Section 4.6, for example). Redox-type reactions of carbonate/oxide/metal are cited in alkali-catalyzed gasification [108], and in addition, evidence of surface complexes of $K^+(O^-)C$ has been seen from in situ FTIR studies [108]. A similar complex has been proposed for the case of alkali-catalyzed char oxidation [109, 110], and this could be particularly important in the case of "young", oxygenated biomass char, where phenolate structures are likely to exist. The complex is also seen as an anchor for dispersing metal/metal salt particles on the active sites of the graphene structures in the char, a process facilitated by the mobility of these particles at elevated temperatures. As well as a "spill-over" redox mechanism from metal salt particles, the complex results in a weakening of the adjacent C-C bond [109] which catalyzes the reaction.

Figures 5.14 and 5.15 illustrate ground-state geometry optimized structures for the complexes described earlier. Cellobiose was modelled to represent the cellulose chain. Structures in Figures 5.14 and 5.15 (a) and (b) carry a plus one charge and represent complexes between a very weak base where the anion does not extract a proton from the OH groups. In these two complexes the metal was attached to the C6 and C2 carbons of the ring respectively (labelled atom 11 and atom 17 in Figure 5.14). Structures in Figures 5.14, and 5.15 (c) and (d) are neutral species and represent complexes between a strong base, where a proton has been extracted from

the carbohydrate. The protons extracted were the C6-O**H** and the C2-O**H** respectively (again, labelled atom 11 and atom 17).

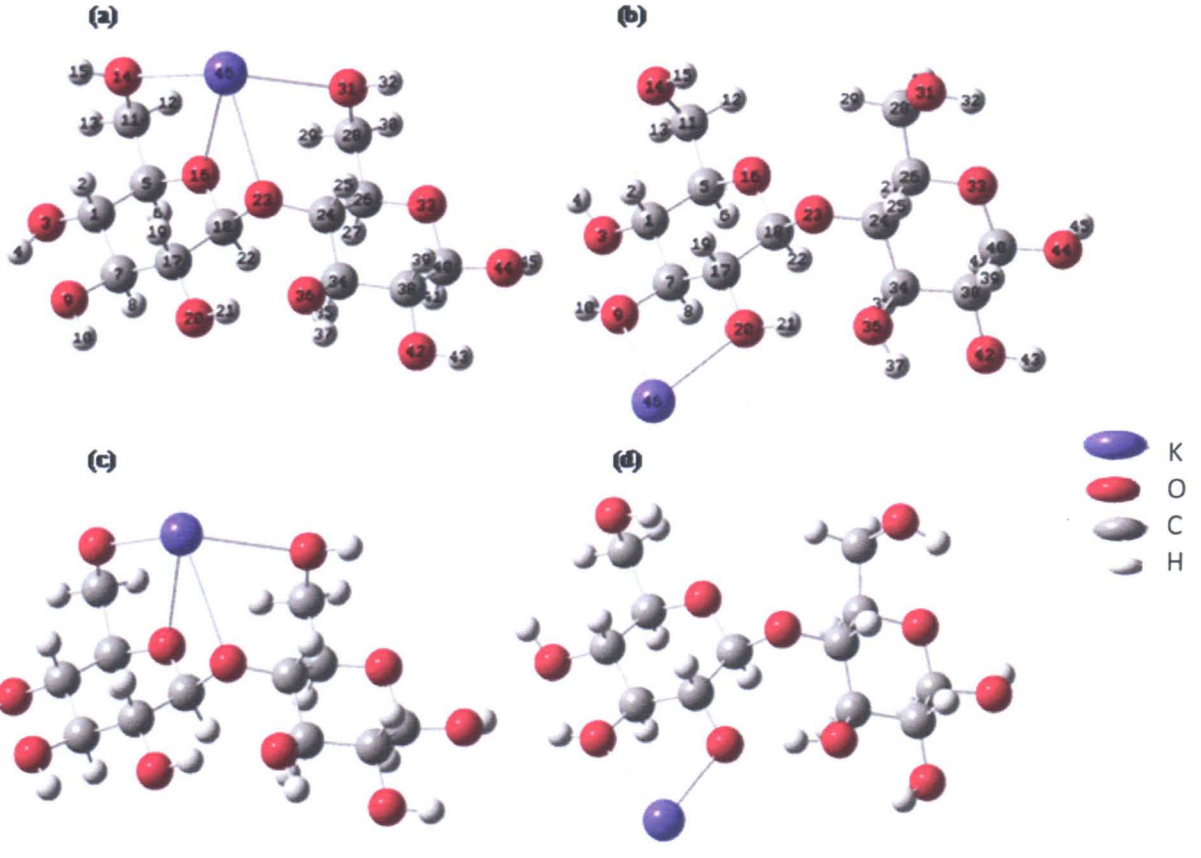

Figure 5.14 Geometry optimized ground state structure of (a) [K-cellobiose]+ (K+ near C6OH group); (b) [K-cellobiose]+ (K+ near C2OH group); (c) K-cellobiose (neutral) (K+ on C6O- group); (d) K-cellobiose (neutral) (K+ on C2O- group). See table 5.5 for geometries and bond lengths.

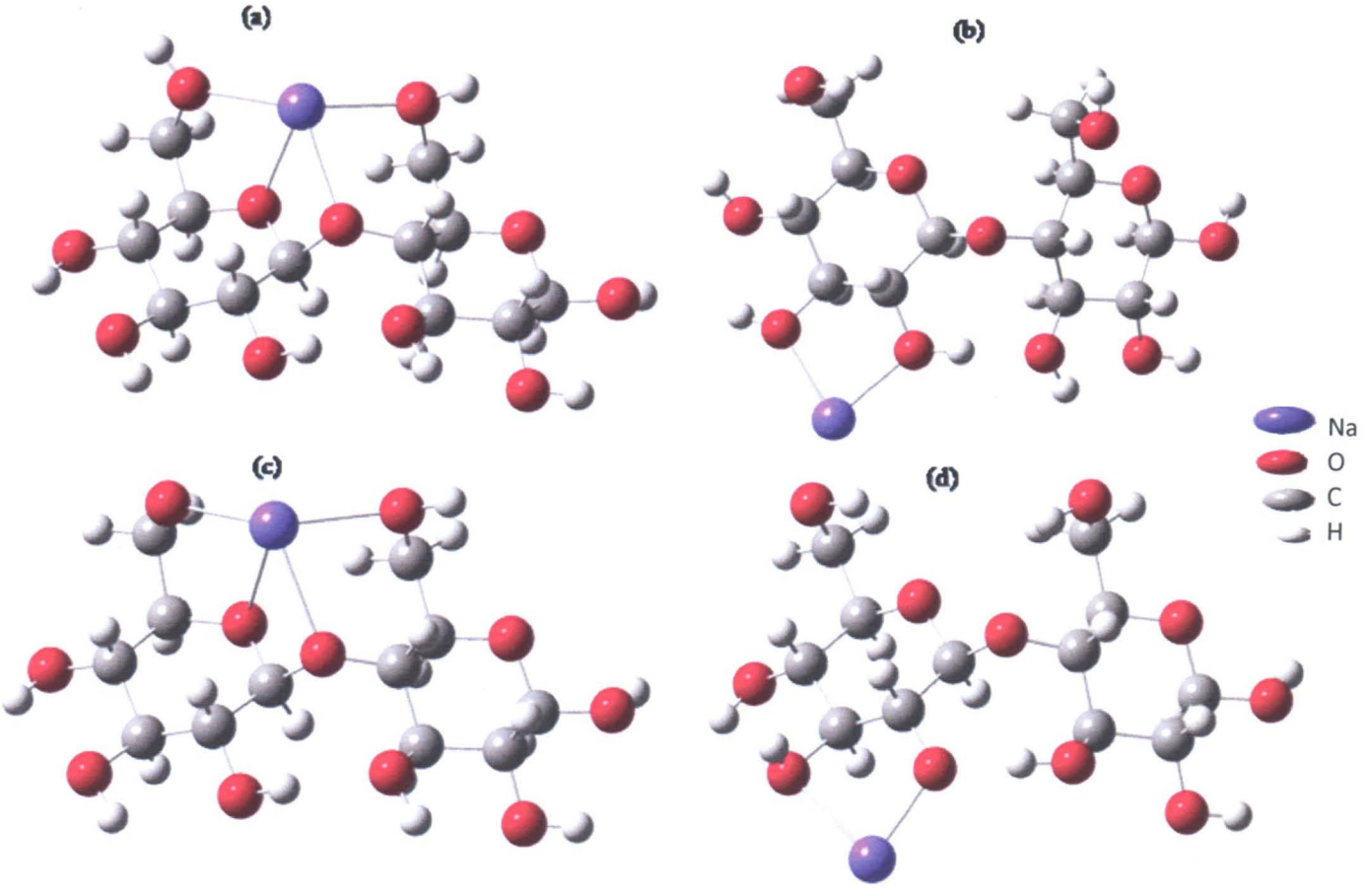

Figure 5.15 Geometry optimized ground state structure of (a) [Na-cellobiose]+ (Na+ near C6OH group); (b) [Na-cellobiose]+ (Na+ near C2OH group); (c) Na-cellobiose (neutral) (Na+ on C6O- group); (d) Na-cellobiose (neutral) (Na+ on C2O- group). The atom numbers are the same as in Figure 5.14 and the geometries and bond lengths are listed in Table 5.6.

5.6.2.1 Potassium

When K^+ is near/attached to the C6-OH group the resulting ground state structures are stabilized by multiple interactions with neighbouring OH and ether groups. When K^+ is near/attached to the C2-OH group the resulting ground state structures contain a bridging K^+ between two OH groups. It is important to note that in cellobiose, where there are long chains, inter-molecular chelation may occur, but the model does not account for this. In both cases the chelated K+ (multiple interactions) have lower energy than the bridging structure; the structure in Figure 5.14(a) is more stable than that in Figure 5.14(b) by 33 kJ/mol, while the structure in Figure 5.14(c) is more stable than that in Figure 5.14(d) by 11 kJ/mol.

Bonding of K^+ into the cellobiose moiety causes subtle changes in bond lengths and angles as the electrons redistribute within the bonding structure. The bond lengths associated with the structures in Figure 5.14 are listed in Table 5.5. K-O bond lengths are in the range 2.42 – 2.80 Å in the different structures. Previous studies have reported K-O bond lengths between 1 and 3.5 Å [109]. The glycosidic linkage bond lengths vary only slightly compared to the analogous free disaccharide (all are in the range 1.39-1.43 Å); similarly the bond angle of the glycosidic linkage (C18-O23-C24) remains virtually unchanged after complexation at ~ 120°. However, the dihedral angles across the two rings of the dimer change dramatically, particularly as a result of chelation of K^+ involving the ether glycosidic linkage, which demonstrates that the rings twist relative to one another in order to accommodate the potassium ion. It is possible, that complexing of potassium at C6 (Figure 5.14(a) and Figure 5.14(c)) stabilizes the glycosidic bond, or an intermediate reaction complex, such that ring opening becomes more favoured. Changes in bond lengths within the rings are small, although the C-O ether bonds change from 1.43 Å in cellobiose to 1.40 Å (C18-O16) and 1.46 Å (C5-O16) in the structure in Figure 5.14(c) implying that the C5-O16 bond has been weakened. This may have implications in the catalyzed ring opening reaction. However, it should be noted that the ring C-O ether bonds in the structures in Figure 5.14 (a),(b), and (d) were very similar in length to the analogous bonds in cellobiose. From fast atom bombardment ionization, and matrix assisted laser desorption ionization studies of

alkali metal–oligosaccharides [102] it is clear that both cracking of the glycosidic linkage and ring opening are assisted by the metal ion. The sequence of events is still not clear however, and it is likely that both routes proceed simultaneously.

Table 5.5 Bond lengths of K-cellobiose structures shown in Figure 5.14.

	cellobiose Å	[K-cellobiose]$^+$ (near C6OH) Å	[K-cellobiose]$^+$ (near C2OH) Å	K-cellobiose ($C6O^-K^+$) Å	K-cellobiose ($C2O^-K^+$) Å
K-O bond lengths					
K-O9	-	-	2.619	-	2.648
K-O14	-	2.799	-	2.413	-
K-O16	-	2.688	-	2.728	-
K-O20	-	-	2.609	-	2.417
K-O31	-	2.744	-	-	-
Glycosidic linkage					
C18-O23	1.401	1.412	1.391	1.426	1.394
C24-O23	1.429	1.431	1.435	1.417	1.432
Bond angle C18-O23-C24	120.2	121.6	120.8	120.8	120.2
Dihedral angle C18-O23-C24-C26	62.9	61.4	66.1	57.7	68.3
Dihedral angle O16-C18-O23-C24	-114.3	-120.4	-106.5	-109.37	-120.28
C-(O (H)) bond lengths					
C7-O9	1.422	1.415	1.438	1.426	1.446
C11-O14	1.417	1.440	1.417	1.350	1.419
C17-O20	1.417	1.410	1.431	1.420	1.372
Ring bond lengths					
C17-C18	1.532	1.536	1.541	1.528	1.552
C17-C7	1.523	1.525	1.519	1.517	1.539
C7-C1	1.524	1.526	1.524	1.527	1.518
C1-C5	1.534	1.532	1.538	1.531	1.536
C5-O16	1.439	1.440	1.437	1.461	1.426
C18-O16	1.423	1.428	1.419	1.399	1.440
C26-C24	1.546	1.546	1.543	1.547	1.540
C24-C34	1.531	1.529	1.525	1.532	1.533
C34-C38	1.523	1.529	1.521	1.526	1.530
C38-C40	1.527	1.532	1.530	1.530	1.525
C40-O33	1.417	1.437	1.424	1.426	1.434
C26-O33	1.431	1.427	1.434	1.437	1.436

5.6.2.2 Sodium

As observed in the case of potassium, when Na^+ is placed near the C6-OH group, the resulting ground state structures are also stabilized by multiple interactions with neighbouring OH and ether groups. When Na^+ is near the C2-OH group, the resulting ground state structures have a bridging Na^+ between two OH groups. Again, as with K^+, the structures with the chelated Na^+ have lower energies and are thus more stable. That is, the energies of the structures in Figure 5.15 follow the pattern 5.15(a) < 5.15(b) by 57 kJ/mol and 5.15(c) < 5.15(d) by 4 kJ/mol .

The Na-O bond lengths range between 2.07-2.40 Å in the Na-cellobiose structures. As seen previously with potassium, the glycosidic linkage bond lengths vary slightly between the Na-cellobiose structures and are in the range of 1.44-1.39 Å. The associated bond angle (between C18-O23-C24, where the numbering follows that of the sister structures in Figure 5.14) varies slightly (122.10-119.65 Å). The dihedral angles vary more significantly, as can be seen in Table 5.6. That is, the two cellobiose rings twist relative to each other to make room for the sodium ion. It is possible that the presence of Na^+ near the C6 atom also stabilizes the glycosidic bond or intermediate complex, thereby favouring ring opening over cleavage of the glycosidic bond.

5.6.2.3 Summary of *ab initio* Modelling Findings

The model presented in Section 5.5 relies on the existence of a biomass-metal ([BM]) intermediate complex which promotes degradation reactions. From the *ab initio* modelling it is clear that the alkali metals readily chelate to hydroxyl and ether groups in the biomass. Changes in bond lengths and angles are subtle, but indicate propensity for the orientation of the rings in the polymer chain to change. As shown in Figure 5.13, modification of the ring orientation is proposed to be a key step in activating cellulose towards cracking and hence, while not completely conclusive, the *ab initio* models do support this.

Table 5.6 Bond lengths of Na-cellobiose structures shown in Figure 5.15, with atom numbers similar to those in Figure 5.14.

	cellobiose Å	[Na-cellobiose]$^+$ (near C60H) Å	[Na-Cellobiose]$^+$ (near C20H) Å	Na-cellobiose ($C6O^-K^+$) Å	Na-cellobiose ($C2O^-K^+$) Å
Na-O bond lengths					
Na -O9	-	-	2.225	-	2.375
Na -O14	-	2.344	-	2.103	-
Na -O16	-	2.294	-	2.404	-
Na -O20	-	-	2.209	-	2.070
Na -O31	-	2.321	-	-	-
Glycosidic linkage					
C18-O23	1.401	1.416	1.389	1.437	1.396
C24-O23	1.429	1.432	1.437	1.418	1.439
Bond angle C18-O23-C24	120.2	122.084	120.938	121.048	119.648
Bond angle					
Dihedral angle C18-O23-C24-C26	62.9	62.708	66.515	60.167	69.991
Dihedral angle O16-C18-O23-C24	-114.3	-118.581	-111.541	-108.960	-119.673
C-(O (H)) bond lengths					
C7-O9	1.422	1.414	1.444	1.423	1.466
C11-O14	1.417	1.447	1.416	1.358	1.417
C17-O20	1.417	1.410	1.435	1.421	1.371
Ring bond lengths					
C17-C18	1.532	1.535	1.541	1.529	1.546
C17-C7	1.523	1.523	1.517	1.515	1.540
C7-C1	1.524	1.526	1.521	1.525	1.522
C1-C5	1.534	1.532	1.540	1.530	1.538
C5-O16	1.439	1.442	1.438	1.470	1.428
C18-O16	1.423	1.430	1.421	1.398	1.432
C26-C24	1.546	1.546	1.546	1.547	1.537
C24-C34	1.531	1.528	1.525	1.532	1.543
C34-C38	1.523	1.529	1.520	1.527	1.530
C38-C40	1.527	1.533	1.530	1.530	1.534
C40-O33	1.417	1.438	1.421	1.427	1.419
C26-O33	1.431	1.426	1.429	1.435	1.432

5.7 Conclusions

In the case of the slow pyrolysis of SRC willow, a Langmuir-Hinshelwood relation can indeed be applied to describe the catalytic effects of both potassium and sodium on biomass pyrolysis. The maximum reaction rate constant of 3.26 x 10^{-3} (sec^{-1}) and the potassium saturation constant of 0.56 wt%, and a maximum reaction rate constant of 3.27 x 10^{-3} (sec^{-1}) and the sodium saturation constant of 0.36 wt% can be accurately used to derive the pyrolysis reaction rate at 300 °C of a willow sample with a known potassium or sodium concentration. A levelling off effect is seen with regard to both metal concentrations and the apparent first-order reaction rate at ca. 4 wt% for K impregnated willow and 3.5% for Na impregnated willow, and this is attributed to maximum active site availability.

Alkali metals in biomass can be in the form of both metal salt particles and chelated species in the organic polymer. A clear acceleration in the pyrolysis reaction rate is observed for metal-impregnated SRC willow, and this acceleration is dependent upon the metal concentration. The Langmuir-Hinshelwood relation can be applied to describe the catalytic effect of these metals in the early stages of biomass pyrolysis. In this model, it is proposed that the metals not only catalyze the decomposition via chelation to hydroxyl and ether groups, but are also evolved during pyrolysis, and new active sites are generated by diffusion of metal ions from salt particles to chelation complexes. *Ab initio* (DFT method) modelling of possible chelated structures indicates that both potassium and sodium ions form multiple interactions with the hydroxyl and ether bonds in the cellulose structure. Structures with metal ions chelated at the C6 position in the ring have interactions with four oxygen atoms, while metal ions at the C2 position have interactions with only two oxygen atoms. Structures are more stable when K^+ and Na^+ can coordinate to more oxygen groups. Inter-molecular interactions were not modelled here. Nevertheless, in all the structures investigated, chelation of the alkali metal ions causes a change in the conformation of the rings (twisting) which may activate the structure towards ring opening.

Chapter 6
Effects of Mineral Content on Torrefied Fuel Characteristics and Quality

6.1 Introduction

As mentioned in Chapters 1 and 2, biomass is considered to be a low-grade fuel. Torrefaction, employed as a fuel pre-treatment technique, improves the fuel's quality, and energy density. Biomass has a lower energy density than coal and it is more difficult to mill due to its fibrous nature. The latter can result in solid handling problems, particularly when firing in existing power stations. The torrefaction process can not only improve the energy density of biomass, but also its grindability properties [11, 111-113]. To produce a torrefied fuel, biomass is heated at temperatures of <300 °C for a short period of time under an inert atmosphere, thereby mildly pyrolysing the fuel. This torrefied fuel is a solid which has properties intermediate between biomass and biochar. The properties of the torrefied biomass are largely determined by process conditions such as the reaction time and more importantly the final temperature [11, 111-114]. Although torrefaction has been shown to improve the biomass fuel properties, a challenge remains because of the large amount of alkali metals still remaining in the torrefied fuel. As stated in previous chapters, potassium, sodium, along with sulphur and chlorine, influence ash chemistry and the behaviour of the fuel in terms of its tendency to corrode equipment and cause slagging and fouling [10, 30]. The main causes of these undesirable slagging effects are attributed to the reactions of alkali metals with silica to form alkali silicates which melt or soften at temperatures as low as 700 °C, and the reactions of alkali metals with sulphur which form alkali sulphates on heat transfer and combustor surfaces [10]. Alkali metals are also important culprits in fouling because many of their salts are highly volatile. When high alkali biomass is utilized in high temperature furnaces and boilers, additives are required to help ameliorate the associated problems, sometimes with considerable additional expense. Demineralization of the fuel, by water washing for example, is

often a simple and effective method for removing a large fraction of the fuel's mineral content, thereby reducing the above mentioned ash problems [4, 33]. Although this approach may be expensive, it could be economically worth-while as a domestic fuel or where large amounts of fuel additives are being considered. In the former case, it may also aid in reducing the emission of inorganic aerosols which can have important impacts on air quality.

The behaviour of torrefied willow was previously examined by a number of techniques to further elaborate on the mechanism of combustion of torrefied biomass [115]. The work in this chapter explores the possibility of combining pre-treatment and torrefaction to create a commodity fuel from biomass. More specifically, the focus lies on determining the effects of minerals on torrefaction, as well as on the combustion and the ash behaviour of the torrefied material.

6.2 Materials, Sample Preparation, and Experimental Methods

The pre-torrefaction biomass feedstocks considered in this work consist of four single species of biomass, Short Rotation Coppice (SRC) willow, eucalyptus, Miscanthus, and wheat straw. The sample sizes ranged from 2x2 to 4x4 cm cuttings for the woody biomasses (SRC willow and eucalyptus) to slightly smaller (2x1 to 3x1 cm) cuttings of the straws (Miscanthus and wheat straw). Prior to some characterization work, however, a portion of the samples was finely milled using a Retsch PM100 ball mill to reduce the particle size of the test sample to <1mm, in accordance with test requirements.

6.2.1 Fuel Characterization

The C, H, N, and S contents of the fuels were determined by using a Thermo Scientific Flash 2000 Organic Elemental Analyzer. Past measurements of C,H, N content of fuels studied with this equipment have shown relative errors of ±1.2 wt%.

The proximate analyses of the samples were determined by following European standard methods (prCEN/TS 14780). As part of the proximate analysis, the moisture, volatile, and ash content of the fuels is measured separately. The moisture content was determined according to CEN/TS 14774-3:2004 and was carried out in a Carbolite MFS Oven in the presence of nitrogen. Volatile content was determined according to BS 1016-104.3:1998 and was carried out in a Carbolite VMF (+PID/CHIM) furnace. Finally the ash content of the fuel was determined by using a Carbolite OAF 10/1 furnace following the CEN European standard DD CEN/TS 14775:2004. The fixed carbon content is then calculated by subtracting the sum of the ash content, moisture content, and volatile matter content from 100. The relative errors for these measurements vary from fuel to fuel but at worst are less than ± 5 wt% and are generally $\leq \pm 1$ wt%.

Ash composition was measured by TES Bretby (www.esg.co.uk) using an ICP-OES method.

6.2.2 Ash Fusion Test

The Ash fusion tests (AFT) were performed using a Carbolite Digital Ash Fusion Furnace. A digital camera was fixed at the front of the furnace to capture images of the ash whilst it was heated at a controlled temperature rate. Also, there was illumination of the sample, so that low temperature melting behaviour could be detected. The ash itself was prepared according to European Standards; it was then ground in an agate mortar. A small amount of demineralized water was added to form an ash paste. The ash paste was then pressed into an upright cylinder stainless steel mould (5mm diameter x 5mm height). The sides of the mould were coated with a thin layer of petroleum jelly prior to the introduction of the ash paste to facilitate the removal of the test piece after it had been given time to properly set. Ash test pieces were then heated to 1500 °C at 7 °C/min heating rate. Images were recorded at temperature intervals of 5 °C for the temperature range of 550 to 1500 °C. The tests were performed in an oxidizing atmosphere with an air flow rate set to 50 ml/min. The key stage temperatures, which correspond to the beginning of shrinkage (SST), sample deformation temperature (DT), hemisphere temperature

(HT), and flow temperature (FT) were determined according to British Standards (DD CEN/TS15370 – 1:2006. Figure 6.1 shows a diagram of the phases that occur during the ash melting process.

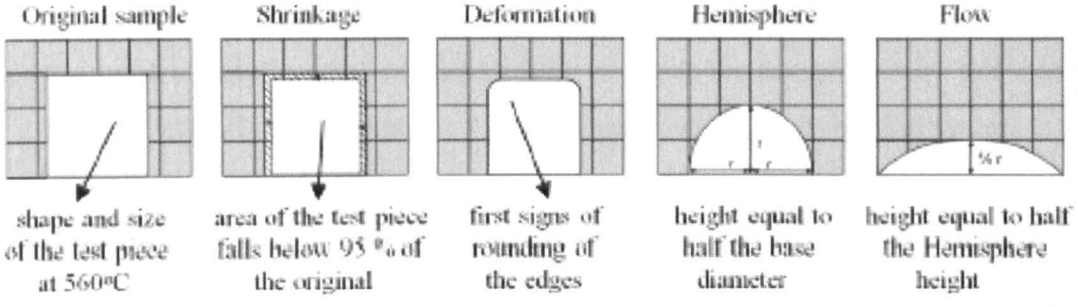

Figure 6.1 Phases that occur during ash melting [116].

6.2.3 Chemical Fractionation

A chemical fractionation procedure, described by Miles et al. in a report for the NREL [117], was modified and employed to progressively remove more of the inherent metal content in the fuels. It consists of three main stages, the first involving washing in de-ionized water, followed by washing in a 1 M ammonium acetate solution, and ultimately by washing the fuel in a solution of 1 M hydrochloric acid.

During the first water washing stage, the sample was immersed in de-ionized water and agitated over-night (20 hours) at room temperature. This sample was then filtered and the filtrate was saved for analysis. The water washed sample was then introduced into the second stage where the sample was agitated in the ammonium acetate solution at room temperature for 3 (60 hours) consecutive days. Again, the sample was filtered and washed with more de-ionized water, and the waste solution was saved for analysis. The fuel sample was then ready for the third and ultimate stage of washing in a 1 M hydrochloric acid solution. The sample in the HCl solution was heated in a closed vessel with cold water reflux (to prevent evaporation of the acid) to a steady temperature of 70 °C and was continuously stirred at this

temperature for another two days (40 hours). The sample was again filtered and rinsed with de-ionized water.

The main deviation from the procedures described by Miles et al. [117] was the fact that the fuel was not pulverized prior to the washings. The biomass was instead kept to ca. 3-4 cm chippings as that is more in keeping with the expected form prior to industrial torrefaction. Due to the larger size of the fuel particles, a higher volume of solution was needed to fully immerse the sample batch. For every 60 g of fuel washed, approximately 1 L of liquid was utilized, be that water, 1 M ammonium acetate, or 1 M HCl.

In the water leaching, simple ionic salts such as alkali chlorides, dissolve very easily. The second solution of ammonium acetate serves as an ion exchanger. That is to say that the inorganic elements in the fuel bound to organic structures in the biomass with an ionic bond will exchange an ion with the solution. Finally, the HCl solution typically dissolves alkaline earth carbonates, sulphates, and sulphides. The residue remaining after the three consecutive leachings is seen to contain silicates and elements bound to the organic matrix with a covalent bond. It has been seen that over 90% of the potassium in biomass occurs as water soluble or ion exchangeable material [117].

The leachates collected from the washings, and the subsequent fuels were extensively analyzed both before and after torrefaction. The ash produced from these samples was studied to determine any improvements in fuel properties due to altered mineral content. First order reaction kinetics from TGA pyrolysis of these fuels were also calculated.

6.2.4 Ion Chromatography

Ion chromatography, using a Dionex DX-100 ion chromatograph, was performed on the leachates of the chemical fractionation procedure to determine the metal ion content that has been removed from the fuels. This particular chromatograph was equipped with a conductivity detector. The eluent for the anions was a mixture of Na_2CO_3 (8.0 mM) and $NaHCO_3$ (1.0 mM), while the eluent for the cations was methyl sulphonic acid solution (1.0 nN). The column used to separate

the cations is positively charged (Dionex IonPac CS12A, 250x4 mm) and the column used to separate the anions is negatively charged (Dionex IonPac AS14A, 250x4 mm). The instrument was pre-calibrated with a series of standard solutions. The anion system was calibrated with solutions of fluoride, chloride nitrite, bromide, nitrate, phosphate and sulphate at 0.5, 1.0, 2.0, 5.0, 10.0, 20.0, and 40 ppm. The cation system was calibrated with lithium, sodium, ammonium, potassium, calcium and magnesium at the same concentrations up to 20 ppm.

6.2.5 Torrefaction

Approximately 50-100 g of dried sample was placed into a reactor tube under a nitrogen flow of 1.2 L/min at standard temperature and pressure. The heating profile experienced by the sample was recorded by three thermocouples placed at 20 cm intervals inside the length of the reactor tube to allow measurement of the inert gas temperature before the sample (T1) and the temperature within the sample (T2), and the temperature after the sample (T3). The reactor tube resided within a three zone horizontal tube furnace that was 750 mm in length with an internal diameter of 75 mm. The heated length was approximately 575 mm. Detailed schematics of the reactor assembly can be found in [118]. The sample was first heated at 10 °C/min to 150 °C and held at this temperature for 50 minutes, before being taken to a final temperature (T_{max}) of 290 °C, again at a heating rate of 10 °C/min, and was held at this temperature for a residence time of (i.e. time with T >200 °C) 60 minutes. This is perhaps at the extreme of residence times typically used in torrefaction. The reason for this is so that differences between fuels and their pre-treatments could be exaggerated. A typical torrefaction heating profile (as recorded by the thermocouples and logging software) for these experiments is shown in Figure 6.2.

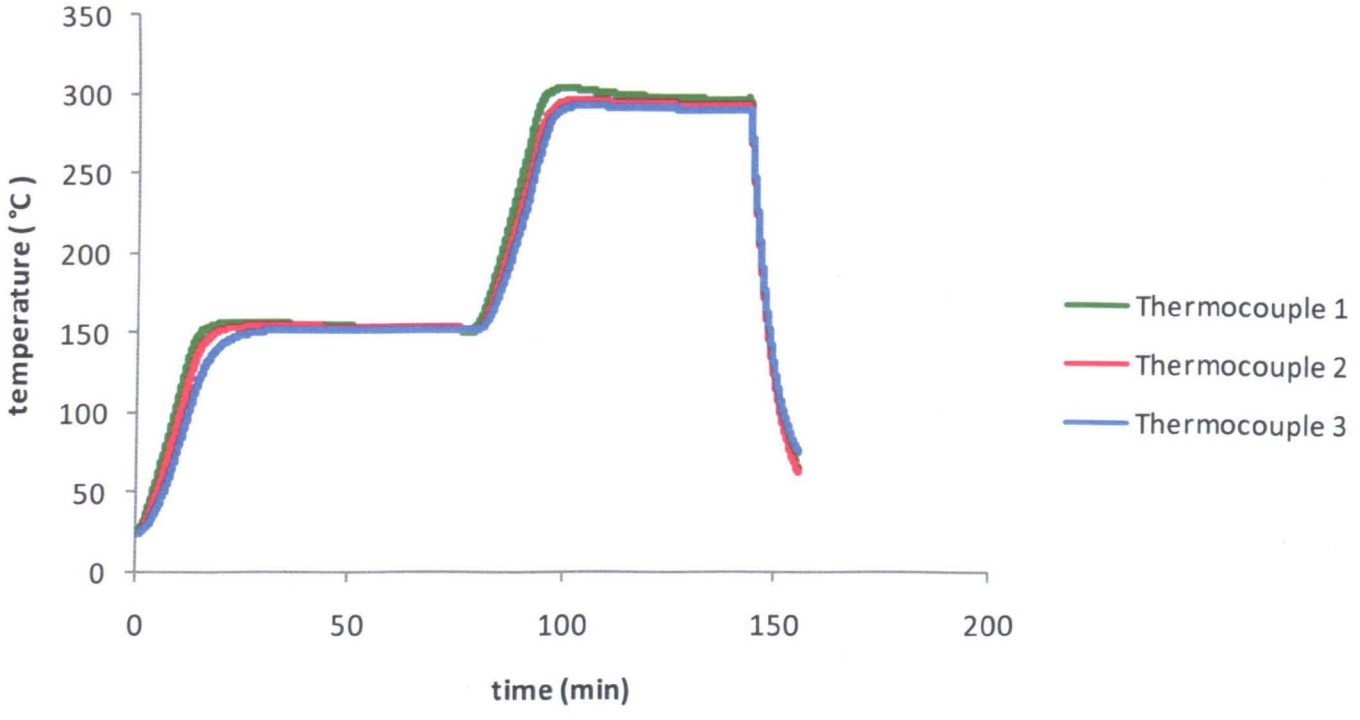

Figure 6.2 Typical torrefaction heating profile.

6.2.6 Thermogravimetric Analysis

The slow pyrolysis of all the fuels studied in this work (including untreated, torrefied, and washed and torrefied) was carried out using a Netzsch STA 449C Jupiter simultaneous analyzer. For these tests, approximately 10 mg of sample was placed in the microbalance and heated at a rate of 10 °C/min to 105 °C. The sample was held at this temperature for 10 minutes and was then heated to 550 °C. Pyrolysis was carried out under flowing helium set to a flow rate of 50 ml/min.

Accurate mass yield measurements could not be made with samples torrefied with the main torrefaction rig (described in Section 6.2.5) as many of the smaller particles became trapped in the quartz wool used to plug either end of the reaction tube. Therefore, TGA with heating profiles set to mimic torrefaction conditions was conducted on all of the fuel samples to obtain more accurate mass yield values.

6.3 Results

The four fuels considered in this work were analyzed both in their untreated state, and also after torrefaction. The samples were also subject to a series of washings and torrefaction reactions thereafter. A diagram showing the sequence of experiments is given in Figure 6.3. This sequence was repeated for each of the four fuels studied.

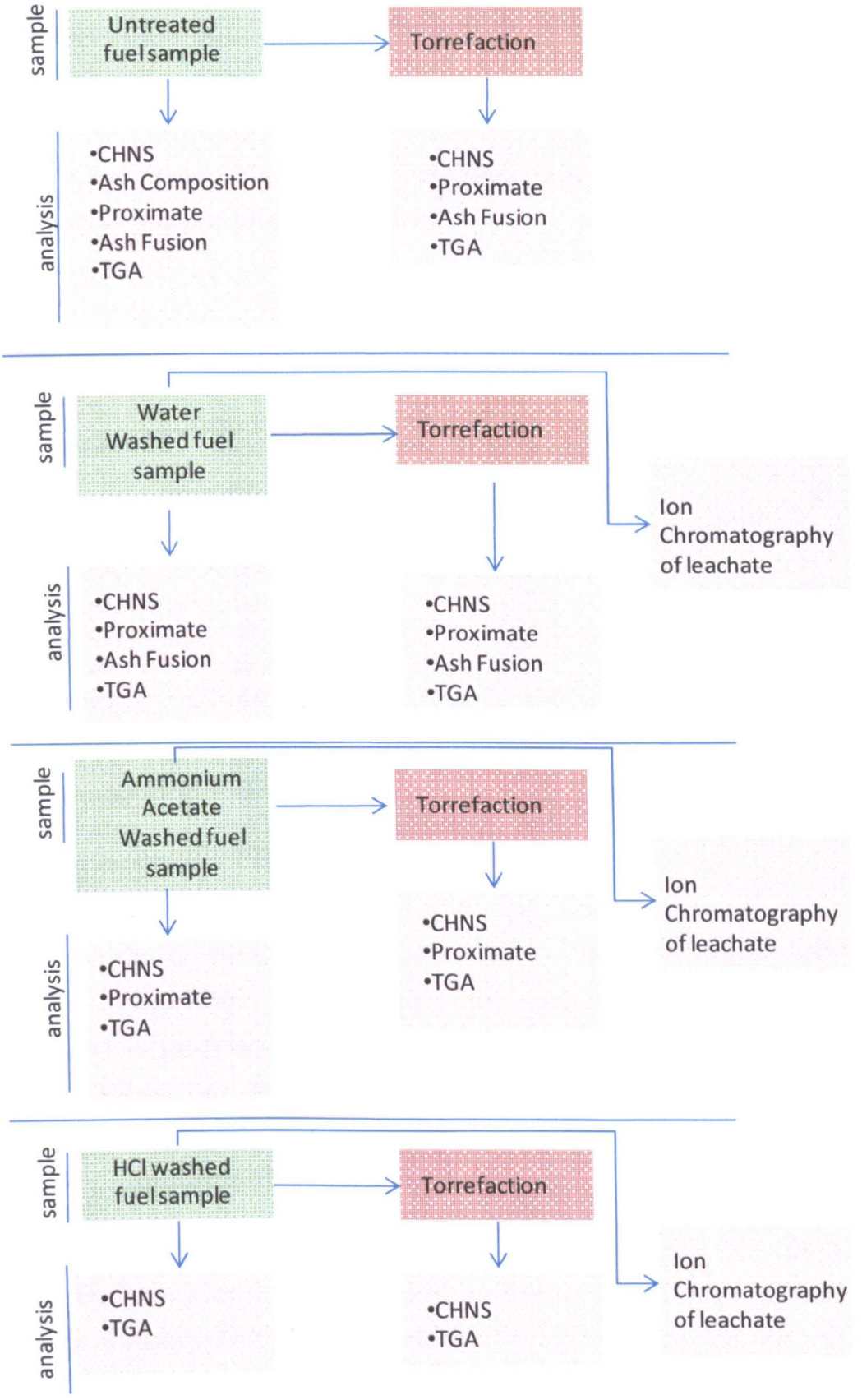

Figure 6. 3 Sequence of experiments.

6.3.1 Untreated Fuel Properties

As indicated in Figure 6.3, the untreated fuels were analyzed for their ash composition, which are listed in Table 6.1.

Table 6.1 Ash composition of untreated fuels (determined by TES Bretby, part of Environmental Scientifics Group).

Elemental Oxide (composition wt % in the ash)	Willow	Eucalyptus	Miscanthus	Wheat Straw
SiO_2	2.2	2.2	52.4	43.5
Al_2O_3	0.5	0.3	0.3	0.5
Fe_2O_3	0.4	1.3	0.4	0.3
TiO_2	<0.1	<0.1	<0.1	<0.1
CaO	33.8	30.6	9	7.7
MgO	4.0	2.4	1.2	1.2
Na_2O	1.2	1.7	0.7	0.1
K_2O	18.1	19.0	16.3	20.0
Mn_3O_4	0.4	0.5	0.2	<0.1
P_2O_5	16.1	3.1	7.2	1.7
SO_3	5.6	2.8	4.5	3.2

The ash composition of a fuel can be used to determine slagging and fouling indices. These indices were originally developed for coal and have been quite successful in predicting deposition problems associated with higher rank coals. Indices derived from analysis of lower rank coals have been less successful in predicting slagging and fouling problems. Nevertheless, these indices have been applied to various types of biomass [116, 119, 120].

A fuel's fouling tendency is predicted by the Alkali Index (AI). Base to acid ratios ($R_{b/a}$) are used to predict slagging tendencies. The AI is expressed as the amount of alkali oxide content in the fuel per unit energy of the fuel and is shown in Equation 6.1:

$$AI = \frac{1}{Q} Y_f^a (Y_{K_2O}^a + Y_{Na_2O}^a) \quad \text{.....Eq.(6.1)}$$

where Q is the HHV on a dry basis, Y^a_f is the fraction of ash (on a dry basis) in the fuel, and Y^a_{K2O}, and Y^a_{Na2O} are the fractions of K_2O and Na_2O present in the ash. If the value of AI >0.17 kg/GJ, then fouling is deemed probable. For AI > 0.34, fouling is virtually certain.

$R_{b/a}$ is calculated according to Equation 6.2:

$$R_{b/a} = \frac{Fe_2O_3+CaO+MgO+K_2O+Na_2O}{SiO_2+TiO_2+Al_2O_3} \quad \text{.....Eq. (6.2)}$$

A $R_{b/a}$ value of < 0.5 indicates a low slagging risk. If $R_{b/a}$ > 1, then there is a severe risk of slagging.

The fouling and slagging indices for the four fuels studied in this chapter have been calculated and are given in Table A.3 in the Appendix.

The C, H, and N contents and the calculated HHVs (on a dry basis) of the untreated samples are detailed in Table 6.2. Measurements were also made for S, however, they were very small (< 0.001 wt%) and these quantities are not recorded here. The HHVs were calculated according to an approximation given by Friedl et al. [121] (Eq. 6.3). This approximation is an average of two other approximations: one based on an ordinary least squares regression (OLS), and the other based on a partial least squares regression (PLS). Both methods were calibrated using 122 different biomass samples. These methods have since been validated through application by Bridgeman et al. [11].

$$HHV=3.55C^2-232C-2230H+51.2C\times H+131N+20{,}600 \quad \text{.....Eq. (6.3)}$$

Table 6.2 Nitrogen, carbon, and hydrogen content on a dry basis, and HHV (d.b.) of untreated fuels.

untreated samples	N (wt %)	C (wt %)	H (wt %)	HHV (MJ/kg)
willow	0.47	45.27	6.16	19.9
eucalyptus	0.34	41.99	5.23	22.9
Miscanthus	0.11	45.96	5.71	19.1
wheat straw	0.35	42.84	5.87	18.1

Results of the proximate analyses of the untreated fuels are given in Table 6.3.

Table 6.3 Proximate analysis for the untreated fuels.

Untreated biomass samples	Moisture (wt%)	Volatiles (wt% d.a.f.)	Ash (wt%)	Fixed carbon (wt% d.a.f.)
willow	8.5	81.8	1.8	18.2
eucalyptus	24.3	77.3	3.2	22.8
Miscanthus	4.5	86.4	3.7	13.6
wheat straw	5.9	83.1	9.2	16.9

6.3.2 Washed Fuel Properties

The fuels were washed successively by deionised water, ammonium acetate and hydrochloric acid according to the chemical fractionation procedure described in Section 6.2.3. The results from the ultimate and proximate analyses conducted on these washed fuels are shown in Tables 6.4, and 6.5. Ion chromatography was used to determine the concentrations of metals leached as a result of the water washings, and these numbers are given in Table 6.6. Ion chromatography was also performed on the leachates of the ammonium acetate and hydrochloric acid treatments, however these results gave large uncertainties in metal concentrations and are

therefore not reported. The changes to the fuel compositions as a result of washing are discussed in Section 6.4.1.

Table 6.4 Nitrogen, carbon, and hydrogen content, and HHV of washed fuels (d.b.).

water washed samples	N (wt %)	C (wt %)	H (wt %)	HHV (MJ/kg)
willow	0.26	45.40	6.12	19.6
eucalyptus	0.24	47.17	5.92	19.9
Miscanthus	0.23	45.74	5.64	19.1
wheat straw	0.29	42.13	5.87	17.8
ammonium acetate washed samples				
willow	0.96	46.41	6.05	20.0
eucalyptus	0.53	46.30	6.08	19.7
Miscanthus	0.70	45.36	6.18	20.0
wheat straw	0.38	42.55	5.99	18.0
HCl washed samples				
willow	0.79	47.19	5.99	20.1
eucalyptus	0.21	46.56	6.25	20.1
Miscanthus	0.08	30.25	4.64	20.2
wheat straw	0.24	41.23	5.97	18.1

Table 6.5 Proximate analysis for the washed fuels.

Water washed biomass samples	Moisture (wt%)	Volatiles (wt% d.a.f.)	Ash (wt%)	Fixed carbon (wt% d.a.f.)
willow	7.4	84.4	1.7	15.6
eucalyptus	5.3	85.8	1.0	14.2
Miscanthus	5.2	85.5	1.4	14.5
wheat straw	6.2	85.6	7.0	14.4
Ammonium acetate washed biomass samples				
willow	6.7	83.8	1.1	16.2
eucalyptus	5.8	85.7	0.6	14.3
Miscanthus	8.6	86.3	1.1	13.7
wheat straw	6.1	87.1	4.3	12.9
HCl washed biomass samples				
willow	5.7	77.3	n.a.	22.7
eucalyptus	7.0	81.7	n.a.	18.3
Miscanthus	39.1	73.8	n.a.	26.2
wheat straw	9.3	78.0	n.a.	22.1

*There was no measurable ash for the HCl treated samples.

Table 6.6 Concentrations of metals leached from washings of biomass samples.

		% of metal leached due to water washing
Willow	Sodium	30
	Potassium	46
	Magnesium	14
	Calcium	3
	Phosphate	56
	Sulphate	10
eucalyptus	Sodium	60
	Potassium	45
	Magnesium	18
	Calcium	4
	Phosphate	27
	Sulphate	8
Miscanthus	Sodium	53
	Potassium	62
	Magnesium	56
	Calcium	19
	Phosphate	49
	Sulphate	33
wheat straw	Sodium	92
	Potassium	54
	Magnesium	32
	Calcium	12
	Phosphate	0.2
	Sulphate	21

6.3.3 Torrefied Fuel Properties

Torrefaction according to the methods described in Section 6.2.5 was performed on all of the untreated and washed fuels. Tables 6.7 and 6.8 list the ultimate and proximate results obtained for these torrefied fuels.

Table 6.7 Nitrogen, carbon, and hydrogen content, and HHV of torrefied fuels (d.b.).

untreated & torrefied samples	N (wt %)	C (wt %)	H (wt %)	HHV (MJ/kg)
willow	0.67	58.99	5.08	23.37
eucalyptus	0.35	59.87	5.09	23.73
Miscanthus	0.21	61.24	5.04	24.30
wheat straw	0.66	55.93	4.37	21.59
water washed & torrefied samples				
willow	0.63	56.55	5.66	22.68
eucalyptus	0.38	56.93	5.46	22.68
Miscanthus	0.28	54.57	5.40	21.59
wheat straw	0.65	54.24	5.25	21.42
ammonium acetate washed & torrefied samples				
willow	1.34	55.59	5.47	22.22
eucalyptus	0.59	55.95	5.53	22.32
Miscanthus	0.37	53.88	5.45	21.34
wheat straw	0.46	50.98	5.13	20.01
HCl washed & torrefied samples				
willow	0.79	56.87	5.26	22.58
eucalyptus	0.23	51.24	5.69	20.30
Miscanthus	0.16	51.46	5.71	20.40
wheat straw	0.40	51.82	5.00	20.28

Table 6.8 Proximate analysis for the torrefied fuels.

torrefied biomass samples	Moisture (wt%)	Volatiles (wt% d.a.f.)	Ash (wt%)	Fixed carbon (wt% d.a.f.)
willow	0.7	60.0	3.5	40.2
eucalyptus	0.4	58.5	3.5	41.6
Miscanthus	1.4	57.6	3.0	42.5
wheat straw	1.0	49.8	13.1	50.2
Water washed & torrefied biomass samples				
willow	3.8	68.8	2.7	31.2
eucalyptus	2.7	67.6	1.4	32.4
Miscanthus	3.5	70.3	2.2	29.8
wheat straw	4.1	64.1	7.4	35.9
Ammonium acetate washed & torrefied biomass samples				
willow	2.0	66.2	1.7	33.8
eucalyptus	1.2	70.2	1.0	29.8
Miscanthus	3.0	71.7	1.7	28.3
wheat straw	3.8	67.5	10.1	32.5
HCl washed & torrefied biomass samples				
willow	2.9	62.3	n.a.	37.7
eucalyptus	3.8	75.3	n.a.	24.7
Miscanthus	3.2	75.6	n.a.	24.4
wheat straw	2.5	58.9	n.a.	41.1

*There was no measurable ash for the HCl treated samples.

The mass (η_M) and energy (η_E) yields were calculated for the torrefaction of all samples according to Equations 6.4 and 6.5 [122], respectively, and are listed in Table 6.9.

$$\eta_M = \left(\frac{M_{torrefied}}{M_{pre-torrefaction}} \right) \times 100 \quad \text{.....Eq. (6.4)}$$

$$\eta_E = (\eta_M) \times \left(\frac{HHV_{torrefied}}{HHV_{pre-torrefaction}} \right) \times 100 \quad \text{.....Eq. (6.5)}$$

where $M_{pre\text{-}torrefaction}$ is the mass of the sample prior to torrefaction, and $M_{torrefied}$ is the mass of the sample after the fuel has been torrefied. $HHV_{pre\text{-}torrefaction}$ is the higher heating value of the fuel prior to torrefaction and $HHV_{torrefied}$ is the higher heating value post torrefaction.

Table 6.9 Mass and energy yields for the torrefaction of all samples.

untreated samples	η_M	η_E
willow	51	60.4
eucalyptus	52.5	54.6
Miscanthus	38	49.4
wheat straw	39.2	47.4
water washed samples		
willow	52	63.3
eucalyptus	54.8	64.8
Miscanthus	55.6	65.7
wheat straw	52.1	66.0
ammonium acetate washed samples		
willow	60	68.3
eucalyptus	56.7	65.3
Miscanthus	56.4	62.4
wheat straw	47.7	55.4
HCl washed samples		
willow	62.1	72.5
eucalyptus	52	54.9
Miscanthus	46.3	48.6
wheat straw	49.2	56.8

6.3.4 Pyrolysis Kinetics

To examine the impact of pre-treatment on biomass reactivity, pyrolysis studies were performed using the TGA analyzer, and 1st order reaction kinetics were used to derive activation energies, E (kJ/mol), and pre-exponential factors, A (s^{-1}), calculated according to the Senum and Yang approach discussed in Chapter 3, and are listed in Table 6.10. The kinetics were calculated over the main devolatilisation peak (generally between 300-360 °C for the un-torrefied fuels, and slightly higher for torrefied fuels). Figures 6.4-6.7 show Arrhenius plots calculated using this data. Reaction rates at 300 °C for all the samples are given in Figure 6.8. The TGA weight loss profiles for the pyrolysis of these samples are shown in the Appendix. For untreated wheat straw (Figure A.6), it is clear that the pyrolysis of the torrefied fuel is very different to the analogous results for the other three samples. In fact, as discussed later, the untreated wheat straw is so reactive that the torrefaction process progresses much farther under the set conditions compared to the others. Consequently, the volatile content is low, and the decomposition reaction being probed in the pyrolysis experiments on the torrefied wheat are expected to be very different also. As a result, the TGA data could not be modelled well using a first-order approach.

Table 6.10 1st order reaction kinetics for biomass samples.

untreated samples	lnA (s^{-1})	E (kJ/mol)
willow	2.63	46.0
eucalyptus	3.59	50.4
miscanthus	7.64	67.5
wheat straw	7.64	67.5
untreated & torrefied samples		
willow	7.34	74.2
eucalyptus	7.35	73.6
miscanthus	7.33	74.1
wheat straw	n.a.	n.a.
water washed samples		
willow	2.92	47.3
eucalyptus	3.76	51.6
miscanthus	4.82	56.1
wheat straw	7.63	68.3
water washed & torrefied samples		
willow	12.01	96.0
eucalyptus	10.48	88.4
miscanthus	11.76	95.0
wheat straw	7.38	72.6
ammonium acetate washed samples		
willow	2.03	43.2
eucalyptus	3.08	47.9
miscanthus	4.24	52.6
wheat straw	4.84	55.0
ammonium acetate washed & torrefied samples		
willow	15.53	114.3
eucalyptus	9.34	83.0
miscanthus	10.12	86.0
wheat straw	11.02	89.8
HCl washed samples		
willow	1.79	42.9
eucalyptus	11.14	87.7
miscanthus	7.62	68.8
wheat straw	4.65	54.9
HCl washed & torrefied samples		
willow	24.03	156.6
eucalyptus	20.06	133.7
miscanthus	7.38	70.8
wheat straw	7.36	72.9

*The untreated and torrefied wheat straw sample had unusual TGA results and therefore the 1st order reaction kinetics could not be accurately determined.

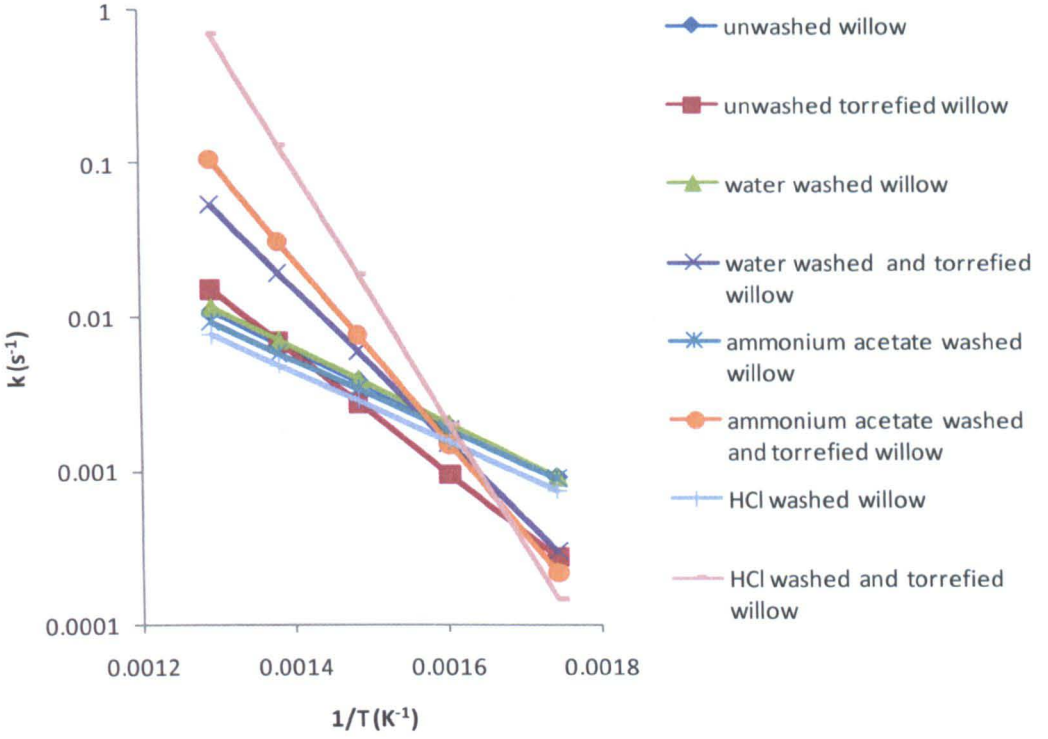

Figure 6.4 Reaction rates at various temperatures (300-550 °C) for the slow pyrolysis of willow samples.

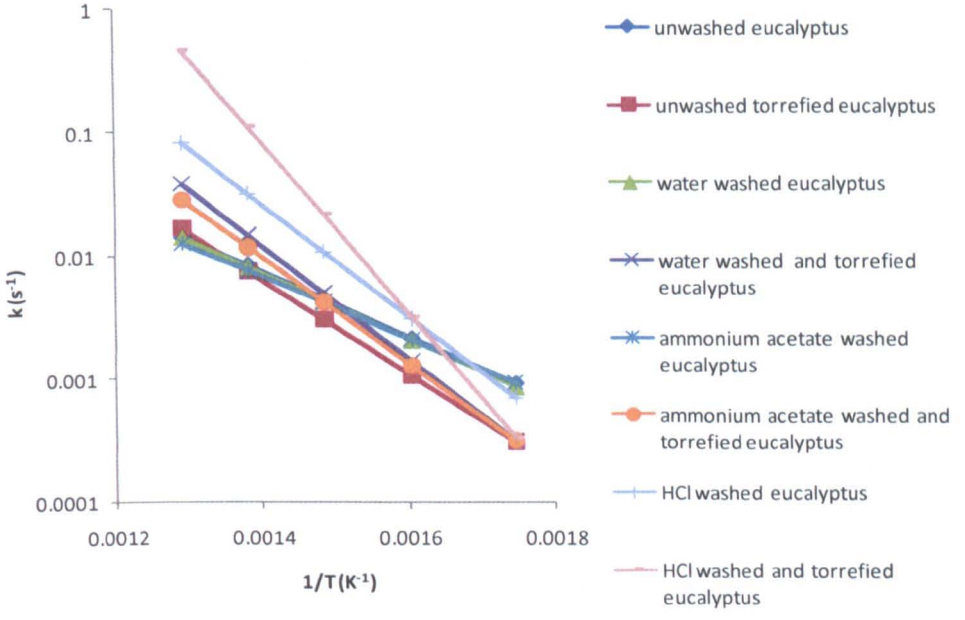

Figure 6.5 Reaction rates at various temperatures (300-550 °C) for the slow pyrolysis of eucalyptus samples.

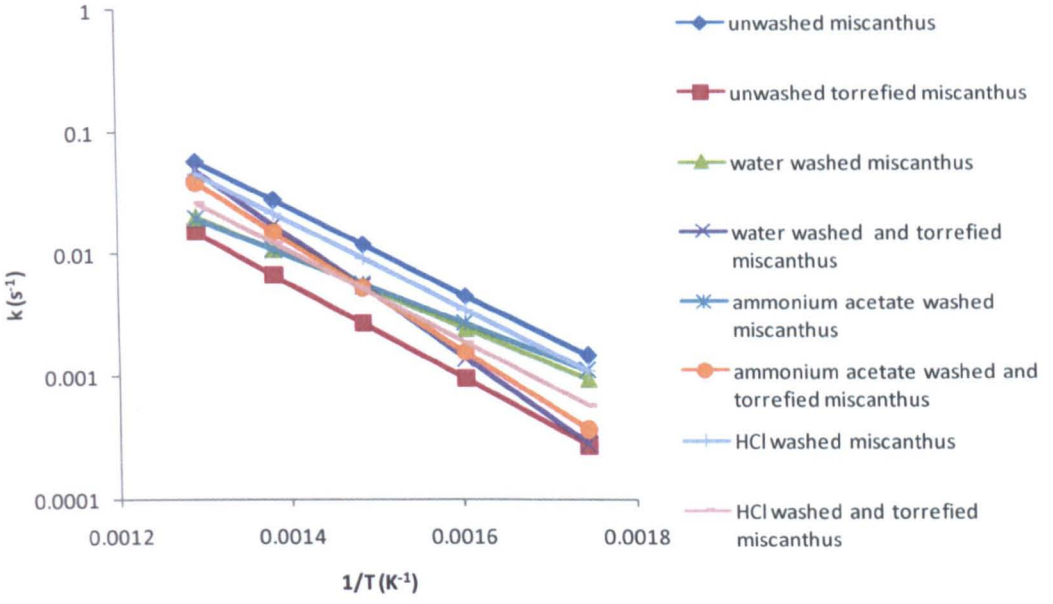

Figure 6.6 Reaction rates at various temperatures (300-550 °C) for the slow pyrolysis of Miscanthus samples.

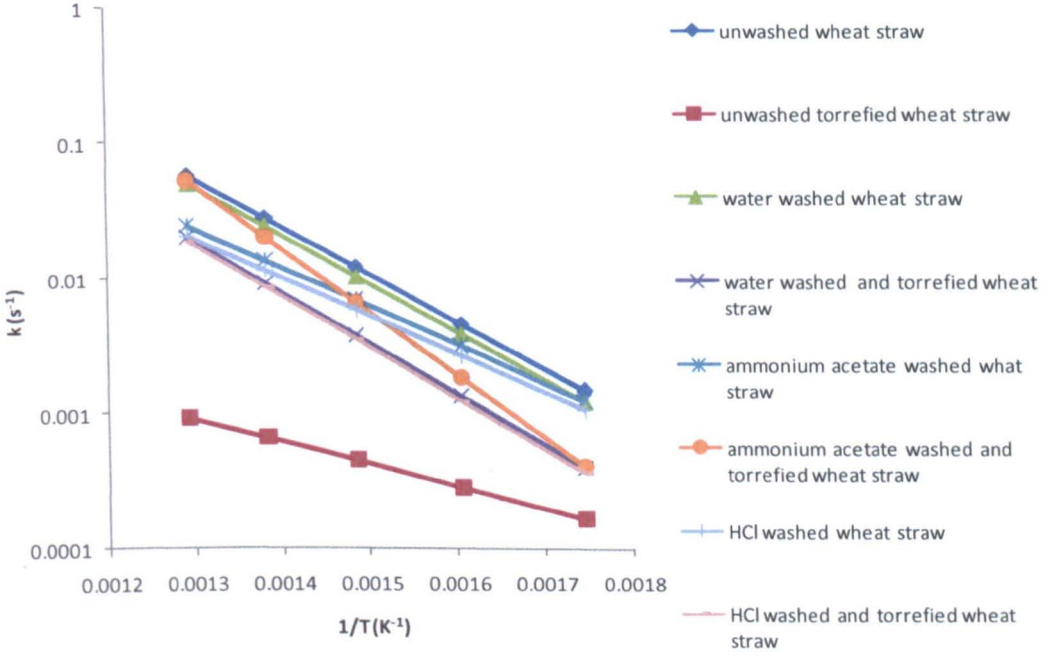

Figure 6.7 Reaction rates at various temperatures (300-550 °C) for the slow pyrolysis of wheat straw samples.

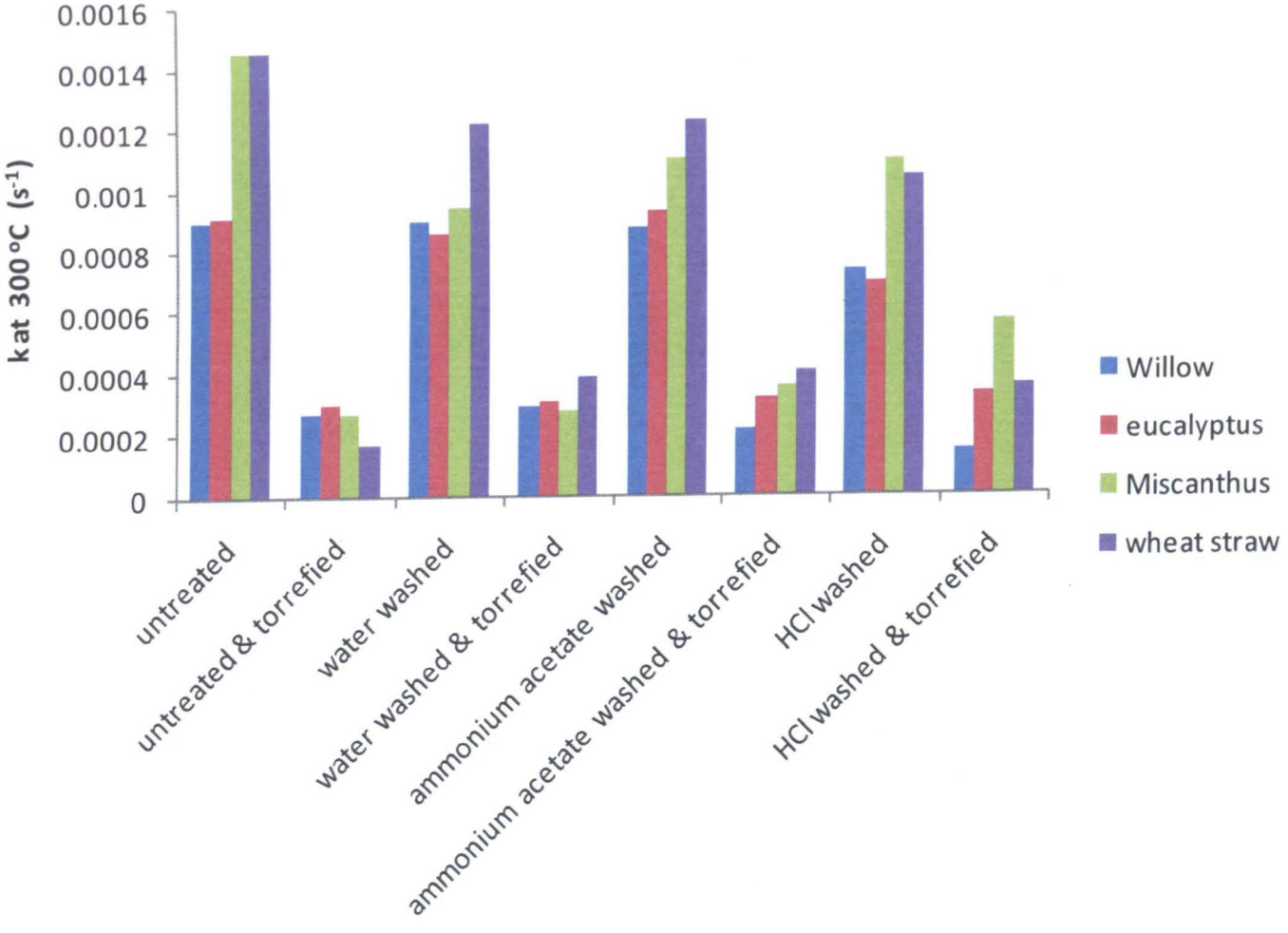

Figure 6.8 Slow pyrolysis reaction rates at 300 °C for all samples.

6.3.4 Ash Characteristics of the Fuels

The ash content of the fuels (given in Tables 6.3, 6.5, and 6.8) is shown in Figure 6.9. The HCl washed samples did not contain measurable quantities of ash and therefore these results are not reported.

Figure 6.10 shows the flow temperature obtained through the Ash Fusion Tests performed on the samples. Again, as no ash was found in the HCl washed samples, these numbers are not present in the figure. Similarly, very little ash remained in the ammonium acetate washed samples, and this amount was not sufficient for making the ash cylinders necessary for the ash fusion test. Table 6.11 contains a list of all four characteristic temperatures of the ash fusion test for the tested samples. In some cases, it was not possible to determine the temperatures as certain samples swelled prior to shrinking. Experiments comparing the AFT with thermogravimetric data were previously conducted and it was hypothesized that the swelling in similar biomass samples could be due to CO_2 and SO_2 evolution from the sample during the AFT [123]. An example of the recorded images at these characteristic temperatures can be seen in Figure 6.11. The cylinders in this figure are made from water washed Miscanthus.

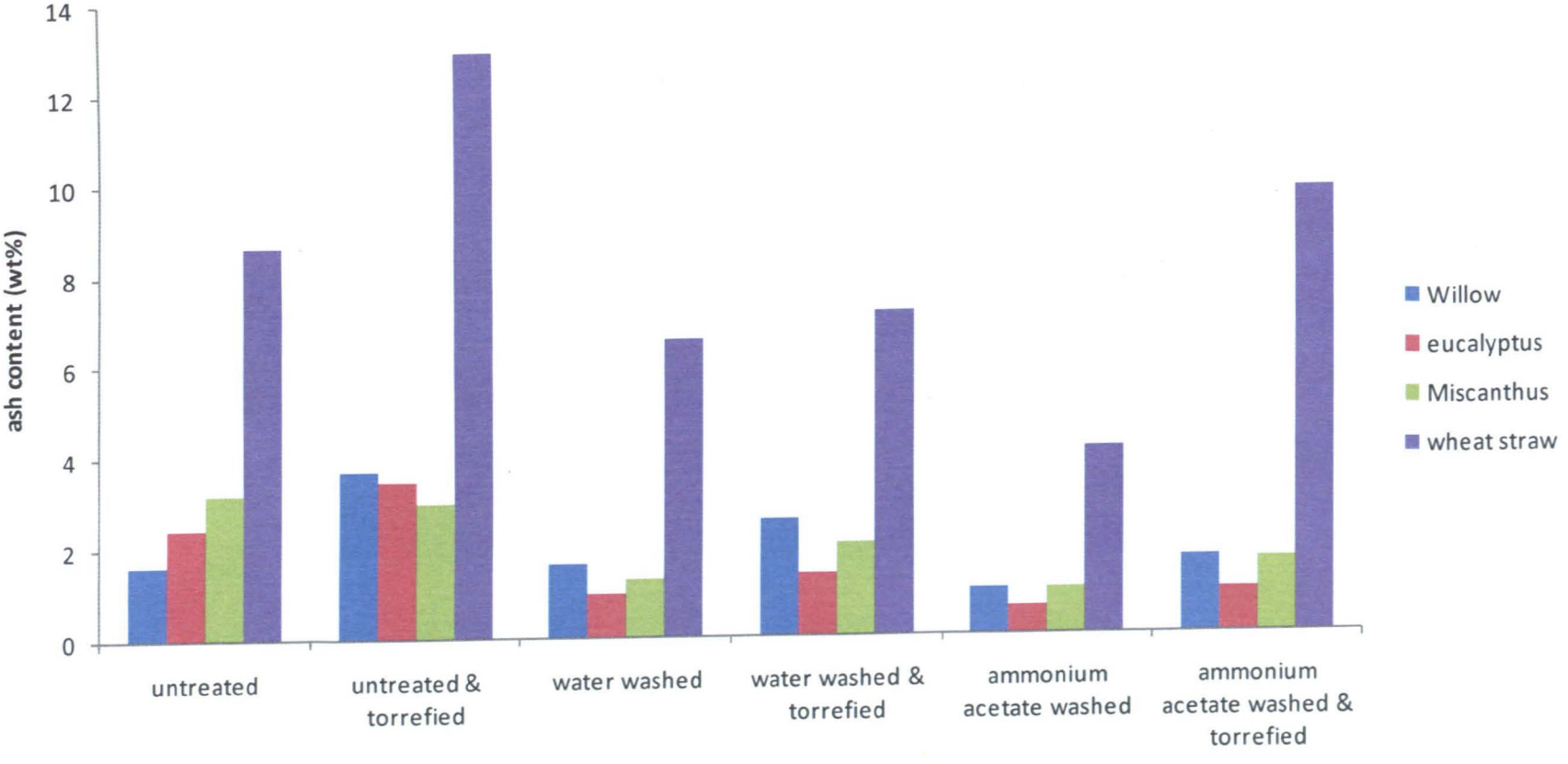

Figure 6.9 Ash content of biomass fuels.

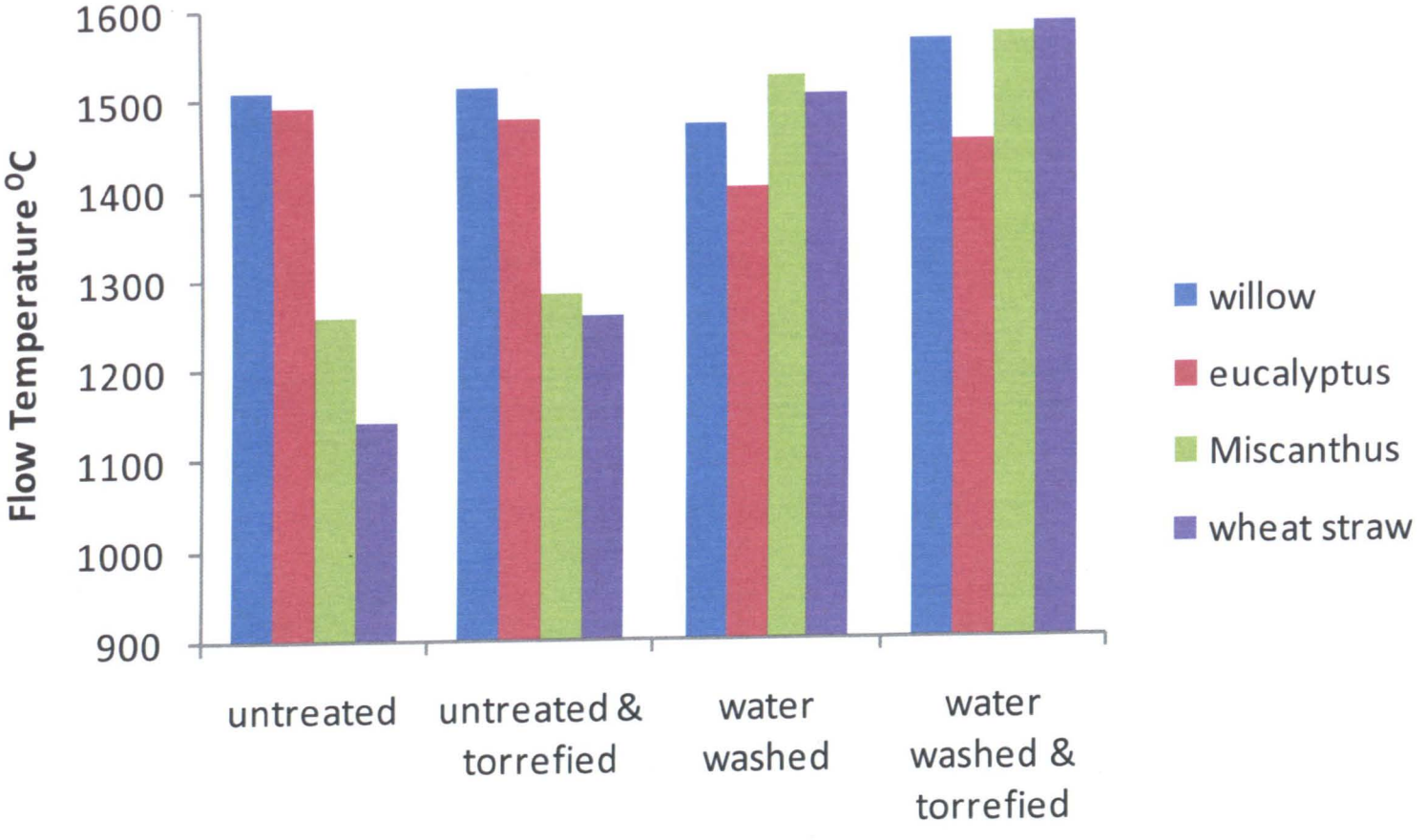

Figure 6.10 Ash flow temperatures of various biomass samples.

Table 6.11 AFT temperatures for various biomass samples.

untreated samples	SST (°C)	DT (°C)	HT (°C)	FT (°C)
willow	1053	1300	cylinder holds shape until FT then immedeately collapses	1510
eucalyptus	n.a.	1470	1480	1493
miscanthus	cylinder swelled at 870, then began shrinking at 1050	n.a. due to swelling	1202	1260
wheat straw	cylinder swelled at 870, then began shrinking at 970	n.a. due to swelling	1095	1140
untreated & torrefied samples				
willow	1055	n.a.	1510	1515
eucalyptus	1120	cylinder holds shape until FT then immedeately collapses	cylinder holds shape until FT then immedeately collapses	1480
miscanthus	cylinder swelled at 870	n.a. due to swelling	1210	1285
wheat straw	cylinder swelled at 830	n.a. due to swelling	n.a. due to swelling	1260
water washed samples				
willow	n.a.	n.a.	1465	1470
eucalyptus	n.a. due to small size of cylinder	n.a. due to small size of cylinder	1380	1400
miscanthus	980	1305	1490	1525
wheat straw	1030	n.a.	1500	1505
water washed & torrefied samples				
willow	n.a. due to shrinking followed by swelling followed by shrinking	1420	1548	1563
eucalyptus	1220	cylinder holds shape until FT then immedeately collapses	cylinder holds shape until FT then immedeately collapses	1450
miscanthus	cylinder swelled at 870	n.a. due to swelling	1527	1570
wheat straw	<850	1505	>1580	>1580

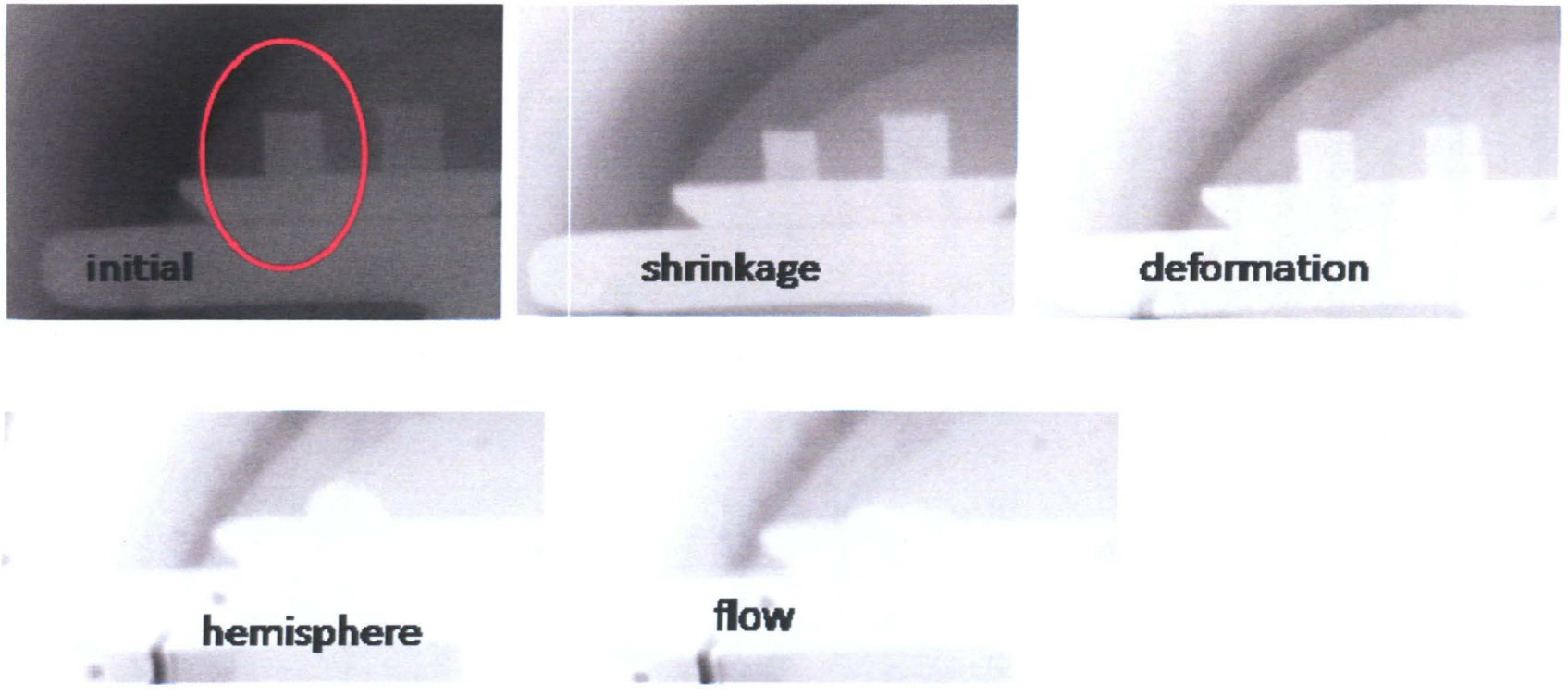

Figure 6.11 AFT images for water washed Miscanthus.

6.4 Discussion – Effects of Pretreatment

6.4.1 Effects of Pretreatment on Fuel Properties

By comparing the ultimate analyses of the fuels before and after the washings (Tables 6.2 and 6.4, respectively), it appears that the washing steps have little effect upon the carbon and hydrogen amounts. However, changes in the nitrogen content are significant. It is clear that the ammonium acetate washing stage increases the nitrogen content for both the washed and the washed and torrefied sample. Presumably this is due to the inclusion of ammonium nitrate into the biomass samples.

The results of the proximate analysis of the untreated fuels (Table 6.3) show that the ash content of the four fuels increases in the following order: willow < eucalyptus < Miscanthus < wheat straw. After the first washing (water washing, Table 6.5), the ash of all the fuels is reduced by approximately 50%. Although further washing with ammonium acetate also reduces the ash content, the reductions are small (0.5 wt% reduction). Washing appears to have a small effect upon the volatile content of the fuel, where a slight increase in volatile content is noted when comparing the untreated with the washed fuels.

Analysis of the ash composition of the fuels (Table 6.1) indicated that the woody biomass samples contain high calcium levels. The potassium levels for the untreated fuels were: willow 3000 ppm, eucalyptus 3000 ppm, Miscanthus 6000 ppm, wheat straw 8000 ppm. The leachates in Table 6.6 are consistent with these compositions. In the water washed samples, the potassium levels leached from the fuels are approximately proportional to the original metal content. When calcium removal is considered, it appears that more calcium is retained during the washing by the woody samples (willow and eucalyptus) than by the herbaceous samples (Miscanthus and wheat straw) as compared to the calcium content in the ash (Table 6.1). The retention of the calcium and loss of the potassium influences the ash melting behaviour and the pyrolysis reaction kinetics, and is discussed later.

6.4.2 Effects of Pretreatment on Torrefaction

Ultimate analysis results indicate that torrefaction increases the carbon and the nitrogen content of the fuels, and reduces the amount of hydrogen present. Proximate analysis results show that the ash content of the willow, eucalyptus, and wheat straw samples increases; that of the Miscanthus, however, decreases slightly.

The ash content of the water washed fuels is unchanged upon torrefaction, and for ammonium acetate washed fuels, the ash content is reduced slightly upon torrefaction. The general trend is for washing to reduce ash content and for torrefaction to increase ash content. This is because in torrefaction there is a reduction in the amount of volatiles in the fuel, and hence ash is concentrated in the solid residue.

Table 6.9 lists the mass and energy yields for the torrefaction process for the unwashed and washed samples. As expected, in the unwashed samples, the mass and energy yields were higher for the woody biomasses (willow and eucalyptus) than for the grasses (Miscanthus and wheat straw) due not only to the higher densities of the woody biomass samples, but also their slower kinetics in pyrolysis as is shown in Figure 6.8 and discussed in Section 6.4.3. The washing procedures, in general, improved the mass and energy yields for all the samples, but had a greater effect on Miscanthus and eucalyptus. Although the progressive washings lead to a slight increase in the mass and energy yields of the samples, most of the benefit is seen after the water washing stage. Since the washings remove much of the potassium content of the fuel, one may expect a decreased mass yield after the samples have been washed, since potassium has been shown to increase the solid product yield in pyrolysis. However, this trend is not observed in the results in Table 6.9 and this is attributed to the lower reactivities of the fuels after removal of K by washing, implying that torrefaction has progressed to a lesser extent.

6.4.3 Effects of Pretreatment on Pyrolysis Kinetics

The kinetic data is shown in Figures 6.4-6.8, and Table 6.10. Here, the kinetic rates are calculated over the temperature range of 300 – 550 °C, and it is clear that

there are significant differences in the rates. These differences in activation energies are shown in Table 6.10, and the reaction rates at 300 °C are shown in Figure 6.8. From this figure it is seen that many of the results lie within a narrow band of reaction rates. However, it is clear that for the straws (Miscanthus, and wheat straw) the fastest rates are achieved by the unwashed samples, and the slowest rates for the unwashed and then torrefied samples. One explanation of this is that during torrefaction, the unwashed fuels are very reactive (due to the catalyzing influence of the high potassium content) and the resultant torrefied fuels are the most pyrolysed (and hence have the lowest reactivity).

In the case of the woody biomasses (willow, and eucalyptus), washing does not appear to have a significant effect upon the reaction kinetics, and examination of Figures 6.4 and 6.5, show similar, low activation energies for all the washed (un-torrefied) fuels. In contrast, the torrefied fuels (all pre-treatment washes) have higher activation energies (see Table 6.10). However, washing with HCl together with torrefaction has the greatest effect on the activation energies, for the woody biomass. One may speculate that this is due to changes in the chemical structure of the fuels. Work presented in Chapter 4 suggests that treatment with HCl causes not only a removal of the organically bound metals, but also partially digests the hemicellulose structure.

The significance of the impact of these changes in composition and reaction rates depends on the end application, power station or domestic heating. In the case of power station applications, washing with water reduces the ash content and increases the ash fusion temperature markedly, which may be advantageous particularly in the case of straw. Washing with ammonium acetate or HCl would not be feasible because of the small advantage gained and the high costs induced. In domestic applications the reduction of ash is not so important. Nevertheless, removal of alkali metals for domestic uses would have potential advantages such as preventing deposit formation, and possibly improving emissions of inorganic aerosols like KCl.

6.4.4 Effects of Pretreatment on Ash

Ash fusion tests were performed on all the samples excluding those washed with ammonium acetate and HCl (as insufficient ash content prevented the production of the cylinders necessary for this test). The AFT results are listed in Table 6.11. In Figure 6.10, the flow temperature stage was selected to help in comparing and contrasting the ash characteristics of all the samples tested. Trends in this figure show that the woody samples have ashes that melt at higher temperatures than the straws. This is due to the fact that the Miscanthus and the wheat straw have high potassium content and the woody biomass samples are high in calcium. This is supported by the ion chromatography analysis of the leachates of the washing experiments (Table 6.6). Thus, of the untreated fuels, the straw samples had the lowest flow temperatures, and the woody biomasses had the highest. The same is seen for the torrefied fuels, that is, the torrefaction alone does not affect ash melting. For the water washed samples, it is seen that the flow temperature of the straws increases to the same level of the woods. Again, upon torrefaction, little change in the flow temperatures is noted. The most problematic fuels in terms of ash are wheat straw and Miscanthus. Water washing has a dramatic impact on these fuels, in particular for HT which increases from typically < 1200 °C to ≥ 1500 °C. This demonstrates that water-washing, combined with torrefaction would be a very attractive process for high alkali residues, such as wheat straw.

6.5 Conclusions

In this chapter, studies were made on pretreatment and torrefaction of four biomass samples: SRC willow, eucalyptus, Miscanthus, and wheat straw. Torrefaction was studied on untreated fuels, or those pre-washed with water, ammonium acetate or hydrochloric acid. Water washing prior to torrefaction significantly reduced the ash content of all the fuels although the nitrogen content was slightly increased. Washing with HCl and ammonium acetate decreased the ash content of the samples further. The washing processes influenced the ash fusion temperatures, but this was dependent of the biomass used. It was particularly beneficial for wheat straw, where the ash flow temperature increased from 1140 to over 1500 °C under oxidizing conditions. The results suggest that water washing is

the most useful pre-treatment for the preparation of torrefied fuels. Torrefaction yields improved after pre-treatment by washing and this was linked to the relative pyrolysis rates of the different fuels. This in turn was related to the removal of catalytic metals (particularly K) by the different washing methods. Thus, torrefaction and pretreatment by different washing procedures are intimately linked. Therefore, re-optimization of torrefaction would be required if ash improvement by pretreatment were to be implemented.

Chapter 7
Summary of Conclusions and Suggestions for Future Work

7.1 Kinetics of the Thermal Degradation of Biomass

This work focused on the kinetics of the thermal decomposition of a SRC willow. It addresses two questions. First, what method of data analysis is appropriate for extracting reliable kinetic data from TGA experiments? Second, what kinetics are most suitable for high heating rate situations such as those present in pulverized fuel power stations?

Kinetic analysis of willow TGA data was conducted using a variety of approaches. A review of previously published work on biomass and its polymeric components helped ascertain the variation in kinetics, reasons for differences, and extrapolation to flame temperatures. The data fell into two main categories: (1) very high E and A values (>100 and up to 270 kJ/mol, and up to 10^{17} s^{-1}) derived when model biomass components are studied, for example, cellulose; or the data is interpreted as the sum of a number of individual first-order reactions, for example, FG-BioMass; (2) intermediate and low E and A values (50–100 kJ/mol and $<\sim 10^5$ s^{-1}) derived using a number of global approaches.

For low heating rate experiments (10^1 K/min), the global first-order reaction kinetic models that tend to yield low E values, such as the reaction rate constant method, work well. High E kinetics can also work well at low heating rate, but only if the reaction is assumed to be due to the sum of a number of individual steps, such as the biochemical components degrading independently, or the functional group approach.

For higher heating rates (>10^3 K/s) high E kinetics predict conversion well, and this can be rationalized since primary cracking reactions will dominate under these conditions. However, at heating rates of 10^5 K/s and temperatures of 1500 °C (i.e., flame conditions), a compensation on the rates is seen and the choice of rate parameters is less critical. Two sets of kinetic data, E = 178.7 kJ/mol, $A = 2.2 \times 10^{13}$

s^{-1} and $E = 48.7$ kJ/mol, $A = 6.84 \times 10^3$ s^{-1}, both predict conversions in keeping with the available experimental data.

Future work: The methods for extracting kinetic parameters studied in this chapter were applied directly only to SRC willow. Although rates derived from experiments on other types of biomass were compared, it would nevertheless be useful to evaluate kinetics of varying types of biomass with all four methods studied. Further validation of the findings would be useful especially at high heating rates and high temperatures.

7.2 Role of Alkali Metals in Biomass Pyrolysis and Combustion

This chapter dealt fundamental work on alkali metals (sodium, potassium, and cesium) to determine if group chemistry has an effect upon the catalytic process observed in SRC Willow thermal degradation, thereby gaining mechanistic insight into the process. Work detailing both pyrolysis and combustion (TGA), and combustion under flame conditions is presented. DTG profiles and first order reaction kinetics comparing the pyrolysis and combustion of the three alkali metal-impregnated, willow samples revealed a strong and similar catalytic effect, i.e. at the same molar concentration, that all three alkali metals have very similar impacts on these reactions. Combustion under flame conditions again showed a stark contrast between the strongly catalyzed degradation of samples with alkali metals, and the uncatalysed degradation of the mineral-free samples. As with the low heating rate results, at flame conditions, the same combustion behaviour was observed for SRC willow samples impregnated with various group 1 metals. These findings imply that a similar thermal degradation mechanism is followed when this woody biomass contains any of the alkali metals.

Future work: In this chapter, preliminary work was conducted on alkali metals to determine if group chemistry has an effect upon the catalytic process observed the thermal degradation of SRC willow. It would be interesting to discover if these trends hold when other types of biomass such as straws are examined. While it was

not an objective of this work, the impact of these metals on combustion is worthy of closer inspection, especially in terms of metal volatilization, and also from a fundamental mechanistic view on char combustion.

7.3 Influence of Potassium and Sodium on the Kinetics of SRC Willow Pyrolysis – Model Predicting Reaction Rates

Both potassium and sodium have been proven to function as catalysts in the decomposition and combustion/gasification of biomass and its chars. This chapter's aim was to develop an expression directly linking biomass degradation kinetics to the inherent potassium and sodium content. This expression is based on the effects of these metals on the slow pyrolysis of short rotation coppice willow. The influence of potassium and sodium on the initial pyrolysis of willow was studied by examining willow samples impregnated with different metal concentrations; from 0 wt% potassium, achieved by acid-washing the willow, to 2 wt% K. Similarly with sodium impregnated samples, concentrations between 0 to 2 wt% Na were investigated.

Thermogravimetric data for these samples was analyzed and apparent first order kinetics derived, which are valid over the experimental temperature range. A novel, modified Langmuir-Hinshelwood relation was developed and applied to link potassium concentration and early pyrolysis. This relation yields a maximum reaction rate and a metal saturation constants that can be used directly to obtain a reaction rate of willow pyrolysis based on the pyrolysis temperature and the concentration of alkali metals in the biomass sample. The maximum reaction rate constant of 3.26×10^{-3} (s^{-1}) and the potassium saturation constant of 0.56 wt% can be accurately used to derive the pyrolysis reaction rate of a willow sample with a known potassium concentration. Similarly, a maximum reaction rate of 3.27×10^{-3} (s^{-1}) and a sodium saturation constant of 0.36 wt% can be used to derive a reaction rate for a willow sample with a known sodium concentration.

A saturation effect was seen with regard to both potassium and sodium concentrations and the apparent first-order reaction rate at ca. ca. 4 wt% for K and 3.5% for Na; this is attributed to maximum active site availability.

Ab initio (DFT method) modelling of possible chelated structures indicates that both metal ions, K^+ and Na^+, form multiple interactions with the hydroxyl and ether bonds in the cellulose structure. Structures with metal chelated at the C6 position in the ring have interactions with four oxygen atoms, while metals at the C2 position have interactions with only two oxygen atoms. Structures are more stable when potassium or sodium can coordinate to more oxygen groups. In all the structures investigated, chelation of potassium or sodium causes a change in the conformation of the rings (twisting) which may activate the structure towards cracking.

Future work: The L-H model presented in this work was successfully applied to K^+ and Na^+ doped SRC willow. Future work could involve testing the modified Langmuir-Hinshelwood relation on other types of biomass. Perhaps of even more use is the possibility of further modifying the mathematical relation to take into account multiple metals simultaneously, and to incorporate the evaporation/volatilization of metals.

7.4 Effects of Mineral Content on Torrefied Fuel Characteristics and Quality

This work explored the effects of combining pre-treatment washing techniques using water, ammonium acetate, and hydrochloric acid, and torrefaction to produce an improved biomass fuel. In particular, the effects of minerals on torrefaction, as well as on the pyrolysis and the ash behaviour of the torrefied material were investigated.

It was found that water washing prior to torrefaction significantly reduced the ash although the nitrogen content was slightly increased. Washing with HCl and ammonium acetate decreased the ash content of the samples further. It was also seen that water washing significantly raises the ash melting temperature of the fuels. This was particularly seen for wheat straw, where the ash flow temperature increased from 1140 to over 1500 °C under oxidizing conditions. The results suggest that water washing is the most useful pre-treatment for the preparation of

torrefied fuels. Torrefaction yields improved after pre-treatment by washing and this was linked to the relative pyrolysis rates of the different fuels. This in turn was related to the removal of catalytic metals (particularly K) by the different washing methods. Thus, torrefaction and pretreatment by different washing procedures are intimately linked. Therefore, re-optimization of torrefaction would be required if ash improvement by pretreatment were to be implemented.

Future work: This chapter showed remarkable success of pretreatment in improving the ash qualities of the fuels studied, particularly those of Miscanthus and wheat straw. It would be useful to conduct TGA combustion studies on these biomass samples to determine how the washings affect the combustion of torrefied fuels. It is suggested that future studies on washing leachates be carried out by ICP-OES rather than by IC to verify results from ammonium acetate and HCl washings. Torrefaction experiments could also be carried out on the washed fuels under various, perhaps less extreme, conditions to optimize the process. Useful information could also be gathered from the collection and examination of the torrefaction tars and gases through the introduction of tar traps and perhaps an online gas chromatograph. To this end, and also as an aid to process optimization, pyrolysis modelling software such as FG Biomass could be employed alongside experimental studies as it provides information on mass yields, volatile release, and helps characterize both solid and liquid products.

References

[1] Annual Energy Outlook. 2011, U.S. Energy Information Administration.

[2] Statistical Review of World Energy June 2009, British Petroleum.

[3] government U, Energy White Paper 2003. 2003, UK government.

[4] Klass DL. Biomass for renewable energy, fuels, and chemicals 1998, San Diego: Academic Press.

[5] International Energy Statistics. 2011; Available from: http://tonto.eia.doe.gov/cfapps/ipdbproject/iedindex3.cfm?tid=90&pid=44&aid=8&cid=regions&syid=1990&eyid=2009&unit=MMTCD.

[6] Miliband E, The UK Renewable Energy Strategy, E.a. Climate, Editor. 2009.

[7] Renewables 2010 Global Status Report. 2010, Renewable Energy Policy Network for the 21st Century.

[8] Thornley P, Upham P, and Tomei J. Sustainability constraints on UK bioenergy development. Energy Policy 2009; 37: p-5623-5635.

[9] Di Blasi C. Combustion and gasification rates of lignocellulosic chars. Progress in Energy and Combustion Science 2009; 35: p-121-140.

[10] Jenkins BM, Baxter L, Miles TRJ, and Miles TR. Combustion properties of biomass. Fuel Processing Technology 1998; 54: p-17-46.

[11] Fuentes ME, Nowakowski DJ, Kubacki ML, Cove JM, Bridgeman TG, and Jones JM. Survey of influence of biomass mineral matter in thermochemical conversion of short rotation willow coppice. Journal of the Energy Institute 2008; 81: p-234-241.

[12] Alberts B, Bray D, Lewis J, Raff M, Roberts K, and Watson JD. Molecular Biology of The Cell. 3rd ed. 1994, New York: Garland Publishing, Inc.

[13] Fiber-Source. 2011; Available from: http://www.afma.org/f-tutor/cellulose.htm.

[14] Sigma-Aldrich. **Enzymes for Alternative Energy Research** 2011; Available from: http://www.sigmaaldrich.com/life-science/metabolomics/enzyme-explorer/analytical-enzymes/enzymes-for-aer.html.

[15] Savage PE. 2011; Available from: http://www.google.co.uk/imgres?imgurl=http://www.engin.umich.edu/dept/che/research/savage/lignin.jpeg&imgrefurl=http://www.engin.umich.edu/dept/che/research/savage/energy.html&usg=__6LPfIR6eypb3BuU9rcl7S76I1O8=&h=206&w=456&sz=276&hl=en&start=3&zoom=1&um=1&itbs=1&tbnid=N39PKvC1HZmUeM:&tbnh=58&tbnw=128&prev=/search%3Fq%3Dchemical%2Bstructures%2Bof%2Blignin%26um%3D1%26hl%3Den%26rls%3Dcom.microsoft:en-us%26biw%3D1131%26bih%3D687%26tbm%3Disch&ei=nPTQTemcDMqChQfk4JGxDQ.

[16] Perry RH, Chilton CH, and Kirkpatrick SD, eds. Perry's Chemical Engineers' Handbook. Fourth ed. McGrawHill Series In Chemical Engineering. 1963, McGaw-Hill Book Company: New ork, San Francisco, Toronto, London, Sydney.

[17] Energy Efficiency & Renewable Energy - Biomass Program - Information Resources. Available from: http://www1.eere.energy.gov/biomass/feedstock_glossary.html.

[18] Government UK. 2011; Available from: http://www.biomassenergycentre.org.uk/portal/page?_pageid=75,20041&_dad=portal&_schema=PORTAL.

[19] Radmanesh R, Courbariaux Y, Chaouki J, and Guy C. A unified lumped approach in kinetic modeling of biomass pyrolysis. Fuel 2006; 85: p-1211-1220.

[20] Shafizadeh F. Introduction to pyrolysis of biomass. Journal of Analytical and Applied Pyrolysis 1982; 3: p-283-305.

[21] Backreedy RI, Fletcher LM, Jones JM, Ma L, Pourkashanian M, and Williams A. Co-firing pulverised coal and biomass: a modeling approach. Proceedings of the Combustion Institute 2005; 30: p-2955-2964.

[22] Ma L, Jones JM, Pourkashanian M, and Williams A. Modelling the combustion of pulverized biomass in an industrial combustion test furnace. Fuel 2007; 86: p-1959-1965.

[23] Weber R. Extracting mathematically exact kinetic parameters from experimental data on combustion and pyrolysis of solid fuels. Journal of the Energy Institute 2008; 81: p-226-233.

[24] Hillier J, Fletcher J, Orgill J, Isackson C, and Fletcher TH. An Improved Method for Determination of Kinetic Parameters from Constant Heating Rate TGA Oil Shale Pyrolysis Data. Prepr. Pap.-Am. Chem. Soc., Div. Fuel Chem. 2009; 54: p-

[25] Staggs JEJ. Modelling thermal degradation of polymers using single-step first-order kinetics. Fire Safety Journal 1999; 32: p-17-34.

[26] Fisher T, Hajaligol M, Waymack B, and Kellogg D. Pyrolysis behavior and kinetics of biomass derived materials. Journal of Analytical and Applied Pyrolysis 2002; 62: p-331-349.

[27] Branca C and Di Blasi C. Global intrinsic kinetics of wod oxidation. Fuel 2004; 83: p-81-87.

[28] Lehto J. Determination of kinetic parameters for Finnish milled peat using drop tube reactor and optical measurement techniques. Fuel 2007; 86: p-1656-1663.

[29] Scott SA, Dennis JS, Davidson JF, and Hayhurst AN. Thermogravimetric measurements of the kinetics of pyrolysis of dried sewage sludge. Fuel 2006; 85: p-1248-1253.

[30] Fahmi R, Bridgwater AV, Darvell LI, Jones JM, Yates N, Thain S, and Donnison IS. The effect of alkali metals on combustion and pyrolysis of Lolium and Festuca grasses, switchgrass and willow. Fuel 2007; 86: p-1560-1569.

[31] Müller-Hagedorn M, Bockhorn H, Krebs L, and Müller U. A comparative kinetic study on the pyrolysis of three different wood species. Journal of Analytical and Applied Pyrolysis 2003; 68-69: p-231-249.

[32] Hsisheng Teng Y-CW. Thermogravimetric Studies on the Kinetics of Rice Hull Pyrolysis and the Influence of Water Treatment. *Industrial & Engineering Chemistry Research* 1998; 37: p-3806-3811.

[33] Vamvuka D and Sfakiotakis S. Effects of heating rate and water leaching of perennial energy crops on pyrolysis characteristics and kinetics. Renewable Energy 2011; 36: p-2433-2439.

[34] Eom I-Y, Kim K-H, Kim J-Y, Lee S-M, Yeo H-M, Choi I-G, and Choi J-W. Characterization of primary thermal degradation features of lignocellulosic biomass after removal of inorganic metals by diverse solvents. Bioresource Technology 2011; 102: p-3437-3444.

[35] Jensen AD-J, K.; Wojtowicz, M. A.; Serio, M. A. TG-FTIR Study of the Influence of Potassium Chloride on Wheat Straw Pyrolysis. Energy & Fuels 1998; 12: p-929.

[36] Sonobe T and Worasuwannarak N. Kinetic analysis of biomass pyrolysis using the distributed activation energy model. Fuel 2008; 87: p-414-421.

[37] Brown RC. Biorenewable Resources. 2003, Ames: Iowa State Press.

[38] Arcate JR, Torrefied Wood, an Enhanced Wood Fuel, in *Bioenergy 2002*. 2002: Boise, Idaho.

[39] Nimlos MN, Brooking E, Looker MJ, and Evans RJ. Biomass Torrefaction Studies with a Molecular Beam Mass Spectrometer. Prepr. Pap.-Am. Chem. Soc., Div. Fuel Chem. 2003; 48: p-590.

[40] Bridgewater AV. Thermal Processing of Biomass for Fuels and Chemicals. in International Conference on Renewable Bioenergy Technologies, Risks and Rewards. 2002. London, England.

[41] Conesa JA, Marcilla A, Caballero JA, and Font R. Comments on the validity and utility of the different methods for kinetic analysis of thermogravimetric data. Journal of Analytical and Applied Pyrolysis 2001; 58-59: p-617-633.

[42] Fitzpatrick EM, Jones JM, Pourkashanian M, Ross AB, Williams A, and Bartle KD. Mechanistic Aspects of Soot Formation from the Combustion of Pine Wood. 2008; 22: p-3771-3778.

[43] Milosavljevic I and Suuberg EM. Cellulose Thermal Decomposition Kinetics: Global Mass Loss Kinetics. 1995; 34: p-1081-1091.

[44] Antal MJ, Varhegyi G, and Jakab E. Cellulose Pyrolysis Kinetics: Revisited. 1998; 37: p-1267-1275.

[45] Gronli M, Antal MJ, and Varhegyi G. A Round-Robin Study of Cellulose Pyrolysis Kinetics by Thermogravimetry. 1999; 38: p-2238-2244.

[46] Koufopanos CAM, G.; Lucchesi, A. . Kinetic Modeling of the Pyrolysis of Biomass and Biomass Components. Canadian Journal of Chemical Engineering 1989; 67: p-75.

[47] Miller RS and Bellan J. A Generalized Biomass Pyrolysis Model Based on Superimposed Cellulose, Hemicelluloseand Liqnin Kinetics. 1997; 126: p-97 - 137.

[48] Ranzi E, Cuoci A, Faravelli T, Frassoldati A, Migliavacca G, Pierucci S, and Sommariva S. Chemical Kinetics of Biomass Pyrolysis. 2008; 22: p-4292-4300.

[49] Hosoya T, Kawamoto H, and Saka S. Cellulose-hemicellulose and cellulose-lignin interactions in wood pyrolysis at gasification temperature. Journal of Analytical and Applied Pyrolysis 2007; 80: p-118-125.

[50] Shuangning X, Zhihe L, Baoming L, Weiming Y, and Xueyuan B. Devolatilization characteristics of biomass at flash heating rate. Fuel 2006; 85: p-664-670.

[51] Biagini E, Barontini F, and Tognotti L. Devolatilization of Biomass Fuels and Biomass Components Studied by TG/FTIR Technique. 2006; 45: p-4486-4493.

[52] Dupont C, Chen L, Cances J, Commandre J-M, Cuoci A, Pierucci S, and Ranzi E. Biomass pyrolysis: Kinetic modelling and experimental validation under high temperature and flash heating rate conditions. Journal of Analytical and Applied Pyrolysis 2009; 85: p-260-267.

[53] L. I. Darvell PH, J. M. Jones, D. J. Nowakowski, M. Pourkashanian and A. and Williams., Impact of minerals and alkali metals on willow combustion properties, in *World Renewable Energy Congress (WREC 2005)*. 2005, Elsevier Ltd.

[54] Chen Y, Charpenay S, Jensen A, Wojtowicz MA, and Serio M, Modeling of biomass pyrolysis kinetics, in *Twenty-Seventh Symposium (International) on Combustion*, T.C. Institute, Editor. 1998, The Combustion Institute: Pittsburgh, PA. p. 1327-1334.

[55] Scott SA, Dennis JS, Davidson JF, and Hayhurst AN. An algorithm for determining the kinetics of devolatilisation of complex solid fuels from

thermogravimetric experiments. Chemical Engineering Science 2006; 61: p-2339-2348.

[56] Varhegyi G, Bobaly B, Jakab E, and Chen H. Thermodynamic Study of Biomass Pyrolysis Kinetics. A Distributed Activation Energy Model with Prediction Tests. Energy & Fuels 2011; 25: p-24-32.

[57] Donskoi E and McElwain DLS. Optimization of Coal Pyrolysis Modeling. Combustion and Flame 2000; 122: p-359-367.

[58] Saddawi A, Jones JM, Williams A, and Woì jtowicz MA. Kinetics of the Thermal Decomposition of Biomass. Energy & Fuels 2009; 24: p-1274-1282.

[59] Chern J-S and Hayhurst AN. A simple theoretical analysis of the pyrolysis of an isothermal particle of coal. Combustion and Flame 2010; 157: p-925-933.

[60] P. Murray JW. Trans. Br. Ceram. Soc. 1955; 54: p-204-237.

[61] C. D. Doyle. Estimating isothermal life from thermogravimetric data. Journal of Applied Polymer Science 1962; 6: p-639-642.

[62] Senum GI and Yang RT. Rational approximations of the integral of the Arrhenius function. Journal of Thermal Analysis and Calorimetry 1977; 11: p-445-447.

[63] Nowakowski DJ, Jones JM, Brydson RMD, and Ross AB. Potassium catalysis in the pyrolysis behaviour of short rotation willow coppice. Fuel 2007; 86: p-2389-2402.

[64] Nowakowski DJ, Influence of Potassium and Phosphorus on the Thermochemical Conversion of the Cell Wall Components of Biomass, in *School of Process, Environmental and Materials Engineering*. 2008, University of Leeds: Leeds.

[65] Solomon PR and Serio MA, Evaluation of Coal Pyrolysis Kinetics, in Fundametals of the Physical-Chemistry of Pulverized Coal combustion, G.P. J. Lahaye, Editor. 1987, Martinus Nijhoff Publishers. p. 126-149.

[66] Wagenaar BM, Prins W, and van Swaaij WPM. Flash pyrolysis kinetics of pine wood. Fuel Processing Technology 1993; 36: p-291-298.

[67] Yu C and Zhang W. Modeling Potassium Release In Biomass Pyrolysis. Progress in Thermochemical Biomass Conversion 2001; 2: p-1107-1115.

[68] Wojtowicz MA, Bassilakis R, Smith WW, Chen Y, and Carangelo RMJ. J. Modeling the evolution of volatile species during tobacco pyrolysis. Anal. Appl. Pyrolysis 2003; 66: p-235-261.

[69] Tsamba AJ, Yang W, Blasiak W, and Wojtowicz MA. Cashew Nut Shells Pyrolysis: Individual Gas Evolution Rates and Yields. Energy and Fuels 2007; 21: p-2357-2362.

[70] Lifshitz A. Gas pyrolsis in combustion single-pulse shock tube studies of N- and O-atom-containing heterocyclics. Combustion and Flame 1989; 78: p-43-57.

[71] Darvell LI, Hrycko P, Jones JM, Nowakowski DJ, Pourkashanian M, and Williams A, Impact of minerals and alkali metals on willow combustion properties, in *World Renewable Energy Congress (WREC 2005)*. 2005, Elsevier Ltd.

[72] Jones JM, Darvell LI, Bridgeman TG, Pourkashanian M, and Williams A. An investigation of the thermal and catalytic behaviour of potassium in biomass combustion. Proceedings of the Combustion Institute 2007; 31: p-1955-1963.

[73] Nowakowski DJ and Jones JM. Uncatalysed and potassium-catalysed pyrolysis of the cell-wall constituents of biomass and their model compounds. Journal of Analytical and Applied Pyrolysis 2008; 83: p-12-25.

[74] Evans RJ and Milne TA. Energy & Fuels 1987; 1: p-123-137.

[75] Antal JMJ and Gronli M. The Art, Science, and Technology of Charcoal Production. Ind. Eng. Chem. Res. 2003; 42: p-1619-1640.

[76] Winter M. WebElements. 2003; Available from: http://www.webelements.com/caesium/bond_enthalpies.html.

[77] Dayton DC, French RJ, and Milne TA. Direct Observation of Alkali Vapor Release during Biomass Combustion and Gasification. 1. Application of Molecular Beam/Mass Spectrometry to Switchgrass Combustion. Energy & Fuels 1995; 9: p-855-865.

[78] Fu Q, Argyropoulos DS, Tilotta DC, and Lucia LA. Understanding the pyrolysis of CCA-treated wood: Part I. Effect of metal ions. Journal of Analytical and Applied Pyrolysis 2008; 81: p-60-64.

[79] Richards GN and Zheng G. Influence of metal ions and of salts on products from pyrolysis of wood: Applications to thermochemical processing of newsprint and biomass. Journal of Analytical and Applied Pyrolysis 1991; 21: p-133-146.

[80] Antal MJ, Varhegyi G, and Jakab E, Cellulose Pyrolysis Kinetics: Revisited. 1998. p. 1267-1275.

[81] Williams PT and Horne PA. The role of metal salts in the pyrolysis of biomass. Renewable Energy 1994; 4: p-1-13.

[82] Philpot CW. Influence of Mineral Content on the Pyrolysis of Plant Materials. Forest Science 1970; 16: p-461-471.

[83] Jones JM, Darvell LI, Nowakowski DJ, Ma L, and Williams A, Fundamentals of biomass combustion, in *XIX International Symposium on Combustion Processes*. 2005: Wisla, Poland.

[84] Frisch MJ, Trucks GW, Schlegel HB, Scuseria GE, Robb MA, Cheeseman JR, and al. e, Gaussian 03 Revision C.01. 2004, Gaussian, Inc: Wallingford, CT, USA.

[85] Jones JM and Jones DH. Modelling the competition between annealing and oxidation in the carbon-oxyten reaction. Letters to the Editor / Carbon 2007; 45: p-668-689.

[86] Froudakis GE and Stratakis M. A DFT Study on the Interaction of Li+ and Na+ with Alkyl-Substituted Ethenes. Eur. J. Org. Chem. 2003; 359-364.

[87] Brown MD, Dyke JM, Ferrante F, Levason W, Ogden SJ, and Webster M. Unexpected Strucutral Diversity in Alkali Metal Azide-Crown Ether Complexes: Synthesis, X-ray Structures, and Quantum-Chemical Calculations. Chem. Eur. J. 2006; 12: p-2620-2629.

[88] Agblevor FA and Besler S. Inorganic Compounds in Biomass Feedstocks. 1. Effect on the Quality of Fast Pyrolysis Oils. Energy & Fuels 1996; 10: p-293-298.

[89] Sivakumar A, Srinivasaraghavan T, Swaminathan T, and Baradarajan A. Extended monod kinetics for substrate inhibited systems. Bioprocess and Biosystems Engineering 1994; 11: p-185-188.

[90] Jensen A, Dam-Johansen K, Wojtowicz MA, and Serio MA, TG-FTIR Study of the Influence of Potassium Chloride on Wheat Straw Pyrolysis. 1998. p. 929-938.

[91] Olsson JG, Jaglid U, Pettersson JBC, and Hald P. Alkali Metal Emission during Pyrolysis of Biomass. Energy & Fuels 1997; 11: p-779-784.

[92] Olsson JG, Pettersson JBC, Padban N, and Bjerle I. Alkali Metal Emissions from Filter Ash and Fluidized Bed Material from PFB Gasification of Biomass. Energy & Fuels 1998; 12: p-626-630.

[93] Knudsen JN, Jensen PA, and Dam-Johansen K. Quantification of the Release of Cl, K and S to the Gas Phase from Combustion of Annual Biomass. Prepr. Pap. - Am. Chem. Soc., Div. Fuel Chem. 2004; 49: p-93-94.

[94] Jensen PA, Frandsen FJ, Dam-Johansen K, and Sander B. Experimental Investigation of the Transformation and Release to Gas Phase of Potassium and Chlorine during Straw Pyrolysis. Energy & Fuels 2000; 14: p-1280-1285.

[95] Rendleman Jr JA, Melville LW, and Tipson RS, Complexes of Alkali Metals and Alkaline-Earth Metals with Carbohydrates, in Advances in Carbohydrate Chemistry. 1967, Academic Press. p. 209-271.

[96] Kalinina KB and Litvinova LS. Thin-Layer Chromatography of Neutral Sugars as Influenced by the Nature of the Cation of Impregnating Salt. Russian Journal of Applied Chemistry 2001; 74: p-1343-1347.

[97] Rodrigues JA, Taylor AM, Sumpton DP, Reynolds JC, Pickford R, Thomas-Oates J, and Derek H, Mass Spectrometry of Carbohydrates: Newer Aspects, in Advances in Carbohydrate Chemistry and Biochemistry. 2007, Academic Press. p. 59-141.

[98] Percival EGV. 251. Addition compounds of the carbohydrates. Part I. Potassium hydroxide-glucose and related compounds. Journal of the Chemical Society (Resumed) 1934; 1160-1164.

[99] Botek E, Debrun JL, Hakim B, and Morin-Allory L. Attachment of alkali cations on β-D-glucopyranose: matrix-assisted laser desorption/ionization time-of-flight studies and ab initio calculations. Rapid Communications in Mass Spectrometry 2001; 15: p-273-276.

[100]Lee S, Wyttenbach T, and Bowers MT. Gas phase structures of sodiated oligosaccharides by ion mobility/ion chromatography methods. International Journal of Mass Spectrometry and Ion Processes 1997; 167-168: p-605-614.

[101]Hofmeister GE, Zhou Z, and Leary JA. Linkage position determination in lithium-cationized disaccharides: tandem mass spectrometry and semiempirical calculations. Journal of the American Chemical Society 1991; 113: p-5964-5970.

[102]Striegel AM, Timpa JD, Piotrowiak P, and Cole RB. Multiple neutral alkali halide attachments onto oligosaccharides in electrospray ionization mass spectrometry. International Journal of Mass Spectrometry and Ion Processes 1997; 162: p-45-53.

[103]Cancilla MT, Penn SG, Carroll JA, and Lebrilla CB. Coordination of Alkali Metals to Oligosaccharides Dictates Fragmentation Behavior in Matrix Assisted Laser Desorption Ionization/Fourier Transform Mass Spectrometry. Journal of the American Chemical Society 1996; 118: p-6736-6745.

[104]Foresman JB and Frisch Æ. Exploring chemistry with electronic structure methods. 2nd ed. 1996.

[105]Shafizadeh F, Melville LW, and Tipson RS, Pyrolysis and Combustion of Cellulosic Materials, in Advances in Carbohydrate Chemistry. 1968, Academic Press. p. 419-474.

[106]Yu, C and Zhang, W. Modeling Potassium Release In Biomass Pyrolysis. Progress in Thermochemical Biomass Conversion 2001; 2: p-1107-1115.

[107]Olsson JG, Pettersson JBC, Padban N, and Bjerle I. Alkali Metal Emissions from Filter Ash and Fluidized Bed Material from PFB Gasification of Biomass. Energy & Fuels 1998; 12: p-626-630.

[108]Cerfontain MB and Moulijn JA. Alkali-catalysed gasification reactions studied by in situ FTIR spectroscopy. Fuel 1983; 62: p-256-258.

[109]Huang HY and Yang RT. Catalyzed Carbon-NO Reaction Studied by Scanning Tunneling Microscopy and ab Initio Molecular Orbital Calculations. Journal of Catalysis 1999; 185: p-286-296.

[110]Backreedy RI, Jones JM, Pourkashanian M, and Williams A. Burn-out of pulverised coal and biomass chars[small star, filled]. Fuel 2003; 82: p-2097-2105.

[111]Bergman PCA and Kiel JHA. Torrefaction for biomass upgrading. in 14th European biomass Conference & Exhibition. 2005. Paris, France.

[112]Arias B, Pevida C, Fermoso J, Plaza MG, Rubiera F, and Pis JJ. Influence of torrefaction on the grindability and reactivity of woody biomass. Fuel Processing Technology 2008; 89: p-169-175.

[113]Bridgeman TG, Jones JM, Williams A, and Waldron DJ. Using existing coal technologies to process thermally pretreated biomass. in 17th European Biomass Conference and Exhibition. 2009. Hamburg, Germany.

[114]Bridgeman TG, Jones JM, Williams A, and Waldron DJ. An investigation of the grindability of two torrefied energy crops. Fuel 2010; 89: p-3911-3918.

[115]Jones JM, Bridgeman TG, Darvell LI, Gudka B, Saddawi A, and Williams A. Combustion Properties of Torrefied Willow compared with Bituminous Coals. Fuel 2011. in preparation.

[116]Baxter XC, Jones JM, Darvell LI, Barraclough T, Yates NE, and Shield I. Study of Miscanthus x giganteus ash behaviour - variation with agronomy and assessment method. Fuel 2011; in press.

[117]Miles T, R., Miles T, R. Jr., Baxter L, L., Bryers R, W., Jenkins B, M., and Oden L, L., Alkali Deposits - found In Biomass Power Plants - A Preliminary Investigation of their Extent and Nature, in *Summary Report*. 1995, National Renewable Energy Laboratory: Golden, Colorado.

[118]Bridgeman TG, Torrefaction of Biomass, PhD Thesis from the *Energy and Resources Research Institute*. 2008, University of Leeds: Leeds.

[119]Gudka B, Darvell LI, Jones JM, Williams A, Kilgallon PJ, Simms NJ, and Goldsmith RL. Fuel Characteristics of Wheat-based Dried Distillers Grains and Solubles (DDGS) for Thermal Conversion in Power-plants. Fuel Processing Technology 2011; in press:

[120]Bryers R, W. Fireside slagging, fouling, and high-temperature corrosion of heat-transfer surface due to impurities in steam-raising fuels. Progress in Energy and Combustion Science 1996; 22: p-29-120.

[121]Friedl A, Padouvas E, Rotter H, and Varmuza K. Prediction of heating values of biomass fuel from elemental composition. Analytica Chimica Acta 2005; 544: p-191-198.

[122]Bergman PCA, Boersma AR, Kiel JHA, Prins MJ, Ptasinski KJ, and Janssen FGGJ, Torrefied biomass for entrained-flow gasification of biomass. 2005.

[123]Baxter X, Combustion Properties of Miscanthus - Impact of Ash and Agronomy. PhD Thesis from the *School of Process, Environmental and Material Engineering*. 2011, University of Leeds: Leeds.

Appendix

Table A.1 First order reaction kinetics for potassium impregnated samples where the units for E are in (kJ/mol), and (s^{-1}) for A and k (Chapter 5).

K wt%	E	Ln A	$k_{300°C}$
HCL	121.27	18.18	6.94E-04
0.10%	66.88	6.83	7.42E-04
0.05%	65.22	6.50	7.51E-04
Raw	65.95	6.83	9.00E-04
0.25%	65.60	6.92	1.05E-03
0.50%	64.27	6.99	1.50E-03
0.75%	63.10	7.04	2.02E-03
1.00%	62.23	7.08	2.52E-03
2.00%	61.29	7.10	3.14E-03
1.50%	61.09	7.11	3.29E-03

Table A.2 First order reaction kinetics for sodium impregnated samples where the units for E are in (kJ/mol), and (s^{-1}) for A and k (Chapter 5).

Na wt%	E	lnA	$k_{300°C}$
0%	75.92	9.04	1.01E-03
0.10%	58.28	5.59	1.30E-03
0.25%	54.34	4.83	1.39E-03
0.50%	47.67	3.57	1.60E-03
1%	41.22	2.75	2.74E-03
2%	36.07	1.70	2.83E-03

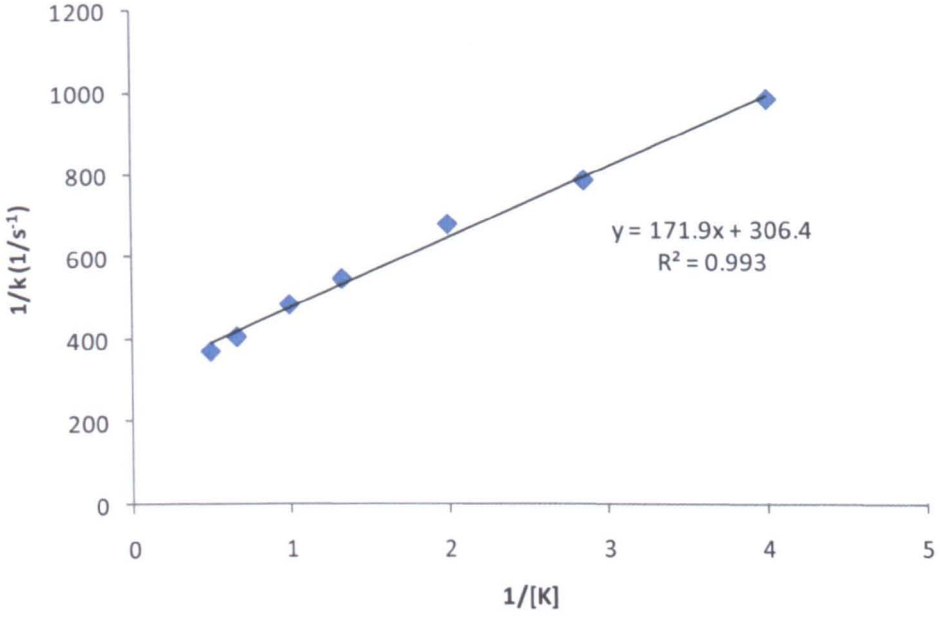

Figure A.1 1/k vs. 1/[M] plot (where [M] = wt% of metal) for potassium impregnated samples as referred to in section 5.5.

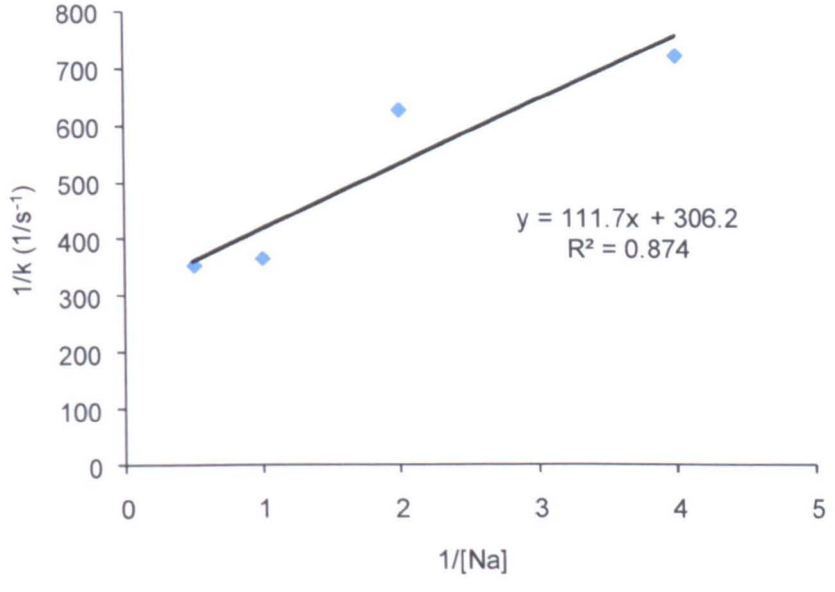

Figure A.2 1/k vs. 1/[M] plot (where [M] = wt% of metal) for sodium impregnated samples as referred to in section 5.5.

Table A.3 Fouling and slagging indices for biomass fuels studied in Chapter 6.

Type of Biomass	AI (kg/GJ)	$R_{b/a}$
willow	0.17	21.30
eucalyptus	0.29	22.00
Miscanthus	0.33	0.52
wheat straw	1.02	0.67

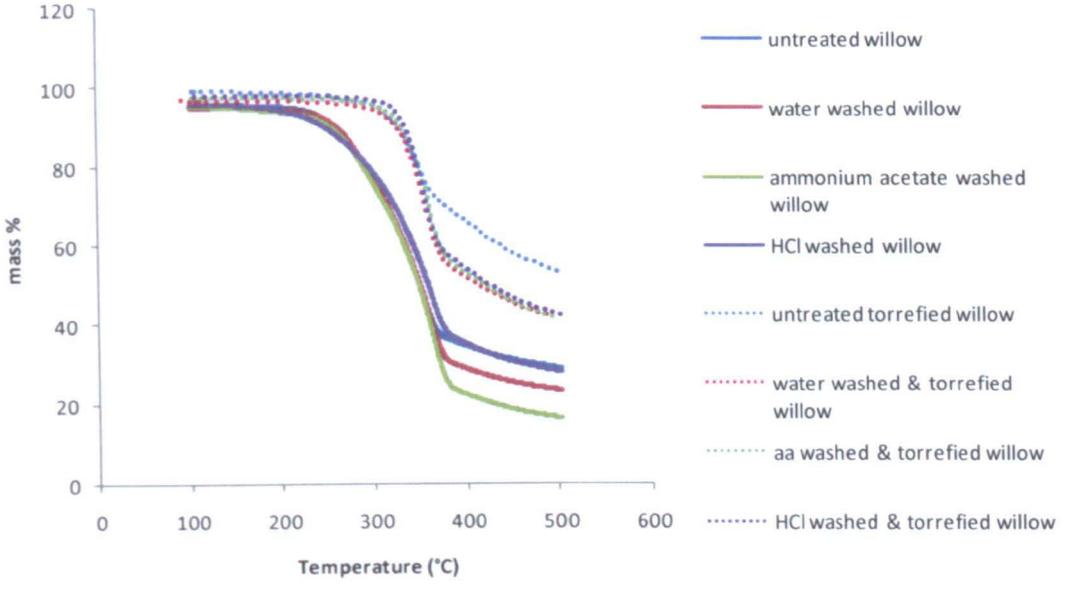

Figure A. 3 TGA pyrolysis weight loss profiles of willow samples at a heating rate of 25 °C/min as discussed in Chapter 6.

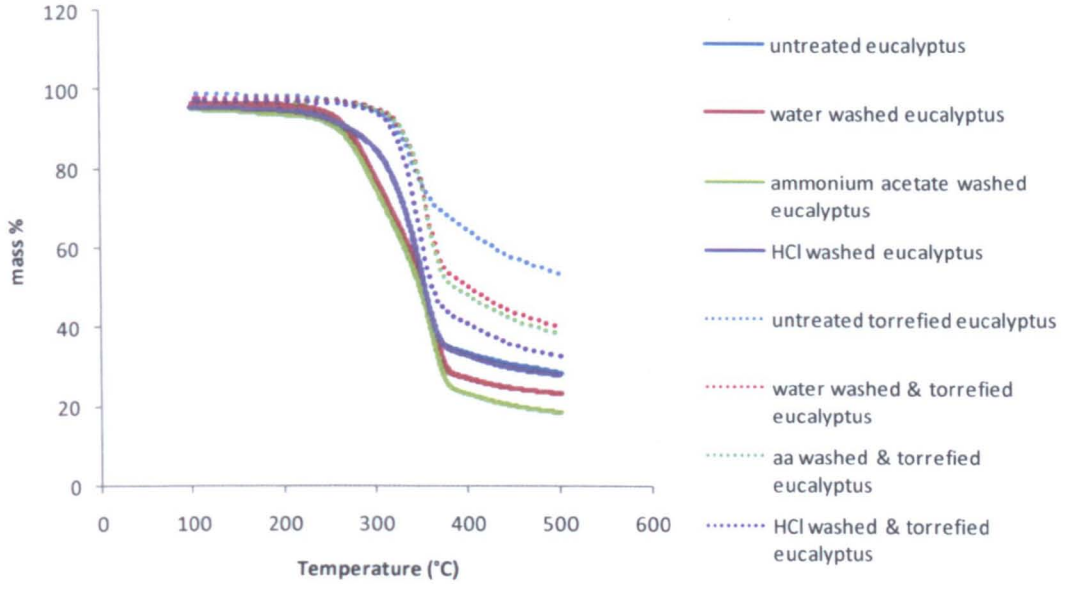

Figure A.4 TGA pyrolysis weight loss profiles of eucalyptus samples at a heating rate of 25 °C/min as discussed in Chapter 6.

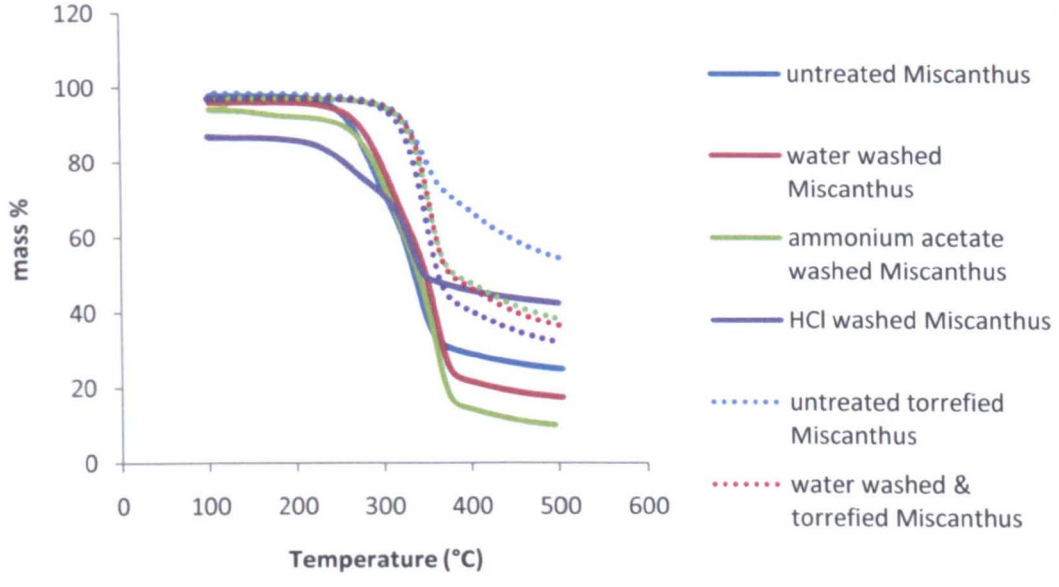

Figure A.5 TGA pyrolysis weight loss profiles of Miscanthus samples at a heating rate of 25 °C/min as discussed in Chapter 6.

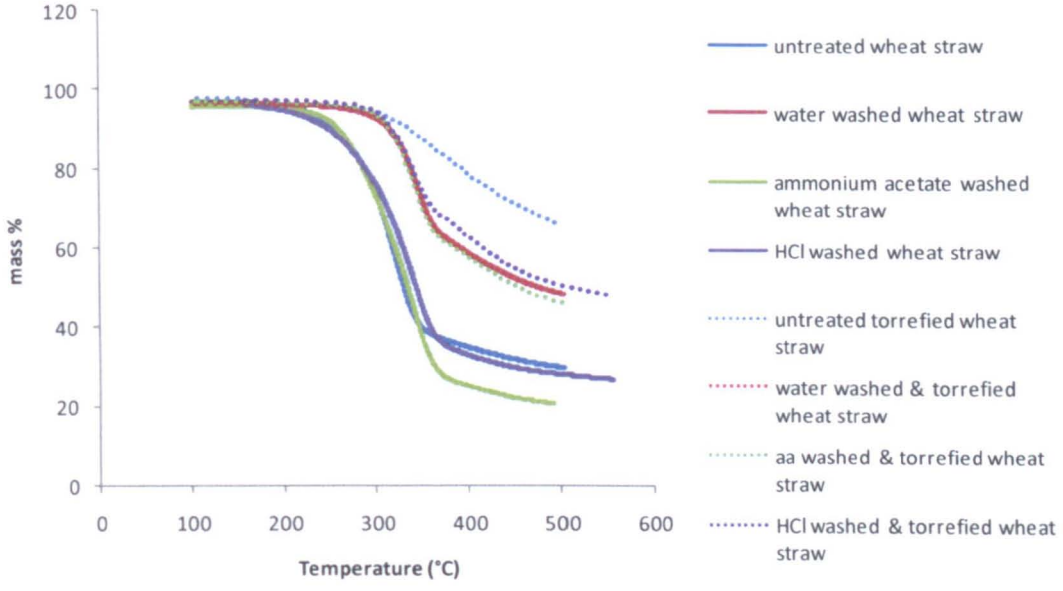

Figure A.6 TGA pyrolysis weight loss profiles of wheat straw samples at a heating rate of 25 °C/min as discussed in Chapter 6.